Max-Planck Institut für Kolloid- und Grenzflächenforschung

Amino acid-derived imidazolium salts: Platform molecules for *N*-Heterocyclic carbene metal complexes and organosilica materials

Dissertation

zur Erlangung des akademischen Grades
"doctor rerum naturalium"
(Dr. rer. nat.)
in der Wissenschaftsdisziplin „Kolloidchemie"

eingereicht an der
Mathematisch-Naturwissenschaftlichen Fakultät
der Universität Potsdam

von

Elliot Steeples

Potsdam, Juni 2016

Table of Contents

I   Acknowledgements

First and foremost, I give my sincere thanks to Prof. Dr. Markus Antonietti for the opportunity to carry out my research within the MPIKG, and to submit this work for a PhD.

My deepest thanks go to Dr. Davide Esposito, who gave me the freedom to pursue this project, and the help, advice, support and patience that I needed to complete it. Thank you for everything.

In advance, I thank the reviewers for agreeing to review this thesis, and the faculty members of my committee. Additionally I'd like to thank anyone who read this and gave me feedback, in particular Nina. Big or small, every effort helped.

I'd like to thank Prof. Dr. Uwe Schilde and Alexandra Kelling for measuring and solving my X-Ray crystallographic data, and for the advice and knowledge surrounding it. I'd also like to thank Dr. Peter Hesemann, for the ongoing collaborative work, ssNMR measurements, and for the direction and advice.

The powerhouse behind the MPI is the all-knowing technicians, who selflessly give advice and measure samples so that we doctoral students can succeed. A collosal thankyou is extended to our group technician Irina Shekova, for the characteristic measurements, and for her unfailing optimism. Likewise I thank Regina, Ursula, Sylvia, Marlies, Heike, Rona and Antje for every sample you've run for me, or piece of advice you've given.

The biorefinery and sustainable chemistry group have been great to me, in every form that my research took. I'd therefore like to thank everyone, past and present. Sarah, Valerio, Michela, Max, Gianpaolo, Zuzka, Sandy, Servann, Binshen, Marcos, and Narashimarao – thank you all for for the pleasure of your company and for your advice.

Life within an MPI is nothing without friends. I couldn't possibly list everyone here, but to everyone within the Colloid Chemistry department and good number outside of it; thank you for all the times we've shared, food we've eaten, drinks we've drank, and hangovers we've survived. Additional thanks go to Remì, for his friendliness, optimism, and neverending search for a party; Afroditi, for always being there for chats I'd never thought I'd have; and Tom, for allowing me to unleash my Englishness every once in a while.

Among my most important acknowledgements I'd like to list Selin. Who has listened to more of my complaints than I thought humanly possible, and without whom I wouldn't have had the strength to finish.

Last, and by no means least, I'd like to thank my parents. They have never stopped supporting me throughout any of my stupid endevours, successful or otherwise. Thank you for everything, this is for you.

II   Motivation

The field of green chemistry is the product of a global initiative to promote a sustainable human lifestyle and preserve resources on planet Earth. The chemical industry has recognized its obligation to play a part in this, by reducing our dependency on crude oil; thereby addressing issues of sustainability and pollution. The first steps that were taken in the mid-late 1980's have now become a global movement which has spread into virtually every field of chemistry with industrial application. Biorefinery is a field which goes hand-in-hand with green chemistry, facilitating the development of platform chemicals and building blocks from sustainable sources such as lignocellulosic biomass, carbohydrates, and protein derivatives that do not depend on crude oil. This field has helped to develop solvents, platform chemicals and materials which are sought after as alternatives to the oil-derived chemicals upon which we can no longer be dependent.

Generally speaking, the most fruitful bio-derived platform products come from carbohydrate sources, in particular products derived from glucose, fructose and glycerol. These products can be used in synthesis to create compounds which may eventually replace oil-derived products. Naturally, producing bio-derived compounds which are competitive with their oil-derived counterparts, whilst still adhering to the 12 principles of green chemistry during their production, is a very difficult task. A huge number of reports within the past two decades have been dedicated to producing such examples, most of which stem from sugars. Potent examples include 5-HMF, levulinic acid, and the vast numbers of oxidation and reduction products of glycerol.

Imidazolium compounds are among those which have been developed using bio-derived and sustainable sources, as part of research previously developed within this research group. Imidazoliums form an integral part of chemical research, within applications such as ionic liquids (and polymers thereof), biologically and pharmaceutically significant compounds, and as addressed in this work: *N*-Heterocyclic carbenes (NHCs). Bio-derived ligands for homogeneous catalysis is a field which up to yet has not received so much attention.

The work presented within this thesis aims to marry together the fields of catalysts derived from sustainable materials, and reactions adhering to green chemical principles. Within chapters **2** and **3**, imidazolium salts derived from amino-acids and sugar-derived diketones (previously researched within this group) were converted into NHC precursor compounds and then subsequently used as ligands for NHC-metal organometallic complexes. A variety of complexes were produced using silver, palladium, and iridium metal centers. The complexes were then

applied in catalytic processes which bare relevance within green chemistry, the most successful of which is the Suzuki-Miyaura C–C cross coupling reaction in aqueous medium.

Within chapter **4**, the incorporation of bio-derived imidazolium salts within materials was investigated. Hybrid organosilica materials were produced via two different strategies, the second significantly greener and more versatile than the first. The resulting materials were investigated for their organic content. This acts as foundation work towards properties such as polarity tuning, hydrophobicity and absorption; and towards applications such as metal scavenging, chromatographic phases and supported catalysts.

This thesis seeks to further investigate the spectrum of bio-derived platform chemicals, and to broaden their significance in fields such as organometallics, homogeneous catalysis and hybrid materials. Concurrently, the 12 principles of green chemistry are adhered to as base rules. Whenever possible, sustainable materials are used, non-toxic solvents and reagents are included, benign synthesis procedures are conducted, and efficient catalytic procedures are investigated to optimize atom economy. The work aims to illustrate the possibilities of applying green chemistry and biorefinery to fields which will require their benefits in order to create a sustainable chemical industry.

1.   Introduction

## 1.1   Green Chemistry and Biorefinery

1.1.1   The 12 Principles and Atom utilization

Our modern society and lifestyle is critically dependent on crude oil, a finite source of compressed hydrocarbons resulting from decomposition of organic matter from organisms that existed on this planet millions of years ago. It has become common knowledge that the use of crude oil and its derivative products is responsible for a number of critical global issues. These issues include greenhouse gas emissions and the rise of global temperature, synthesis of non-degradable plastics which accumulate in nature, and international political rifts based on the search for more oil. A global effort to reduce the potentially disastrous consequences of crude oil use continues to persist, but the biggest goal of this movement within the chemical industry in particular is that of "sustainability"; that is to say the use of resources which are renewable or re-usable. This involves a gradual reduction and eventual abolition of our dependency on crude oil by using sustainable resources such as biomass to make platform chemicals which we would otherwise refine from oil, and also to reduce the effect of issues already caused. This movement is now known as "Green Chemistry".

The initiative towards sustainability and process efficiency was investigated within industrial chemistry from the early 1980's following cues from the United Nations,[1] however it was not until the early 1990's that the term "Green Chemistry" was coined by Anastas and Werner. It has since become an established research field, with ever-growing numbers of researchers and journals making a contribution. Several of the main aims of the green chemistry initiative were already priorities within industrial chemistry, for example selectivity, avoidance of toxic substrates and reduction of surplus energy costs. However it was not until after the Pollution Prevention act of 1990,[2] and subsequently the US Environmental Protection Agency's (EPA) conception of the "US Green Chemistry Program" in 1993 before these aims were conveyed into a list. In a 1994 ACS symposium, Anastas and Warner proposed the *12 principles of green chemistry*,[3] which have since been used as a guideline for sustainable research and are paraphrased and explained as follows:

1. Waste prevention instead of remediation
2. Atom efficiency
3. Less hazardous/toxic chemicals
4. Safer products by design
5. Innocuous solvents and auxiliaries
6. Energy efficient by design
7. Preferably renewable raw materials
8. Shorter syntheses (avoid derivatization)
9. Catalytic rather than stoichiometric reagents
10. Design products for degradation
11. Analytical methodologies for pollution prevention
12. Inherently safer processes

In order to judge the "greenness" of a chemical process or product thereof, several measurement scales have been conceived which assess the degree to which a process adheres to the 12 principles. These are generally focused around the ratio of product produced to precursor used. The two main measurements are atom economy (AE),[4] introduced by Trost in 1991 and the E-factor, introduced by Sheldon the following year.[5] Atom Economy, initially the most widely used measurement, is simply a theoretical number to describe the reagent mass which becomes product assuming 100% yield. Whilst this model gives an insight into process efficiency, it disregards many important factors as it focuses simply on the theoretical stoichiometric equation. Solvents, acids, bases and any other entity which is assumed to be in excess is disregarded. The E-factor is a more sophisticated model and is now used extensively in pharmaceutical and fine-chemical production. The number simply represents the mass ratio of waste to desired product from a process. This takes account of all substances used, including reagents, reactants, solvent and catalysts; however production of water is in most cases excluded. The exclusion of water is usually permissible for fine chemical production; however for bio-relevant processes such as fermentation and biorefinery (covered later) the inclusion of waste water streams can be an important issue. E-factor has been a significant tool in judging the efficiency of bulk chemical manufacture compared to fine chemical and pharmaceuticals. E-factor was often observed to be staggeringly high for smaller processes, particularly in pharma; helping to expose inefficiency. An example which illustrates both models is outlined (Scheme **1.1**) in the production of Phloroglucinol from TNT.[6] Aside from the very dangerous and toxic reagents used in this reaction, AE regards this as an inefficient process, as only 5% of atoms within used reagents are incorporated into the product. Likewise, theE-factor of 40 represents 40kgs of waste per kg of product, which is also regarded as highly insufficient.

O$_2$N, NO$_2$, NO$_2$ K$_2$Cr$_2$O$_7$ H$_2$SO$_4$, SO$_3$ → HO$_2$C, O$_2$N, NO$_2$, NO$_2$ K$_2$Cr$_2$O$_7$ H$_2$SO$_4$, SO$_3$ → HO, OH, OH

Phloroglucinol
MW = 129

Cr$_2$(SO$_4$)$_3$ 2KHSO$_4$ 9FeCl$_2$ 3NH$_4$Cl CO$_2$ 8H$_2$O
392   272   1143   160   44   144

byproducts

Atom Utilization = 126/2282 = ca. 5%
E Factor = ca. 40
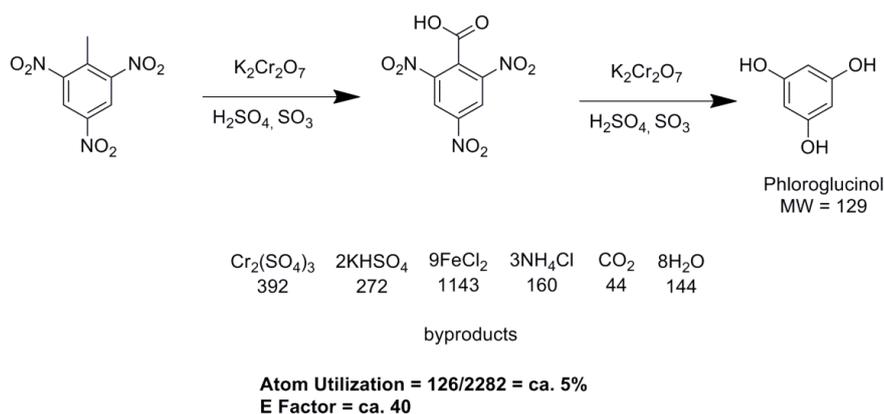
Scheme 1.1 AE and E-factor of the production of Phloroglucinol from TNT

For a more in-depth perspective on the sustainability of a process, one must additionally consider the factors that exist outside the process itself, and the full life-cycle of every substance involved. This can be achieved using the Life Cycle Assessment (LCA), developed in 2004 as part of GlaxoSmithKline's investigation into its pharmaceutical processes.[7] This method takes account of each part of the process and their individual cycles from conception to use, giving a picture of the processes' energy requirements, supply, demand, environmental impact, even the effect of the transport required. Performing a full LCA of a process reveals the effect of said process on known environmental issues, such as greenhouse gas emissions and eutrophication, which would otherwise not be obvious from E-factor or AE. For example a 2013 review on LCA analysis of biopolymer processing revealed that while biopolymers are preferable to polyalkenes for their biodegradability,[8] other issues are likely to arise as a result of their mass-production. This includes the increase in nitrogen-rich biodegradation products, subsequently causing eutrophication. .

This work considers a few particular green chemistry principles as guidelines; which will be subsequently discussed in further detail.

1.1.2   Principle 7: Platform Molecules from Biorefinery

For a process to be fully sustainable, either the source of each process "ingredient" must be infinite, or the products must be infinitely recyclable. Since crude oil is the source for most chemical building blocks, such as alkenes, alkanes and aromatics; research has been conducted into alternatives from living matter. Biorefinery is the process of refining chemical products from biomass, usually plant matter, which are renewable in theory. Whilst biorefinery stems from an initiative to produce energy sources, platform chemicals and building blocks from biorefinery have now become just as fruitful a research topic. The main streams of biorefinery

are focused on plant oils, protein-derivatives, agricultural residues and lignocellulosic biomass (figure **1.1**).
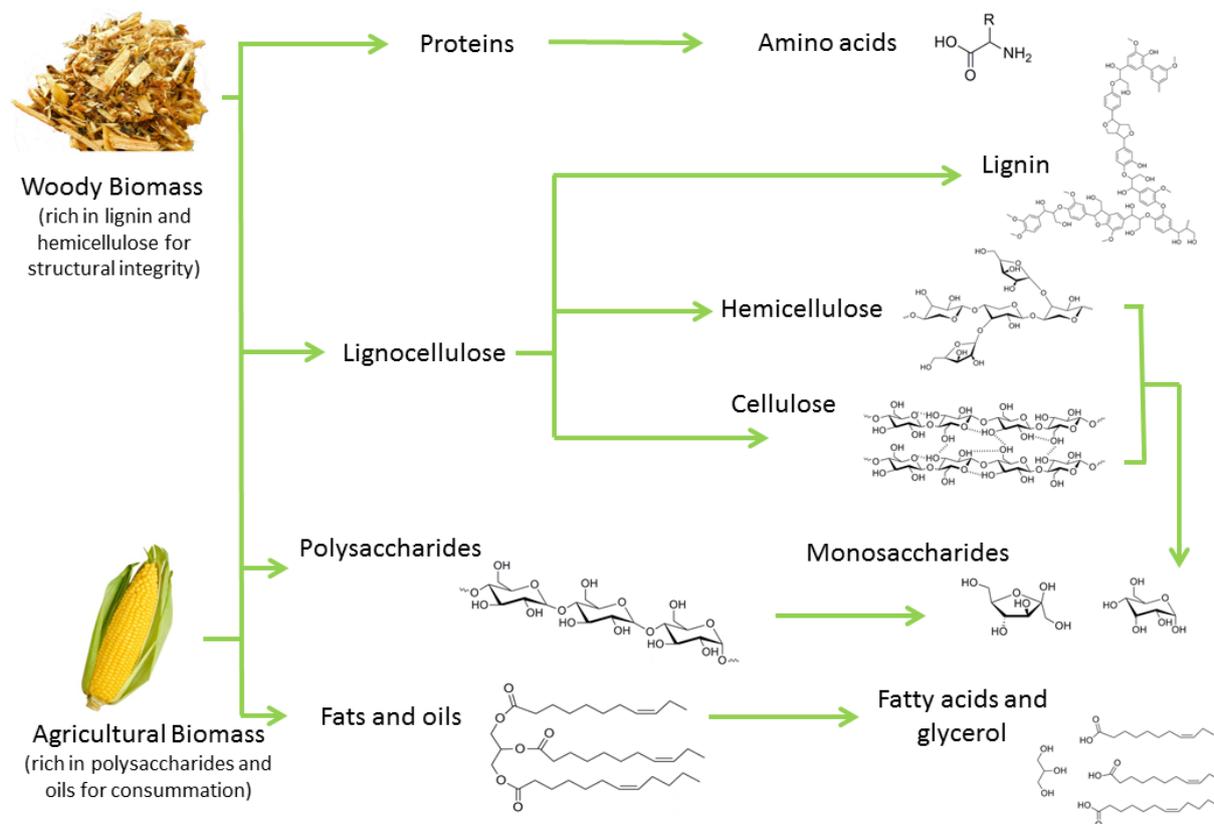

Figure 1.1 Biomass sources and their corresponding refinery products

There are three main methods of approaching biorefinery: biological, thermal, and chemical. Biological methods focus on technology which has already been available for a number of decades through the brewing and agricultural industry, utilizing bacteria and enzymes to convert digestible bio-molecules into smaller value-added products. The most obvious example of this is fermentation, such as the fermentation of glucose to produce alcohols. But less well-known examples are also significant in the production of biofuels, such as microbial methanogenesis, which is used for the production of methane.[9] Thermal processes have a greater impact on the production of chemical building blocks, generally involving the high temperature treatment of dried plant matter. Pyrolysis (heat treatment in the absence of oxygen) under certain conditions produces bio-oil; a complex mixture of monomeric and oligomeric fragments of lignocellulose and their oxygen-rich decomposition products.[10] Typically bio-oils contain monomeric sugars, hydroxyaldehydes, carboxylic acids and furans from cellulose and hemicellulose; as well as phenolic fragments from lignin. However the composition of each different bio-oil depends on the biomass source and the pyrolysis method. As a general trend, pyrolysis which is performed at lower temperatures and slow heating rates

tends to produce more char and solid combustion products, whereas faster methods at higher temperatures produces more high-value liquid products, alongside gaseous byproducts. Hydrothermal treatment is another recent biorefinery development, which uses high temperature and pressure to cleave polymeric biomolecule linkages via the use of near- or supercritical water.[11] This has proven to be an effective method of cleaving particularly challenging chemical bonds, such as C–C or C–O–C linkages within lignin and various polysaccharides.

Finally, chemical methods present the greatest potential in producing value-added chemicals from biomass fragments, as a result of their relatively mild conditions and versatile tunability. Chemical methods come in two broad categories: pre-treatment and catalytic processing, the latter of which will be discussed in more detail. Pre-treatment involves the separation of each individual biopolymer from its corresponding biomass source, for example the separation of lignocellulosic biomass into its three components: cellulose, hemicellulose and lignin.[12] This typically involves treatment with strong acids and/or bases, and various different solvents. Depending on the desired biomass component, often several methods are used in combination, as each one is suited to the isolation of particular components. For example, alkaline methods (treatment of the biomass in aqueous alkaline solutions) such as sodium and calcium hydroxide treatment typically produce high yields of cellulose, and additionally offer the advantage of hydrolysis into glucose.[13] However the lignin structure is then tainted with metal ions and salts, which may impede its further refinery. On the other hand, "organosolv" methods (separation through selective dissolution in organic solvents) are able to effectively dissolve the lignin and hemicellulose in organic solvents without effecting its composition.[14] Lignin is typically more soluble in certain organic solvents owing to its aromatic content; however its complex irregular structure facilitates only partial solubility. Cellulose and hemicellulose on the other hand, whilst insoluble in water, are much more amenable to aqueous-phase treatment techniques due to their weaker glycosidic bonds. A combination of these two methods can offer an effective process for the separation of lignocellulosic biomass components.

| Biomass Feedstock	Intermediate Chemicals	Primary Chemicals
Carbohydrates:	Sugars:	
Starch	Glucose	Methanol
Cellulose	Fructose	Ethanol
Hemicellulose	Xylose	Propanediols
	Lactose	Carboxylic acids
	Sucrose	Furfural
		Ethylene
Lignin	Phenolics:	
	Gallic acid	
	Ferulic acid	
Oils		
Long-chain triglycerides	Fatty acids	Fatty alcohols
	glycerol	Propanediols
		Propylene
		3-hydroxypropionaldehyde
Proteins	Amino acids	

Table 1.1 Biorefinery step processes: from feedstocks, to biopolymers, to platform chemicals

The highest-value (bio-derived) chemical building blocks are currently derived from carbohydrates (table **1.1**). These mostly consist of 5- and 6-membered sugars from agricultural residues, cellulose, and hemicellulose from plant biomass. The most easily obtainable of these is glucose, prepared from the hydrolysis of polysaccharides. It is therefore the most researched, and the source of the most platform molecules from bio- and catalytic processes. However other 6-membered sugars such as mannose and galactose, and 5-membered sugars such as ribose and xylose are used either alone or in combination with glucose as precursors for value-added compounds with shorter carbon chain lengths. In 2004, the US department of energy released a list of the top-ten value added compounds obtainable from the resultant monosaccharides, judged based on a number of criteria, as a goal for biorefinery catalysis research.[15] One of the most published examples within the top-ten is hydroxymethylfurfural (HMF), which earned its place in the top-ten based on its potential as a platform molecule for other 5-membered heterocycles and levulinic acid.[16] HMF can be synthesized using 6-membered sugars, however the 5-membered fructose is by far the most utilized precursor. Dehydration of the ring-bound hydroxyl groups yields the olefin groups within the heterocycle; this is performed using an acid catalyst, usually HCl or H_2SO_4. Further research is dedicated to producing HMF in different reaction media.
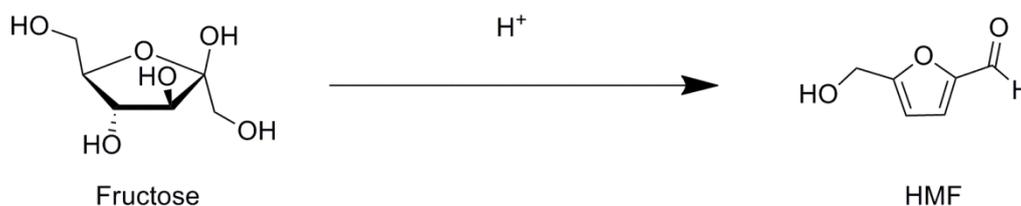
Scheme 1.2 Conversion of fructose to HMF via acid catalysis

Vegetable oils and fats are composed of long complex tri-esters of glycerol. Glycerol appears on the top-ten list as a precursor for a number of high-value three-carbon (C3) and two-carbon (C2) building blocks.[17] One fruitful example of a glycerol conversion process is hydrogenolysis, which yields a series of industry related polyols, ketones and aldehydes. 1,2-propane diol (used for polyester synthesis) can be selectively yielded using a number of heterogeneous catalysts based on copper and nickel.
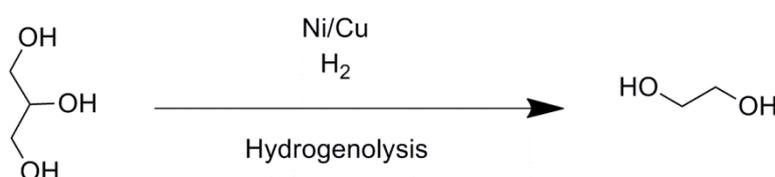
Scheme 1.3 Hydrogenolysis of glycerol into ethylene glycol

Lignin obtained from lignocellulosic biomass is a heterogeneous biopolymer consisting of aromatic functionality joined together by aryl and benzyl ethers and C–C bonds. Lignin has no defined structure, meaning that there are many different bonding arrangements depending on the plant from which it is derived.[18] The complex amorphous structure of lignin makes it a challenging substrate for biorefinery, due to its sparse solubility in common solvents and inert chemical linkages. It is however the only naturally abundant source of aromatic moieties, making it a very desirable candidate for the production of phenols and benzenes. Chemical conversion of lignin to produce value-added chemicals is still a field very much in its infancy, however a number of examples exist of defined products from chemical treatment.[19] The earliest example is that of vanillin, which is produced on industrial scale by the paper industry; oxidation processes using copper or cobalt catalysts produce vanillin from lignin by means of oxidative cleavage.[20] Research is currently ongoing to produce catalysts capable of selective depolymerization of lignin, mainly aimed at hydrogenolytic cleavage of aryl ether linkages.[21] However catalysts that are selective, active, and robust enough to cope with the sulfur present in commercial sources of Kraft® lignin are still one of the many barriers that need to be crossed before catalytic lignin depolymerization is efficient enough for industrial scale.

The final primary chemical building-blocks of interest are amino acids, derived from proteins.. Amino acids are mostly used in pharmaceutical research and the food industry, particularly in supplements and sweeteners (aspartame).[22] Most naturally-occurring amino acids are produced by fermentation processes on the industry scale, mainly from large-scale crops such as corn and beans.[23] However a number of alternative examples have been drawn to light in the interest of sustainability and utilization of waste: seafood shells were the focal point of a recent Nature comments article, a naturally abundant source of proteins, chitin, and various other minerals.[24]

1.1.3 Principle 9: Sustainable Catalysis

The central principle of sustainability within catalysis comes from the use of catalysts in reactions rather than using stoichiometric or an excess of reagent, or excessive heat. This allows the process to become more efficient, and save energy that would otherwise be required to push a reaction towards the desired products. The properties of the catalyst also play a role in the sustainability of a process (table **1.2**), and can be tuned depending on the reaction.

For example, heterogeneous catalysts are inherently separate from the reaction medium; this allows the catalyst to be easily separated from the products, and makes for simple facilitation of recycling and suitability for flow systems. However heterogeneous catalysts often require much higher temperatures than their homogeneous alternatives, since adsorption to the active site must occur, which is not required when the catalyst is within the same medium as the substrate. Furthermore the selectivity of heterogeneous processes is often inferior to that of homogeneous processes. Homogeneous catalysts are typically more selective, since they do not require such high temperatures; and the possibility of coordinating tunable ligands make them easily adaptable to a particular reaction.[25]

	Homogeneous catalysis	Heterogeneous catalysis
Activity (relative to metal content)	High	Variable
Selectivity	High	Varible (typically low)
Reaction conditions	Mild	Harsh
Service life of catalysts	Variable (typically short)	Long
Sensitivity toward catalyst poisons	Low	High
Diffusion problems	None	Can be important
Catalyst recycling	Expensive	Not necessary
Variability of steric and electronic properties of catalysts	Possible	Not possible
Mechanistic understanding	Plausible under certain conditions	More or less impossible

Table 1.2 Comparison of heterogeneous vs homogeneous catalytic methods[25]

Another consideration lies in the choice of metal for metal-based catalysts. Typically the most active metals are within periods 5 and 6 of the periodic table, for example palladium, for use within C–C cross coupling. Whilst these metals are very active, and only extraordinarily small amounts of catalyst need to be used, they are precious metals and thus not abundant in the Earth's crust; therefore not particularly suitable for large-scale production. However using nickel for the same process is much more sustainable in terms of element availability, however much higher catalyst loadings and higher temperatures are typically required to produce the same degree of reactivity.[26] A great deal of catalysis research is directed towards optimizing more abundant transition metal systems into catalysts which are competitive with the rarer d-block metals.

1.1.4   Principles 3 and 5: Aqueous-phase Organic Synthesis

Solvents are among the main discussion topics when considering green chemistry, since they are used in large quantities in both academic research and industrial chemistry. The FDA (Food and Drug Administration) issued guidelines for the use of solvent within the pharmaceutical industry, categorizing solvents into four different classes.[27] Pfizer were among the first to adhere to this, eventually issuing their own solvent selection guide based on the FDA guidelines.[28] In each case the preferred solvents are non-toxic, non-volatile, and obtainable from renewable resources. Water is sometimes regarded as the "holy grail" within these guidelines, owing to its inert, safe, non-flammable nature, its high heat capacity, and its abundance on the planet.[25] Water was long regarded as unsuitable for organic synthesis since most organic substrates are insoluble or immiscible in water, however early examples of known reactions performed in water were actually accelerated compared to their performance in organic solvents. A pioneering example was performed by Breslow *et al* for a Diels-Alder cycloaddition between cyclopentadiene and methyl acrylate (figure **1.2**).[29] Initially this high performance was simply linked to a mutual repulsion of the reagents by the water, thereby increasing the chance of the reagents coming together.[30] However several contributions were postulated to contribute to this effect. The cohesive tension of water was assumed to have a "cohesive pressure" effect on the reaction, particularly significant for Diels-Alder reactions which accelerate under traditional external pressure.[31] Another contribution was alleged to be the overall gain in entropy, since water molecules are released into the surrounding medium upon forming one product from two reactants. However as the literature expanded on this topic, it became clear that the hydrophobic effect accelerated more organic syntheses than simply the "two-reactants one-product" model of the Diels-Alder reaction. The factor which is now assumed contributes the most to the acceleration of organic synthesis in water is hydrogen bonding, suggested by theoretical Monte-Carlo simulations.[32] The clathrate cages produced by hydrogen bonding are

seen to destabilize the initial and transition states, encouraging product formation entropically. Since the reactants are not dissolved, this type of reaction is assumed to be biphasic; the term "on-water" was coined by Sharpless to distinguish the difference between reactions where some or all of the reagents are dissolved in water (in-water).[33]
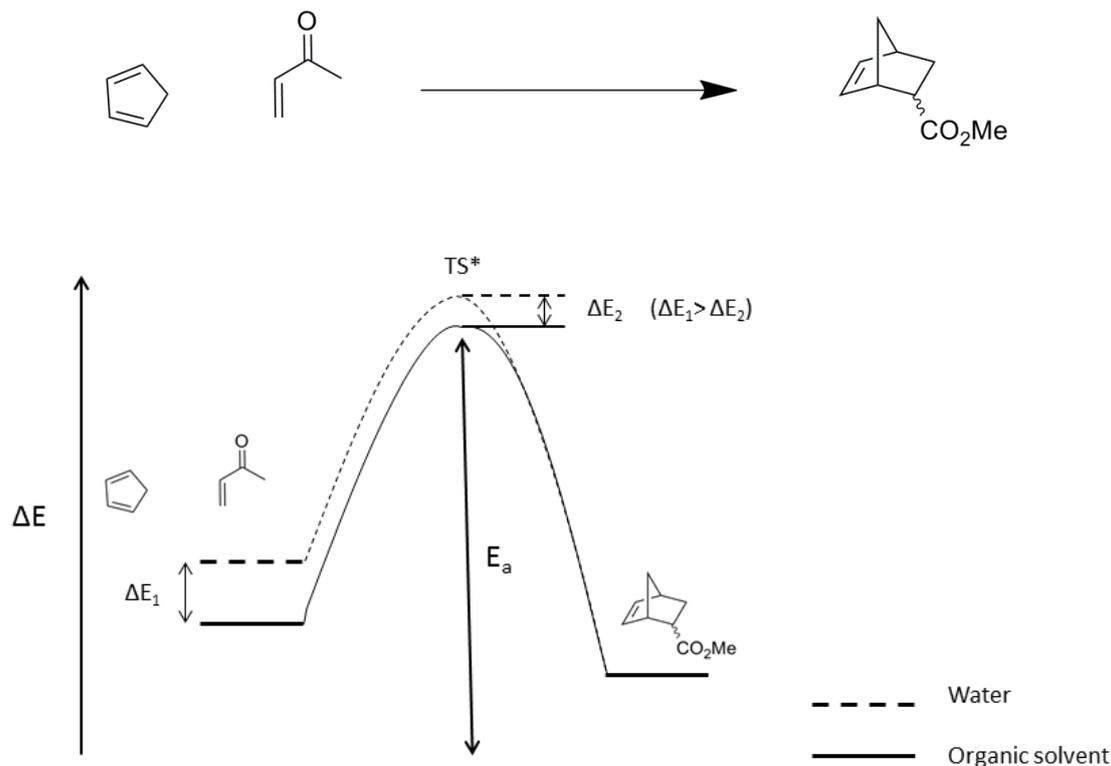

Figure 1.2 Reaction scheme and reaction coordinate profile of the Diels-Alder cycloaddition between cyclopentadiene and methyl acrylate in water and organic solvent

As well as purely organic and organocatalytic reactions, transition metal-catalyzed reactions in aqueous phase have also seen a surge in research popularity. Aqueous-phase transition metal catalysis poses a great number of advantages over common organic solvents; the most significant of which is the separation of products from the catalyst and subsequent catalyst recycling, which is very difficult in a monophasic system. As with organic systems, water was ignored by metal researchers. Its properties as a neutral ligand for first-row transition metals, and the history of moisture-sensitivity within organometallic complexes initially painted the picture of water being a nuisance. However a number of complexes were determined to be stable in water as a medium.[34] Water solubility of the catalyst is desirable for recycling; since the catalytic layer and the substrate layer are immiscible, this allows for simple separation and re-use of the aqueous layer. The most common way of inducing water solubility is by the coordination of water-soluble ligands.[35] Typically introduced water-soluble moieties are

sulfonate, carboxylate or ammonium ionic groups. The first, and to date most common class of water-soluble ligands are phosphines: Chatt reported the mono-sulfonation of triphenylphosphine to produce *m*-TPPMS,[36] and Kuntz later reported its tri-sulfonated derivative *m*-TPPTS.[37] These were subsequently used *in situ* with palladium and rhodium to perform C–C cross coupling reactions in aqueous phase with good success (scheme **1.4**);[38, 39] the rhodium example was taken on by industry for the production of butyraldehyde.[40] Since then, a monumental increase in publications relating to water-soluble ligands and complexes has come forth. The most successful ligands include (but are not limited to) phosphines and *N*-heterocyclic carbenes, as a result of their strong non-labile coordination to metals, preventing metal leaching into the organic layer. Metal catalyzed reactions performed in aqueous media include Pd, Rh and Ir catalyzed cross-coupling, Ru and Rh catalyzed metathesis, Ir catalyzed hydrogenation, Cu catalyzed "click" chemistry, and perhaps most remarkably, Pd catalyzed C–H activation.[35, 41-43]
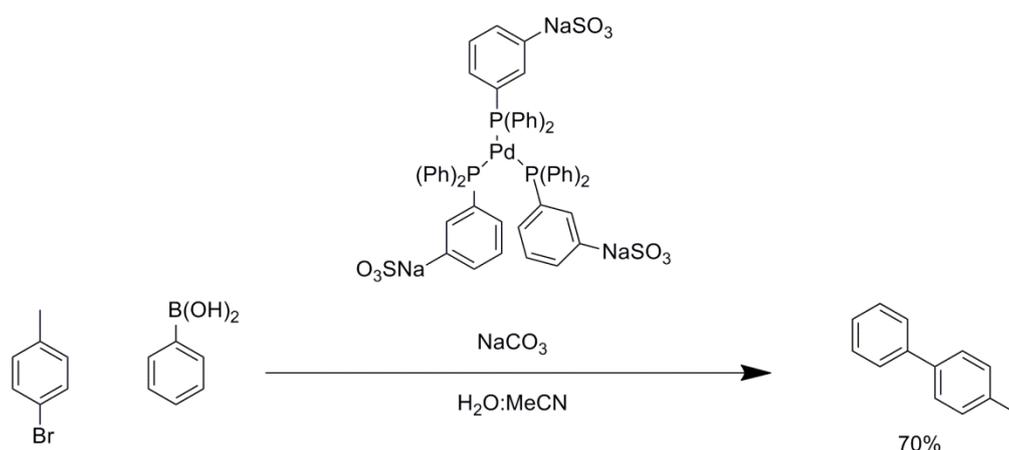
Scheme 1.4 Biphasic Suzuki-Miyaura coupling of 4-bromotoluene with phenylboronic acid using *m*-TPPTS$_3$Pd(0) as a catalyst [38]

Since the reaction is biphasic, the mechanism of interaction with the catalytic water layer can be described in a number of different fashions. Four different interaction models were proposed by Shaughnessy (figure **1.3**).[35] The first is the reaction in bulk water, assuming that reactant can be sparingly soluble in the water layer (A). The second is reaction in a surfactant-supported micelle, assuming a surfactant, supramolecular structure, or surfactant-like catalyst such as a polymer supported catalyst is involved (B). The third is reaction at the interface, assuming the catalyst can exist at the interface between the two phases(C). Finally the fourth is a solvent-switchable catalyst system, assuming the catalyst can exist in both phases (D). The interaction largely depends on the nature of the catalyst and substrates, as well as any additives.
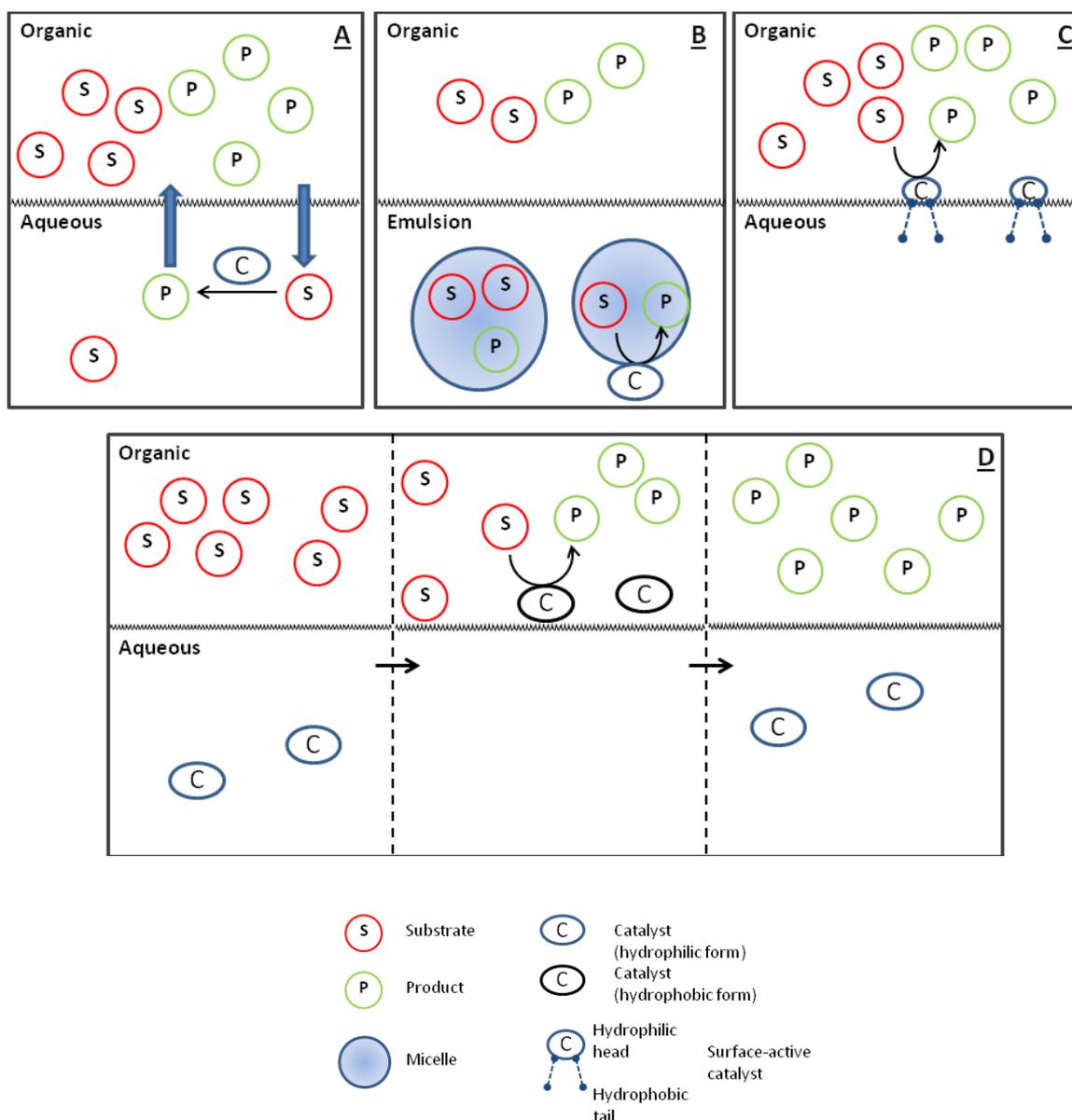
Figure 1.3 Mechanisms of interaction of a homogeneous organic reaction in water with a water-soluble catalyst[35]

An important factor to keep in mind with aqueous-phase organic synthesis is the environmental impact that may result from industrialization of this idea. Whilst water is indeed sustainable and environmentally friendly, contamination of water with organics and inorganics presents a hazard to ecosystems. Organic contaminations are notoriously hard to remove from water even through high-energy purification techniques such as distillation. Potential methods of contamination removal could be found through the use of porous membranes or carbon and silica materials. However this begs the question of whether the whole process is indeed green if such techniques are required, due to the energy and material costs. When considering water as a reaction medium for industry, the catalyst must be as recyclable as possible, and a full assessment of waste water streams must be performed before scaling up.[44]

1.2   *N*-Heterocyclic carbenes

1.2.1   Discovery and development

N-Heterocyclic carbenes (NHCs) are a class of carbene – centred on an sp^2–hybridised carbon atom residing between two heteroatomic species, at least one of which is nitrogen, within a ring structure. A huge number of known NHC structures exist within the literature combining many different heteroatom combinations and ring sizes; however the most common precursor structures are imidazolium and imidazolinium 5-membered rings with two amino groups, between which lies the carbenic carbon.[45] NHCs were initially discovered as ligands within transition metal complexes. Based on the initial reports of Wanzlick, metal-NHC complexes were synthesized and characterized independently by Ölefe and Wanzlick,[46, 47] respectively for a mono-NHC chromium complex and a bis-NHC mercury complex. Both syntheses involved direct metallation from its respective imidazolium salt. After this discovery, great interest was sparked in synthesizing stable free-NHCs (scheme **1.5**), a goal which was eventually achieved by Arduengo in 1991 with his adamantyl-substituted imidazol-2-ylidine species (IAd), which was isolable and stable in inert atmosphere.[48]

Scheme 1.5 Formation of a free NHC from an imidazolium cation

This opened up a field of research dedicated to the synthesis and application of an enormous library of NHC structures (figure **1.4**). The greatest potential of these species has been realized within the field of catalysis. Since the foundation work by Breslow,[49] NHCs have been widely applied as organocatalysts; mostly for the generation of reverse-polarity or Umpolung intermediates of acyl groups. This field is now largely dominated by triazolylidine species, after initial work at BASF suggested triazolium salts were better suited for selectivity and stability than imidazolium salts.[50] The most recognized application for NHCs is the use of NHC-metal complexes in catalysis. After the initial work performed by Herrmann recognizing their potential as spectator ligands (ligands which do not actively participate in the catalytic cycle) for Pd-catalyzed Heck couplings;[51] a bulk of work was produced hailing NHCs as competitors for hugely popular phosphine ligands within a number of different metal complexes. Possibly the most notable example is the 2nd generation Grubbs catalyst, a ruthenium complex featuring the now-commercial imidazolinydine ligand SIMes (figure **1.5**).[52] This complex was seen to be far more active and stable than its phosphine counterpart, and became part of the bulk of work for which Grubbs shared the Nobel Prize with Schrock and Chauvin in 2005. Since these achievements, a

number of imidazolium and imidazolinium-based structures became commonly used, and are now commercially available.
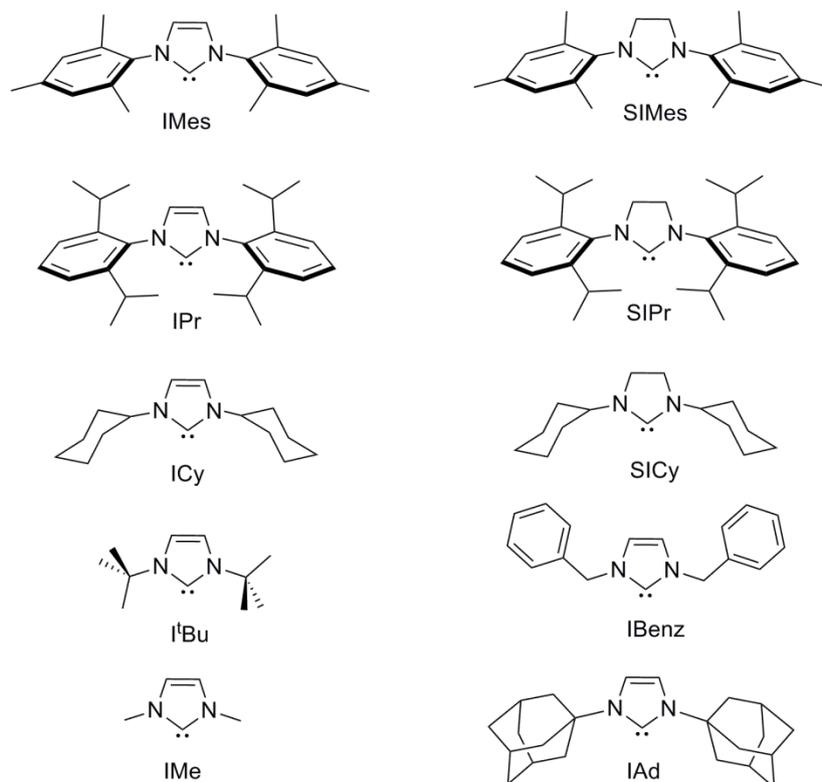

Figure 1.4 Skeletal diagrams of common NHC structures
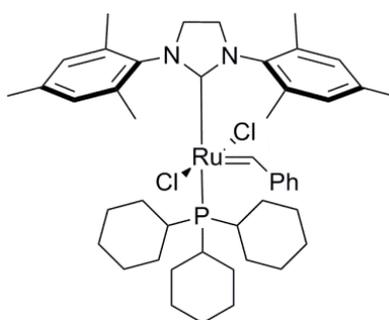
Figure 1.5 Skeletal diagram of the Grubbs 2nd generation ruthenium NHC catalyst [52]

1.2.2 Electronic structure

Carbene species (in general) are either sp or sp^2 hybridised, depending on this hybridization, the species adopts either a linear (for sp) or bent (for sp^2) geometry.[53] The two degenerate non-bonding p-orbitals within an sp-hybridized carbon atom house one electron of the carbene electron pair in each orbital. These two electrons are able to have the same spin state since they occupy different orbitals; therefore the electron pair in linear carbenes exist in a triplet state (figure **1.6**).[54] For sp^2-hybridized carbon atoms, orbital degeneracy is no longer present,

meaning that the p_x orbital develops s-character, becoming a σ-orbital. Within this orbital structure, the electron pair can occupy the σ-orbital, the p_π-orbital, or a combination of both with aligned or opposite spin states. Therefore bent carbenes can have both singlet and triplet multiplicity (figure **1.7**). The multiplicity of the carbene depends on the energy difference between the p_π and σ-orbitals, which can be influenced by the substituents located α to the carbenic carbon.[54]
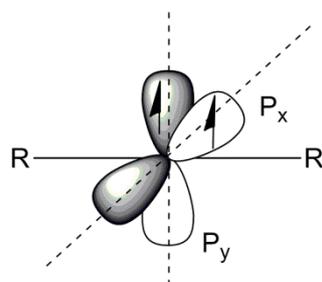

Figure 1.6 Orbital diagram of a linear carbene with filled P_x and P_y orbitals. The electron spins are aligned in triplet state
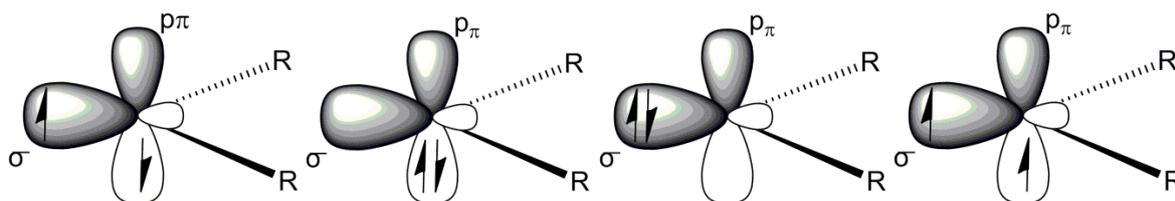

Figure 1.7 Orbital diagram of each possible electron and spin state arrangement within a bent carbene. All are aligned in singlet states aside from the far right, which is in a triplet state

The electronic contribution of the α-substituents can be characterized by two different components: the inductive (I) effect and the mesomeric (M) effect. The inductive effect simply pertains to the polarization of a bond by withdrawing electron density towards the more electronegative element. The mesomeric effect (or resonance effect) describes the movement of π-electron density within a conjugated system.

Within NHCs, the two α-substituents are often both nitrogen atoms, which produce a combined -I and +M effect throughout the planar N–C–N system (figure **1.9**).[54] This effect, combined with the confined ring forcing the bent N–C–N angle between 100-110°, means that NHCs are always bent in geometry with singlet multiplicity of the carbene lone pair. The imidazolium backbone is also reported to have an influence on the -I effect. More examples exist of stable free-NHCs derived from imidazolium salts as opposed to imidazolinium, this is attributed to the double-bond within the backbone contributing to electron withdrawing ability through aromaticity.[55]

Likewise, NHCs which feature electron-withdrawing substituents on the imidazolium backbone display remarkable stability. The dichloro-substituted 1,3-dimesitylimidazol-2-ylidene (IMe) synthesized by Arduengo *et al* was the first documented free carbene to actually be stable *in air* for limited exposure times.[56]
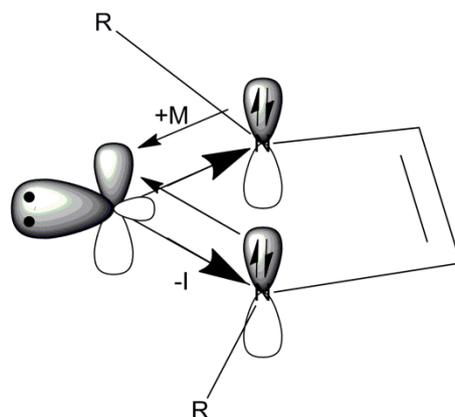

Figure 1.9 Illustration of the combined -I and +M effects within an NHC

Additionally to electronics, sterics were also regarded to play a role in the stabilization of the carbenic lone pair. This is derived from the observation made by Lough *et al* that *N*-substituents featuring bulky, sterically demanding groups are less susceptible to dimerization than those with less bulky groups.[57] However a good number of non-bulky free NHCs have been synthesized,[58] thus steric effects are now largely regarded to be unimportant.

1.2.3   NHC–Metal complexes

1.2.3.1   Bonding properties

For traditional carbene–metal bonding, carbene-containing complexes are classified as either Fischer-type or Schrock-type carbenes, depending on the nature of the interaction. Fischer-type carbenes are often found bound to low-oxidation state metals, and feature an α-substituent capable of donating a lone pair of electrons. Donation of electron density into the p_{π} orbital (LUMO) increases the orbitals' energy with respect to that of the metal d orbitals, therefore the π-electron density along the M–C bond is more concentrated around the metal. Schrock carbenes on the other hand are often found bound to metals of a higher oxidation state, and feature α-substituents incapable of donating mesomeric electron density. As a result, the carbenic p_{π} orbital is lower in energy with respect to the metal d orbitals; therefore π-electron density can be polarized towards the carbene carbon, making it nucleophilic.

For many years after their discovery as ligands, it was assumed that NHCs were simply σ-donors.[59] The NHC–M bond is a 2-electron (L) type donation, with single-bond character, much

more akin to Fischer carbenes as opposed to Schrock carbenes, which is the reason that the NHC–M bond is usually denoted with a single bond in skeletal diagrams. However in time it was revealed that σ-donation does not complete the full story of the bond nature (figure **1.10**). Numerous reports contributed evidence to suggest NHCs were capable of π-back donation from the metal d orbitals into the carbenic carbon π* orbital,[60] [61] [62] although the degree of π-back donation is minimal in most cases. This is a result of the +M effect of the nitrogen atoms to the carbenic carbon p_π-orbital (LUMO), thereby raising it above the level of the metal d-orbitals. The final contribution to NHC–M bonding is the π-bonding capability, which is donated from the nitrogen lone pairs; this was recognized only in recent years.[63] [64]
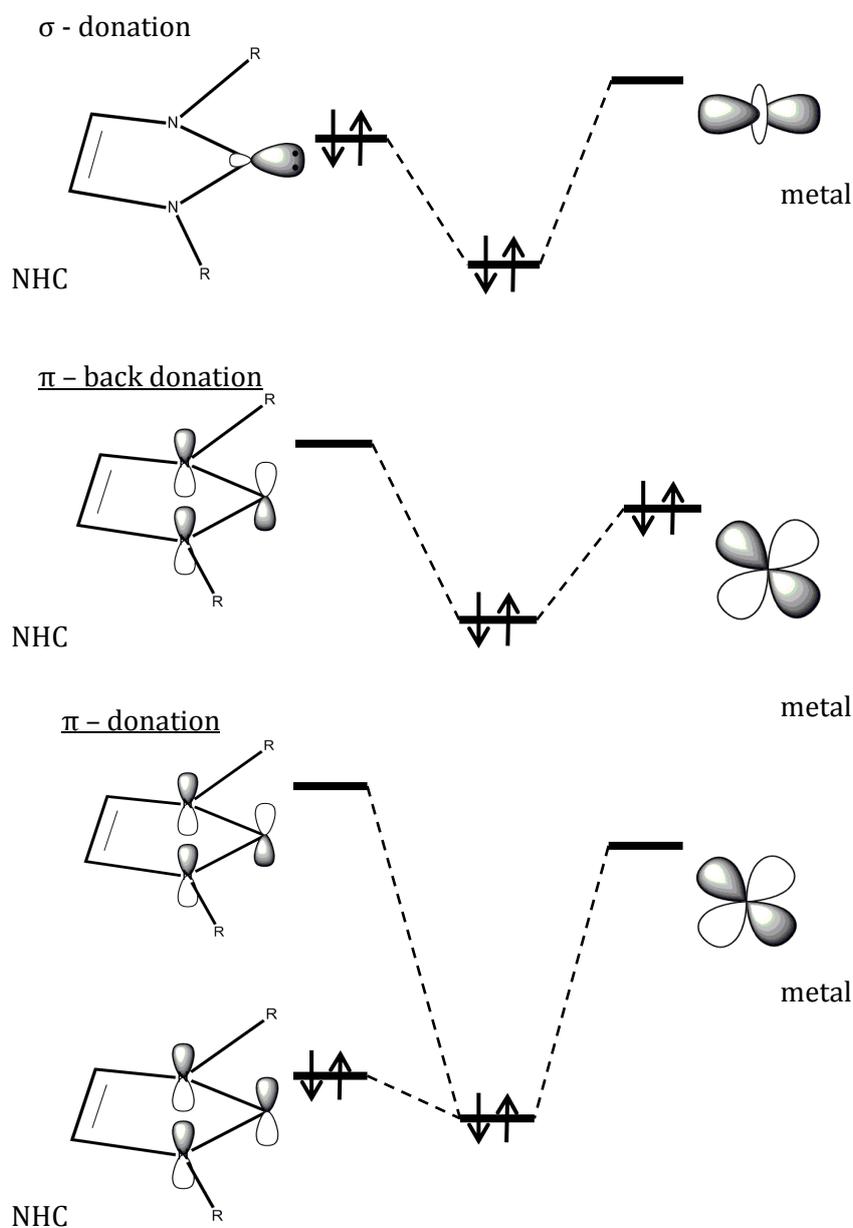

Figure 1.10 Orbital diagrams of the different types of NHC–M bonding modes and their relative orbital energy levels

The major advantage of NHCs as ligands is that each of the different bonding properties can be tuned by modifying the structure of the NHC precursor. For example, electron-withdrawing substituents on the imidazolium backbone are known to increase the ability of the complex to π-back donate;[65] [56] [66] this can contribute to the weakening of σ-donation ability. Despite the stability difference observed in free carbenes, no significant difference in ligand properties is observed between imidazolium and imidazolinium-derived NHCs, showing that the olefin backbone does not contribute significantly to the electronic properties of the bound ligand.[67] Likewise *N*-bound substituents also provide very little difference in electronic character to the bound ligand;[68] however the contribution of *N*-bound substituents to the ligand's steric character is significantly altered.[69] The combination of the ligand's steric and electronic properties contributes a significant difference to the catalytic activity of the resulting complex.

1.2.3.2   Synthesis methods

A diverse number of methods have been developed for the synthesis of NHC-metal complexes. The three most commonly applied methods are: *in-situ* deprotonation followed by metallation, complexation from a free NHC, and transmetallation from an NHC–Ag precursor.

The first method was that utilized by Wanzlick for his synthesis of a bis-NHC mercury complex (scheme **1.6**).[47] Hg(OAc)$_2$ was used as the only other reagent aside from the imidazolium precursor, meaning that deprotonation of the C2 position could be performed simply using the basic metal counter-anion, in this case acetate. This can be performed using a library of different basic metal precursors such as actetates, oxides, amides, or alkoxides. It was later discovered that less-basic metal precursors could also be used in the presence of an additional base. [70] As a result of the high pK$_a$ of the imidazolium C2–H, it was often considered that only strong bases such as *t*-BuOK could be used in the same fashion as the free-carbene synthesis. However weaker bases such as K$_2$CO$_3$ and NEt$_3$ can also be used, provided that species with a lower pK$_a$ are not present.
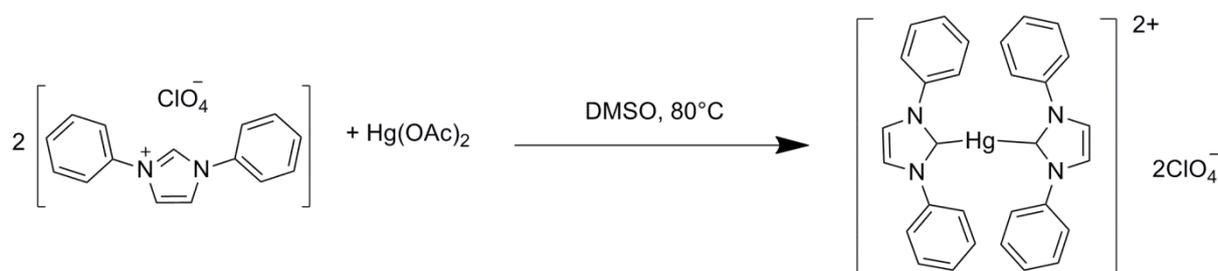

Scheme 1.6 The first discovered NHC complex synthesized by *in situ* metallation. As reported by Wanzlick *et al*[47]

Free-NHC complexation is often described as the best method, since it produces the best yields. However since it involves synthesis and isolation of a free-NHC, the procedure is complicated and requires very thorough use of inert gases and Schlenk techniques, and is not feasible for many NHC precursors. The typical method of free NHC synthesis involves deprotonation with a strong base; usually stoichiometric NaH in THF solvent at low temperatures (scheme **1.7**).[48] Once formed, the carbene is incredibly nucleophilic; the dry metal precursor is added under inert gas and forms the complex immediately.
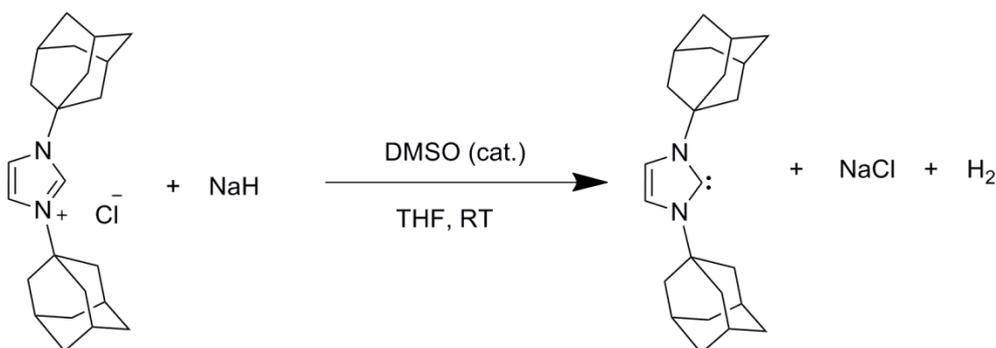
Scheme 1.7 The first synthesis of a free NHC IAd. Reported by Arduengo *et al* [48]

The most versatile method is arguably the silver-transmetallation method. Silver oxides are inherently very basic, and so insert into the C–H bond without the use of additional base, producing silver halides as by-products. Ag–NHC complexes are often air and light-sensitive due to the relative weakness of the Ag–C bond; however this works well for transmetallation, since formation of another NHC–M bond is thermodynamically favorable, alongside the precipitation of the silver halide by-product. This method was first described by Lin *et al* in 1998, where isolated Ag–NHC complexes derived from benzimidazolium precursors were transmetallated onto Pd and Au precursors (scheme **1.8**). [71]
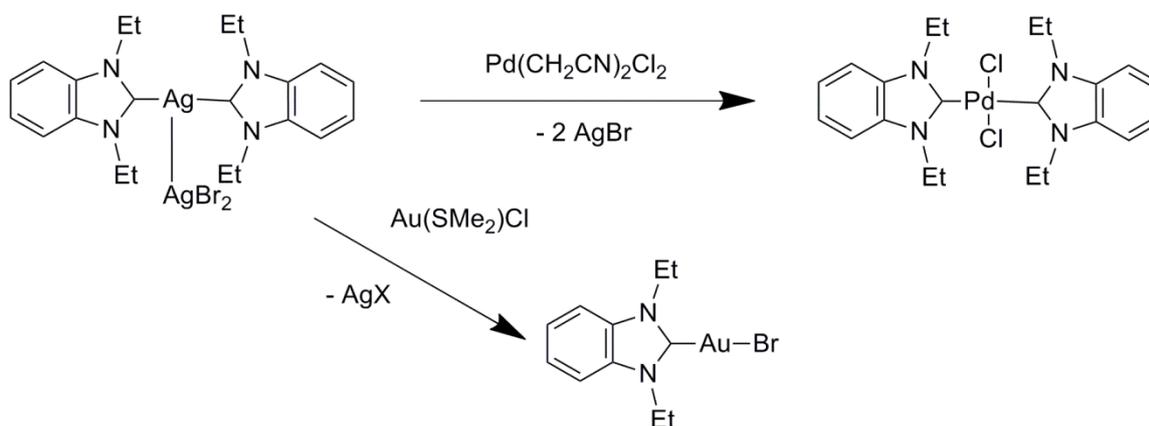
**Scheme 1.8** The first reported transmetallation of an Ag–NHC complex by Lin *et al* [71]

Aside from these methods, many other novel complex synthesis methods have been described. Early examples include oxidative-addition into C–X bonds, [72] and insertion into NHC C=C dimers (often known as the Lappert method). [73] This follows on to modern sophisticated methods including electrochemical syntheses,[74] thermal elimination of a C2 protecting group,[75] templated synthesis from metal-isonitrile complexes,[76] and even direct oxidation of metal powders.[77] A number of these methods are often used in current NHC-complex research. Promising examples include the electrochemical synthesis initially reported by Chen *et al* and further developed by Willans *et al* for the synthesis of first-row transition metal complexes,[74 78] with ongoing research in the development of flow-reactor synthesis. Another is that of Waymouth and Hedrick: thermolysis of C2-protected groups, in particular pentafluorobenzene, has been shown to produce free-NHCs at moderate temperatures, even for particularly unreactive NHC precursors.[79]

### 1.2.4   Water-soluble NHC complexes

Following on from the development of water-soluble phosphine ligands for inducing metal complex water-solubility, the next logical step was the use of water-soluble NHCs to induce water solubility. NHCs pose a huge advantage in this field due to their robust nature, strong bond formation with metal complexes, and their extensive opportunities for simple functionalization. Water-soluble NHC complexes are almost always researched for their application in aqueous-phase catalysis, however a number of reports have also reported their use in anti-cancer and anti-bacterial applications. The most common water-soluble moieties introduced onto NHCs are sulfonates, carboxylates, amine/ammonium groups and alcohols and ethers. Water-soluble polymer- and macrocycle-supported NHC complexes are also commonly researched for their catalytic applications in water. Polyethylene glycol (PEG) as well as many other polyethers and polyesters have been attached to NHC backbones in order to induce solubility. [35 42 80]

The bulk of research is based on sulfonate-functionalized NHCs, this owes to their unparalleled water-solubility, stability, and non-coordinating behavior preventing the formation of by-products and coordination polymers. NHC precursors featuring alkylsulfonate groups are typically synthesized using a sodium or potassium salt of a haloalkylsulfonate substituted onto an imidazole, or alkylation by cleavage of a sultone (cyclic sulfonate ester); zwitterions are typically formed. Examples of such precursors were initially introduced by Shaughnessy, and subsequently used to produced bis–Ag–NHC complexes; the charged sulfonate becomes a counterion for the Ag(I) ion (scheme **1.9**).[81] Transmetallation of these complex-types to Au was reported by Joò, yielding both mono and bis–NHC complexes.[82] Similarly, direct metallation to Pd was described within the Shaughnessy report using *t*-BuOK as a base;[81] highlighting the

stability of these precursors towards strong bases, and the stability of the complexes towards high temperatures. Arylsulfonates are also popular due to their similarity to current popular NHC structures. Plenio *et al* successfully synthesized sulfonated analogues of the popular IMes, SIMes and IPr precursors via traditional routes using sulfonated anilines,[83] and could directly sulfonate pre-synthesized precursor salts using chlorosulfonic acid in a following report (scheme **1.10**).[84] Likewise for the alkylated precursors, metallation was primarily achieved through transmetallation from silver. Although *in situ* generation of the free carbene was reported by Roy *et al* for the synthesis of Pd complexes.[84]
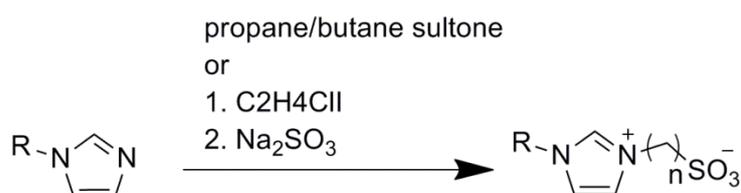

Scheme 1.9 Synthesis of alkylsulfonate NHC precursors by Shaughnessy *et al* [81]
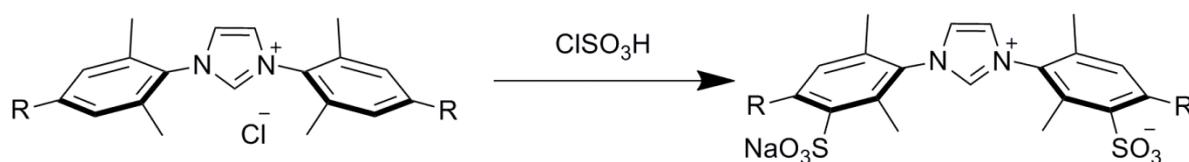
Scheme 1.10 Synthesis of arylsulfonate NHC precursors by Plenio *et al*[84]

Amine and ammonium groups are less common than sulfonate or carboxylate groups in NHC water solubility. The disadvantage of this route is that the amines are not often water soluble, so water solubility normally has to be introduced via a quaternization step to produce the ammonium, similar to that seen within ionic liquids. However ammonium species usually produce very good water solubility, and are often sensitive to pH; which can be a desirable strategy towards catalyst recycling. Özedemir was the first to report water-solubility via an ammonium-functionalized NHC.[85] Initially an imidazolinium dimer was synthesized, which was coordinated to rhodium and ruthenium via C=C insertion (Lappert's method). However water solubility was only induced after complexation via generation of a quaternary salt using HCl (scheme **1.11**). Another notable example is an IMes analogue introduced by Grubbs *et al* with a Boc-protected amine attached to the NHC backbone, rather than the *N*-bound groups. [86]
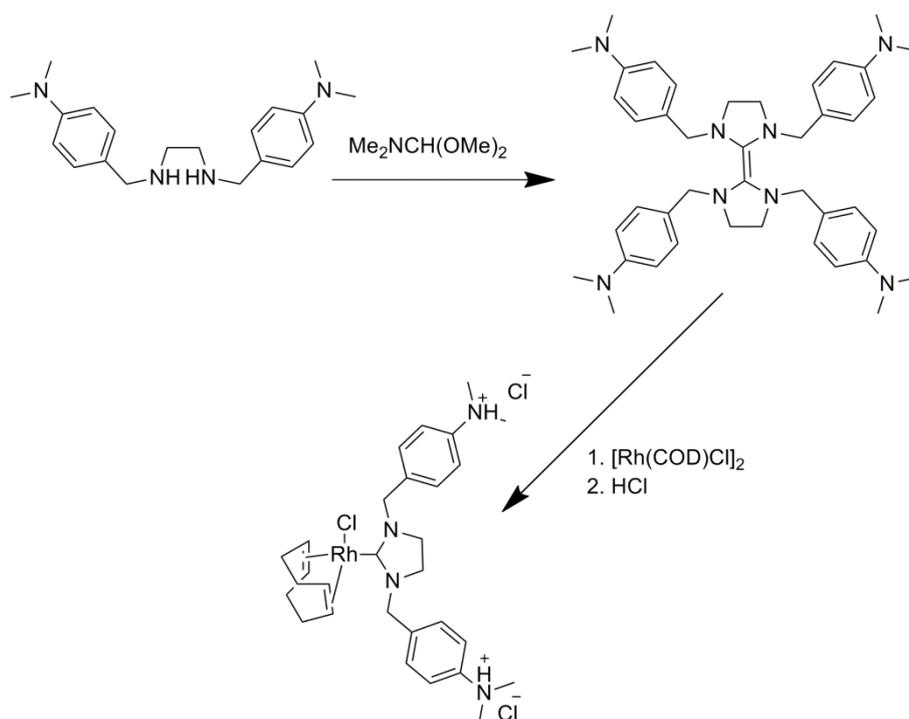
Scheme 1.11 Synthesis of an amine-functionalized NHC precursor, and subsequent metallation and quaternization into an ammonium-functionalized NHC–Rh complex, reported by Özedemir *et al*

Alcohol or ether functionalization is the least common of the four methods outlined here, since these groups are not as polar, so water solubility is often limited. A number of examples do exist, the first of which was a pyridyl-bridged tridentate ligand synthesized by Youngs *et al* featuring tethered alcohol groups (scheme **1.12**).[87] Metallation of these compounds is usually performed via Ag transmetallation or direct metallation; free carbenes have the capacity to form adducts with alcohols, and so this route has not been reported. Youngs' group was able to form Ag and Pd complexes using the aforementioned routes. Another notable example is a centipede-like coordination polymer produced by Karimi et al featuring *N*-bound groups functionalized by triethylene glycol.[88] The so-called Janus-type ligand has two opposite-facing C2 carbenic units, which allowed for the formation of a Pd coordination polymer with Pd(OAc)$_2$.
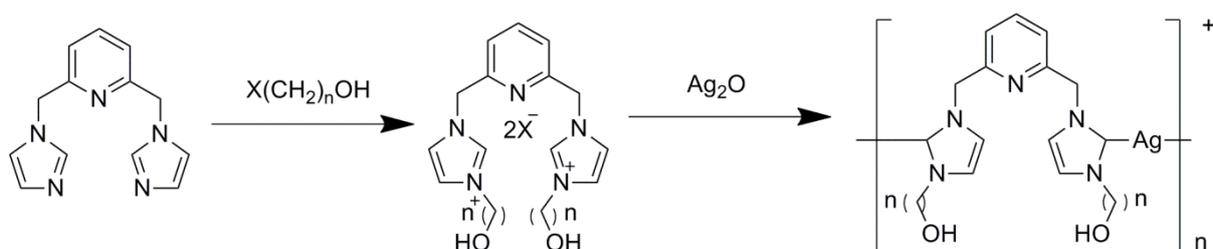
Scheme 1.12 Synthesis and Ag complexation of a tridentate chelating NHC precursor, featuring alcohol *N*-bound groups. Reported by Youngs *et al* [87]

Carboxylate-functionalized ligands are the final functional group used to induce water solubility. Whilst functionalization is simple, these groups can cause problems by giving unexpected coordination patterns, since carboxylic units have been reported to coordinate with metal centers. Since carboxylate-functionalized NHCs form an integral part of this work, examples of these types of NHCs and complexes will be further discussed in the second chapter

1.2.5 NHCs in nanoparticle stabilization

Metal nanoparticles are an increasingly important field, particularly within the area of catalysis. These "naked" metal particles, between 1 – 100 nm in size, are by definition heterogeneous; however the reactivity in terms of catalysis is often considered to walk the line between homogeneous and heterogeneous.[89] Whilst nanoparticles are very active species in catalysis, they are usually unstable in common solvents, preferring to agglomerate into bulk metal. Stabilizers and solid supports are typically employed to prevent agglomeration into an inactive species. Within solution, surfactants and supramolecular species are often employed to produce colloidal dispersions of nanoparticles; however the nature of this stabilization depends on the structure and characteristics of the stabilizer.

NHCs are increasingly employed as nanoparticle stabilizers. A number of accounts have been produced over the last decade reporting stabilization of nanoparticles species with addition of free NHCs or imidazolium salts. The first account of this behavior was reported in 2005 by Finke *et al*, whereby H/D exchange was observed within an imidazolium ionic liquid species in the presence of an iridium source.[90] This was followed up by an XPS investigation from Dupont *et al* in which two different binding energies for the C2 position was observed.[91] Since these investigations were performed on imidazolium ionic liquid species, this opened up a debate into the mechanism of nanoparticle stabilization with ionic liquids.

The nature of this supposed NHC interaction with nanoclusters and surfaces remained ambiguous until a pioneering study by Chaudret *et al* in which free NHCs were investigated under various conditions in the presence of an Ru(0) source (scheme **1.13**).[92] Solid state magic angle-spinning NMR (MAS-NMR) analysis on the colloidal dispersions revealed the presence of a carbenic C2 resonance in solid state; the location of the NHC coordination site could even be ascertained, revealing coordination on the edge sites of a hexagonal-close-packed nanoparticle. The stabilized nanoparticles were seen to be active in catalysis for the hydrogenation of arenes and olefins. Since this report, the characterization of nanoparticles within surface interactions has become much more sophisticated, and even modifications of surface-bound NHCs have been reported. Johnson *et al* reported coordination of NHCs on a gold monolayer supported on a

silicon wafer.[93] The *N*-bound groups of these NHCs were olefins, susceptible to ROMP (ring-opening metathesis polymerization) from a Grubbs generation II catalyst.
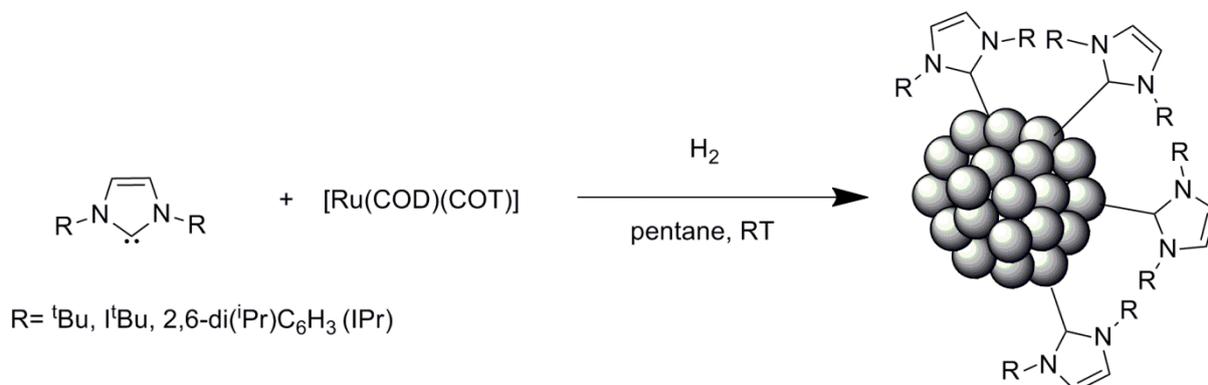
Scheme 1.13 Formation of Ru nanoparticles stabilized by NHCs bound to the surface. Reported by Chaudret *et al* [92]

The agglomeration of organometallic complexes into nanoparticles during catalysis is a common observation; however before these reports it was never considered that NHC–metal complexes could form stabilized nanoparticles with the NHC still coordinated to the surface. It is worth mentioning that bulkiness of an NHC is said to play a role in the prevention of agglomeration. Nanoparticle formation is typically undesirable within homogeneous catalysis, since the nanoparticles are either inactive or less active than the molecular species. Ligands such as IPr or IMes are said to sufficiently stabilize the molecular species as to prevent agglomeration, an attribute that may partially explain their success within NHC–metal catalysis.

1.3   Palladium-catalyzed cross-coupling

1.3.1   The Suzuki-Miyaura cross-coupling reaction

Cross-coupling reactions are carbon–carbon and carbon–heteroatom bond forming reactions which act as an irreplaceable tool in the toolbox of organic synthesis. Typically these reactions proceed by coupling an aryl or alkyl halide with a nucleophilic fragment, usually an organometallic or organoboron species. Since the idea of cross-coupling was first reported with Grignard reagents,[94] a lot of research throughout the late 20_{th} century was devoted to cross-coupling with organometallic species. Eventually it was discovered that palladium species could be used as catalysts for a number of different cross-coupling reactions. This was expanded to include organozinc,[95] organosilicon,[96] and organostannanes,[97] until eventually organoboranes were reported by Suzuki and Miyaura in 1979.[98] Palladium was also used earlier in the similar coupling reaction of alkenes and aryl halides by Mizoroki and Heck,[99] [100] which was later expanded to include alkynes by Sonogashira utilizing a Cu(I) co-catalyst.[101] Suzuki, Heck and

Negishi shared the Nobel Prize for chemistry in 2010 for their independent work involving palladium-catalyzed coupling reactions.

The Suzuki-Miyaura reaction is by far the most popular due to the availability of boronic acids, their stability towards moisture and base, and the relative non-toxicity of the by-products. The reaction proceeds based on a similar mechanism observed for all Pd-catalyzed cross-couplings (figure **1.11**). A Pd(0)/Pd(II) redox cycle allows the reaction to proceed in presence of a base: starting with a Pd(0) species, oxidative addition allows insertion of Pd into the C–X halide bond. This Pd(II) intermediate undergoes ligand exchange with the base, and that subsequent species undergoes transmetallation with the boron reagent to generate an organopalladium(II) intermediate. This intermediate then undergoes reductive elimination, forming the desired C–C bond and restoring the Pd(0) species.[102] [103] The base plays a number of roles in the reaction. The most significant include assisting transmetallation by formation of the more reactive palladium hydroxy or alkoxy intermediate, and assisting reductive elimination via the formation of a more nucleophilic boron species. [104]
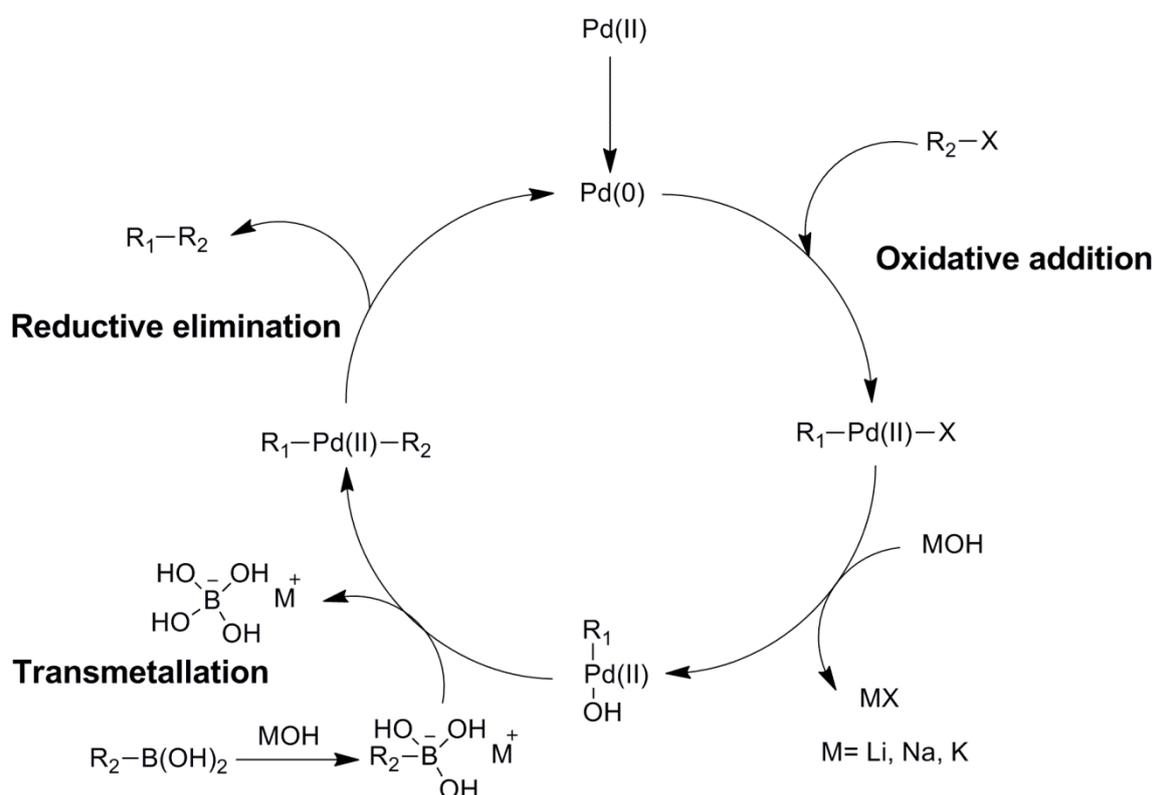

Figure 1.11 Catalytic cycle of the Suzuki-Miyaura cross-coupling reaction. Including generation of the Pd(0) active species from a Pd(II) precatalyst

1.3.2   Pd–NHC catalysts in the Suzuki-Miyaura reaction

The first example of an isolated Pd–NHC complex used as a catalyst for Suzuki-Miyaura couplings was published by Herrmann *et al* in 1995 (scheme **1.14**). [51] A bis-chelating NHC ligand Pd complex, and an analogous non-chelating *cis*–NHC Pd complex were tested for the coupling of aryl boronic acids with aryl chlorides and bromides. Both complexes could sufficiently activate the substrates. This was the first account which demonstrated NHCs as competitor spectator ligands to phosphines.
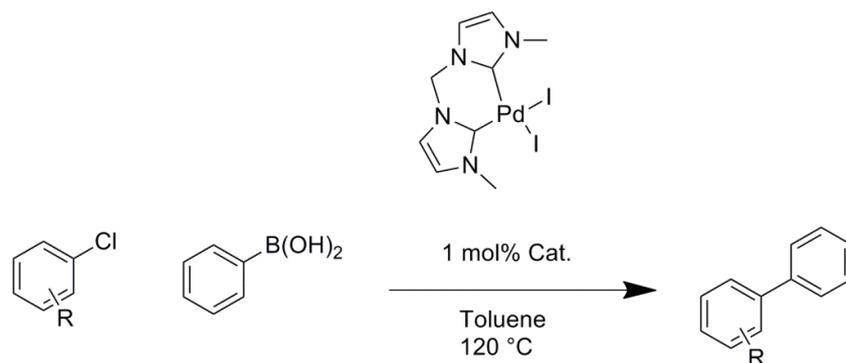

Scheme 1.14 First reported example of a Pd–NHC complex used as a catalyst for the Suzuki-Miyaura coupling [51]

This account lead to a surge in publications investigating NHCs in cross coupling catalysis, much of this was led by Nolan. An initial report in 1999 investigated the activity of the IMes imidazolium precursor (IMes.HCl) for the coupling of aryl chlorides using Pd$_2$(dba)$_3$ as palladium source for *in situ* catalyst generation (scheme **1.15**).[105] After the success of this report, a more detailed study in 2002 included optimization of conditions and investigation of a series of different imidazolium salts,[106] including: IPr.HCl, ICy.HCl and IAd.HCl. Major conclusions drawn were that IPr and IMes were vastly superior for coupling various aryl chloride substrates, and that a 1:1 ligand:metal ratio afforded a faster reaction rate. Following on from this result, an investigation into isolated bis-NHC–Pd complexes in comparison to *in situ* imidazolium salts was reported (scheme **1.16**).[107] Bis-IMes–Pd complexes of both traditional (C2–Pd bond) and abnormal (C4–Pd bond) geometry were synthesized and compared to the *in situ* IMes.HCl and Pd(OAc)$_2$ system for aryl chloride coupling. Bizarrely, the traditional geometry complex was completely inactive whilst the abnormal complex lead to catalytic activity. However the active complex was seen to be inferior compared to the *in situ* system with both 1:1 and 1:2 ligand:Pd(OAc)$_2$ ratios.
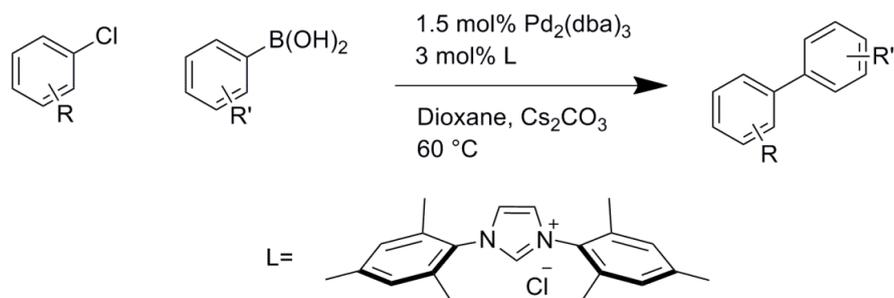
Scheme 1.15 Suzuki-Miyaura cross coupling catalyzed by *in situ* NHC ligand formation with Pd$_2$(dba)$_3$. Reported by Nolan *et al* [105]
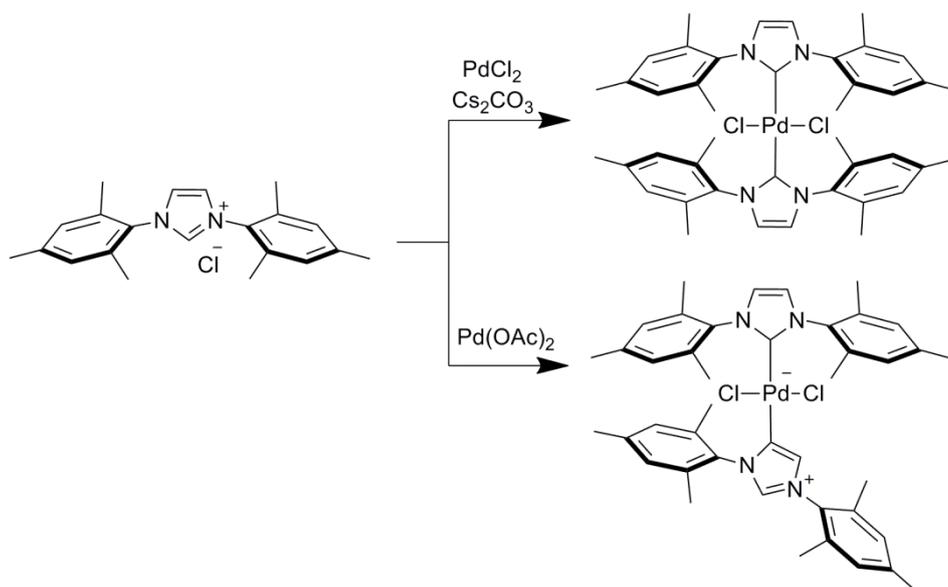
Scheme 1.16 Synthesis of normal and abnormal bis-NHC Pd(II)Cl$_2$ complexes for subsequent use in Suzuki couplings. Reported by Nolan *et al*[107]

New reports subsequently rose investigating novel structures for NHC precursors. Perhaps the most notable of these is the IBiox family of bisoxazoline-derived salts reported by Glorius *et al* (figure **1.12**).[108] These feature a tricylic system, in which the *N*-bound substituents are bonded to the imidazolium backbone by an ether linkage. The substituents have a restricted flexibility, which could contribute a great deal to the steric factor of the resulting NHC. The IBiox.HOTf salts were used *in situ* with Pd(OAc)$_2$ for Suzuki-Miyaura couplings of aryl chlorides. The precursors featuring longer chain lengths displayed better activity than their shorter-chain analogues, suggesting a greater steric influence. Whilst good activities were observed, this system suffers in terms of high catalyst loadings, expensive strong bases, anhydrous conditions and high temperatures.
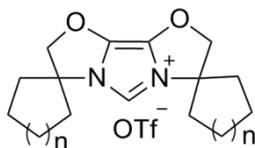
Figure 1.12 IBiox ligand family general structure. Reported by Glorius *et al[108]*

The discovery that bis-NHC–Pd complexes are largely inactive lead to the hypothesis that steric crowding may be hindering coordination of the substrates. A number of reports featuring mixed-ligand complexes were subsequently reported. Mixed NHC-phosphine complexes were among the first of these, produced by Herrmann *et al,* producing better yields than bis-NHC complexes.[109] NHC(allyl)Pd complexes were synthesized subsequently by Nolan *et al* (figure **1.13**).[110] It was ascertained that the mechanism of pre-activation involved the attack of the η^3-allyl ligand by the alkoxide base to produce an NHC–Pd(0) species (figure **1.14**).[111] These pre-catalysts were tested in catalytic screenings with remarkable activity and stability, with no deactivated palladium black observed. Aryl-substituted allyl ligands were found to produce the active catalyst more quickly and to stabilize the active catalyst, producing very good activity, and even activating aryl triflate moieties.[112] This discovery lead to the assumption that a sterically bulky NHC aids in reductive elimination, however including a labile co-ligand aids in the coordination of the substrates.
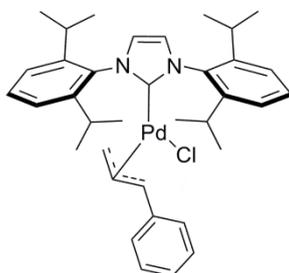
Figure 1.13 Skeletal diagram of a NHC(allyl)Pd complex used in catalysis by Nolan *et al* [112]
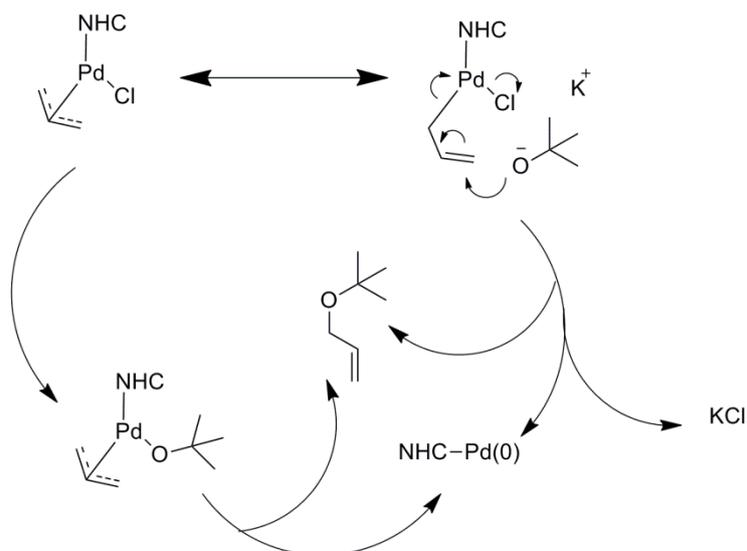
Figure 1.14 Activation pathway of the active catalyst from the NHC(allyl)Pd precatalyst.
Adapted from reference [112]

By far the most successful complexes to date for Pd–NHC catalyzed cross-couplings are the PEPPSI (pyridine-enhanced precatalyst preparation, stabilization and initiation) complexes reported by Organ *et al* (scheme **1.17**). [113] These utilize the labile ligand effect through coordination of a pyridine ligand *trans* to the NHC, which is easily activated by gentle heating in basic solution. Their popularity stems from simple synthesis and compatibility to a vast number of substrates, bases, and ambient atmosphere. Organ's initial publication reports high yields ofsubstrates with deactivated aryl rings using very low catalyst loading alongside hydroxide and carbonate bases. In line with the general trend observed for other NHC complexes; the more sterically demanding NHCs IMes and IPr produce better yields compared to less bulky NHCs.[114] In a later report, IPr was even proven to be capable of the solvent-free coupling of aryl chlorides in microwave conditions.[115]
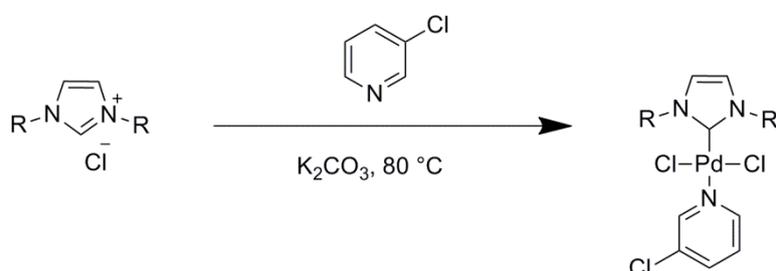
Scheme 1.17 General synthesis for Pd–NHC PEPPSI-type complexes. Reported by Organ *et al* [113]

1.3.3 Aqueous-phase Suzuki-Miyaura reaction

The benefits of water in Suzuki-Miyaura couplings have been reported extensively.[43, 116 117] This mainly pertains to the increase in activity, as a result of removal of salts and boronic by-products into the non-catalytic layer, pushing the equilibrium forward. However these accounts mainly utilize water as a co-solvent in biphasic medium, or as the reaction medium in hydrophobic "on-water" conditions with hydrophobic catalysts. Whilst these reports are not within the scope of this thesis, one particular account is worth mentioning. While the hydrophobicity of the substrates has been shown in many accounts to accelerate reaction rates in water, reactions which require inorganic bases are often hindered; since the base is water soluble, and the reagents only meet at the interface. In biphasic reactions, phase-transfer-catalysts (PTCs) are often utilized to aid with the shuttling of base between the two layers. Jeffery first demonstrated the role of tetraalkylammonium salts in a Heck reaction with $Pd(PPh_3)_4$ as catalyst.[118] Coupling yields were drastically improved using tetrabutylammonium chloride (TBAC) at lower temperatures. This was later extended to Suzuki reactions by Zhang *et al*, where aryl bromide coupling was improved using tetrabutylammonium bromide (TBAB) with microwave heating, producing full conversion within 10 minutes.[119] It was concluded that the surfactants added were acting as PTCs.

As stated previously, the utilization of hydrophilic complexes is desirable for catalyst recycling applications. C–C cross couplings are among the many catalytic processes that this philosophy has been applied to. The first water-soluble ligands to be used for Suzuki-Miyaura couplings were the sulfonated phosphine ligands. Casalnuovo *et al* reported the synthesis of a (*m*-TPPMS)$_3$Pd(0) complex and its application for Heck coupling.[38] Inspired by this, Genêt *et al* used *m*-TPPTS for *in situ* catalysis with $Pd(OAc)_2$ for coupling of aryl bromides with a 2.5 mol% catalyst loading.[120] The system was seen not to be active for aryl chlorides, which still remain as challenging substrates for aqueous-phase Suzuki-Miyaura couplings. Aside from sulfonated phosphines, various other hydrophilic groups have also been used in Heck couplings (figure **1.16**). Phosphonate and carboxylate phosphine ligands are among some of the more novel ideas, benefiting from a typically better water solubility than sulfonates. The *in situ* system using *p*-TPPMP (disodium 4-(diphenylphosphino)phenylphosphonate) (figure **1.16**) and $Pd(OAc)_2$ gave higher yields for Heck couplings of aryl iodides under microwave-irradiated conditions.[121] Likewise the *m*-TPPTC (trisodium tri(3-carboxyphenyl)phosphine) ligand gave slightly better yields for sulfonated systems under the same conditions. [122]
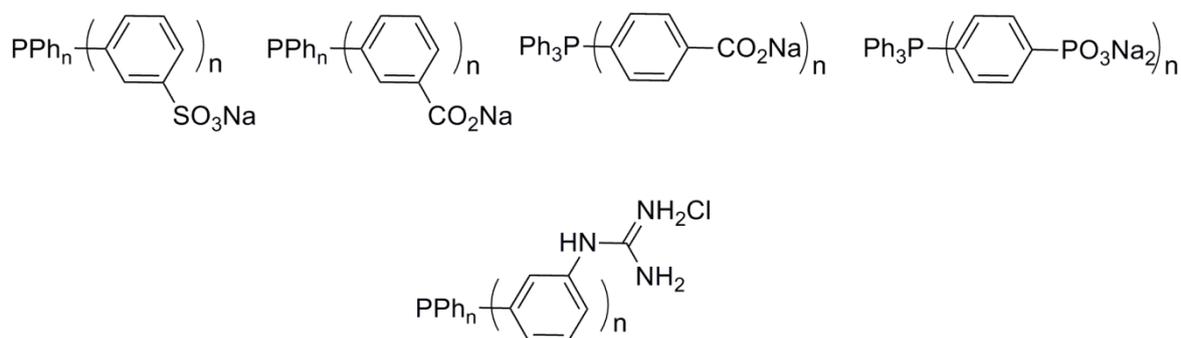
Figure 1.16 General structures of the sulfonate, carboxylate, phosphonate and guanadinium families of water-soluble phosphine ligands. Adapted from reference [123]

Other phosphine-based systems include ligands substituted with water-soluble biomolecules, including guanadine, glucose and glucosamine.[123] Beller's reports of the sugar-substituted phosphine ligands were reported to be very active for aryl bromide couplings in Suzuki reactions;[124] however the formation of glycosidic bond with the phosphine entity is inherently weak. Sterically-demanding phosphine ligands such as the sulfonated CataCXium F developed by Plenio *et al* were also used for *in situ* Suzuki catalysis (scheme **1.18**).[125] This ligand was able to catalyse aryl chloride couplings in water using Na_2PdCl_4 over longer reaction times, and was recyclable for at least 5 extra runs.
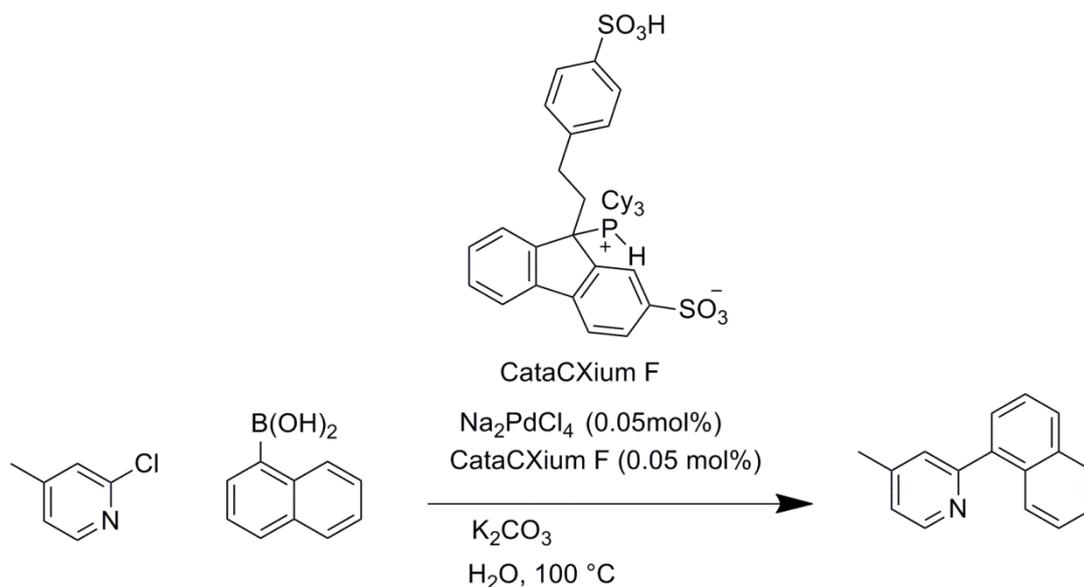
Scheme 1.18 Suzuki-Miyaura reaction in water catalyzed by the CataCXium F ligand with Na_2PdCl_4. Reported by Plenio *et al*[125]

Other ligand systems include nitrogen-donor ligands such as the ammonium-substituted 2-(2-imidazolyl)pyridine-derived cyclic palladium complex produced by Hong *et al* (scheme **1.19**). [126]

This complex was reported to be capable of coupling aryl chlorides with the use of TBAB, however Pd nanoparticles were proven to form at some point in the reaction.
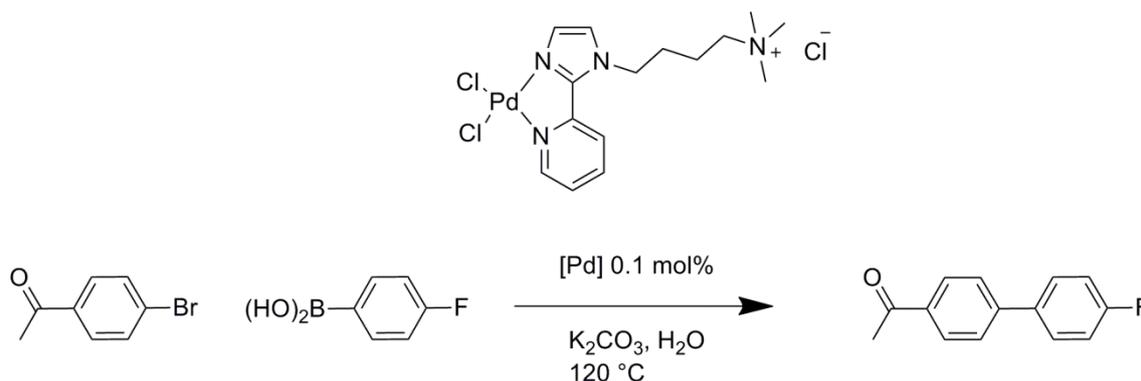
Scheme 1.19 Chelating ammonium-functionalized Pd(II) complex and its use in aqueous-phase Suzuki couplings. Reported by Hong *et al* [126]

Palladacycles with hydrophilic groups have also been used. The oxime-derived complex produced by Najera was the first published complex to catalyze aryl chlorides in water with the use of TBAB.[127] The complex was also reported to be readily recyclable in comparison to Pd(OAc)$_2$.
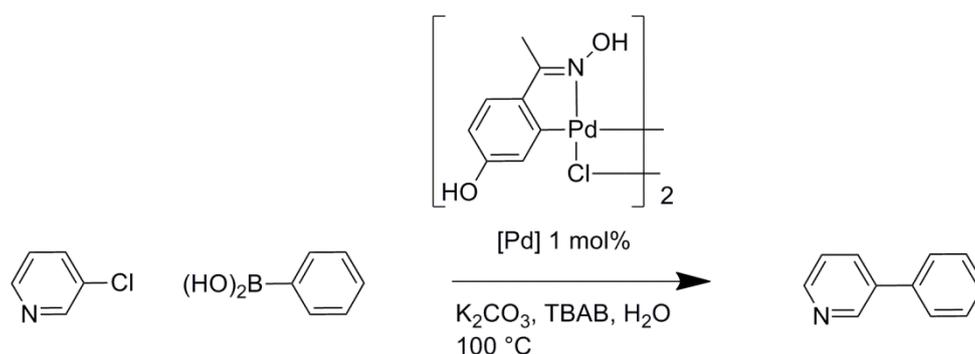
Scheme 1.20 Water-soluble palladacycle and its use in aqueous-phase Suzuki catalysis. Reported by Najera *et al* [127]

Second to phosphines, NHCs are the most popular ligands for the introduction of hydrophilicity. NHCs have been extensively used within the last decade within aqueous-phase cross-couplings; the bulk of research is applied towards Suzuki-Miyaura couplings. The most successful examples are those modelled upon systems that already performed well for Suzuki couplings in organic medium. Plenio et al for instance applied the sulfonated analogues of IMes and IPr to in-situ couplings of aryl halides in water.[83] Activities were reported to be excellent, even for aryl chlorides, however only conversions were reported rather than yields (scheme **1.21**). In a later report, NHC(allyl)Pd complexes analogous to those reported by Nolan were synthesized using

the sulfonated IPr ligand and applied to Sonogashira couplings, this time within a biphasic reaction mixture.[84] Sulfonates remain a popular polar moiety for inducing water-solubility.
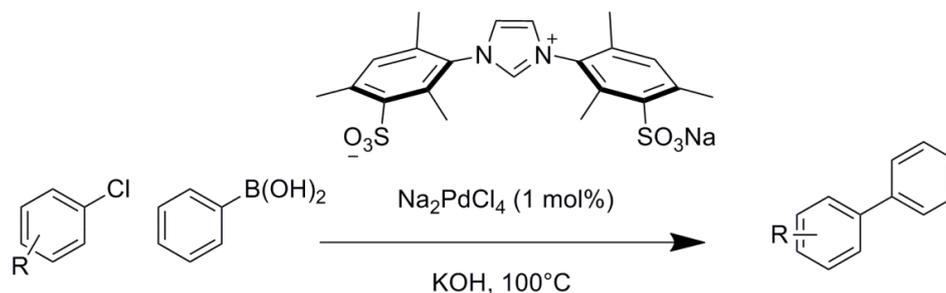
Scheme 1.21 Plenio's *in-situ* Suzuki coupling in water with sulfonated IMes[83]

A very recent study by Kühn et al is one of the most active examples to date, which highlights the importance of bulky NHCs (scheme **1.22**).[128] Aryl chlorides were easily coupled using their most bulky Pd–PEPPSI complex, which was recyclable for 3 additional runs. Although nanoparticles were observed to appear as part of the reaction, mercury poisoning studies determined that nanoparticles played no part in the catalytic activity.
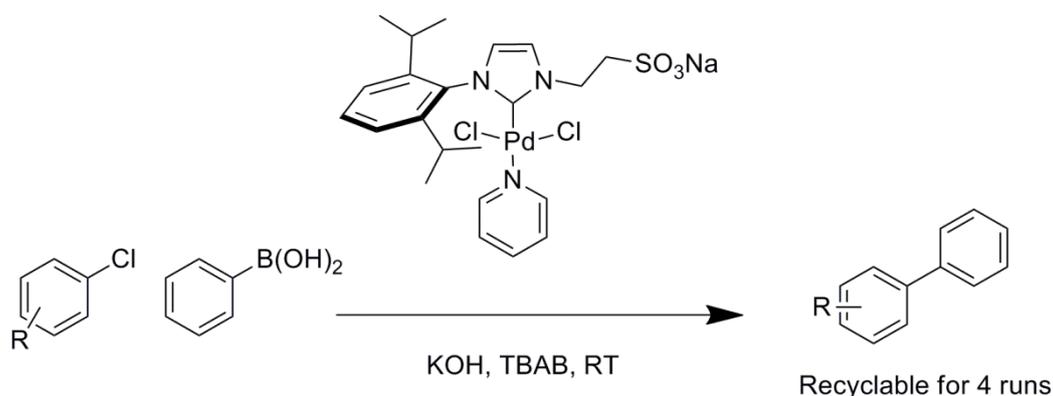
Scheme 1.22 PEPPSI-type catalyst synthesized by Kühn *et al*, used as a recyclable catalyst for aryl chlorides[128]

Carboxy-functionalized NHCs have also been well-reported. One of the first examples was that of Domìnguez *et al* who reported a carboxy-functionalized pincer complex as an active catalyst for aryl bromides without the use of TBAB, highlighting the stability of pincer complexes.[129] A later study involved an extensive catalyst poisoning study upon this and two similar catalysts, revealing that Pd(0) nanoparticles were involved in the coupling in most cases.[130] A novel example was presented by Wang *et al*, in which carboxylic acid-functionalized NHC chelating complexes were synthesized with easily interchangeable counter-ions (scheme **1.23**).[131] This was seen to show unique pH-sensitive properties, which were used to recycle the catalyst via

precipitation for an additional 4 runs. This catalyst was active for aryl bromides, however chlorides were once again difficult to activate.
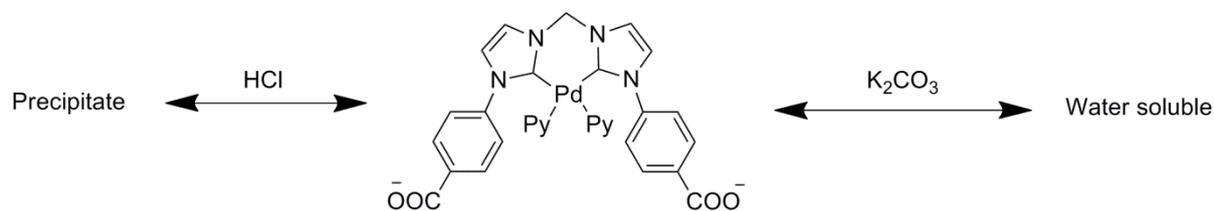
Scheme 1.23 Unique pH-induced solubility of chelate complex reported by Wang *et al*[131]

Although not common, biomolecule-derived NHC complexes have been reported for application within aqueous-phase Suzuki couplings. Yang *et al* reported an NHC with glucopyranoside N-bound groups, which was complexed to palladium and used in TBAB-free aqueous-phase couplings.[132] Both aryl bromides and chlorides were seen to be activated at relatively low catalyst loadings. A very novel example was reported later by Luo *et al* (scheme **1.24**).[133] Caffeine was quaternized with methyl iodide to produce a backbone-substituted imidazolium salt, which was complexed to palladium using the direct metalation route. The novel complexes were active for Suzuki, Heck and Sonogashira couplings; although limited examples were explored, and activities were not comparably high with previous literature.
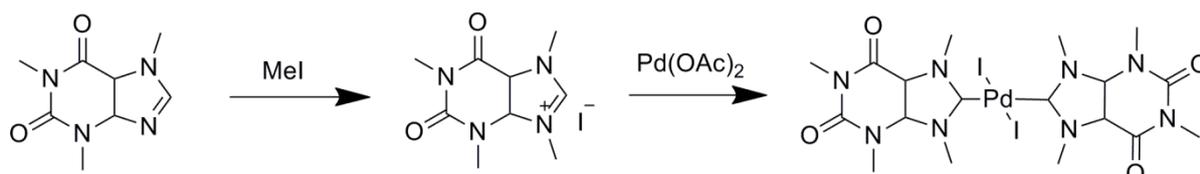
Scheme 1.24 Luo *et al*'s report of a caffeine-derived NHC ligand [133]

1.4 Organosilica materials

1.4.1 Hybrid materials and PMOs

Mesoporous silicas are ordered, nanostructured silica materials with pores 2 – 50 nm in size. They are synthesized by the hydrolysis of silicate compounds in the presence of a soft template, which is subsequently washed out forming an ordered porous inorganic network. The research into these materials began with MCM-41, a silica structure with hexagonally-arranged cylindrical pores which was synthesized by the Mobil Corporation.[134] This was discovered to form via co-condensation of the tetrasilicate ester precursor around cylindrical intercalated rods formed by the self-assembly of the trimethylalkylammonium surfactant molecules, in their case cetyltrimethylammonium bromide (CTAB). The Mobil Company was able to create a library of different porous silica materials using different self-assembled soft templates. [135] Later in 1998, Zhao *et al* produced a new type of porous silica with hexagonally-arranged pores, this time using a block copolymer as a surfactant. [136] This material became known as SBA-15, and is to date one of the more desired mesoporous silica materials due to its larger pore size and structural integrity. Since then a huge number of different porous silica materials with different pore arrangements, pore sizes and morphologies have been reported.

Organosilicas are silica materials interconnected by typical Si–O–Si linkages, which feature organic moieties within the structure covalently bonded via an Si–C bond, simply named organic-inorganic hybrid materials. These are synthesized by two different methods: using a triorthoorganosilicate precursor in a co-condensation reaction or by post-modification ("grafting") of an organic unit onto the silanol surface groups (figure **1.17**).[137] For co-condensation, the structure and morphology of the resulting material can be heavily influenced as a result of steric influence and intermolecular interactions which depend upon the nature of the organic group.
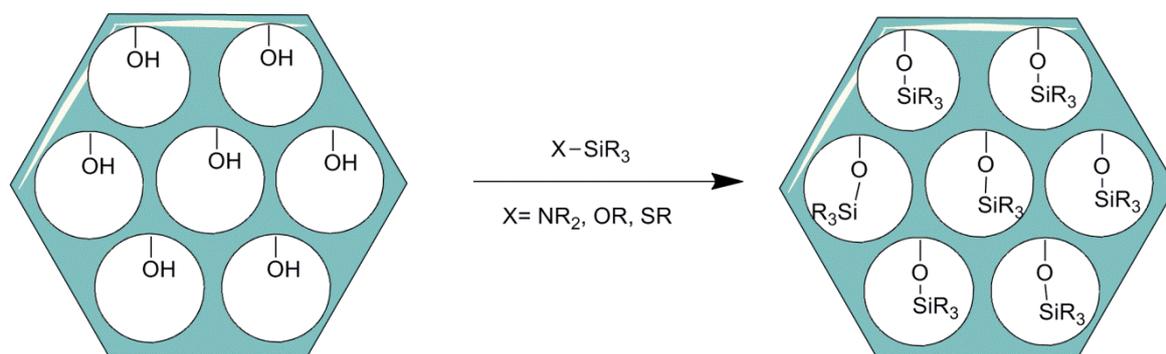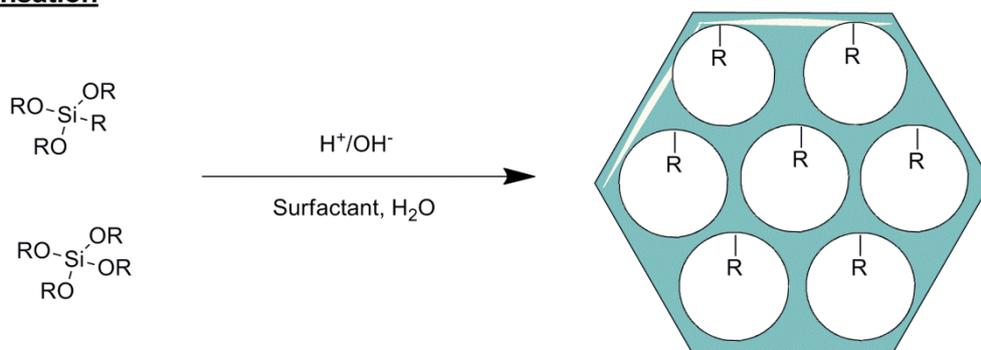
Figure 1.17 Different synthesis strategies for synthesizing organosilica materials: grafting and co-condensation

The addition of a surfactant during co-condensation of the silica material with an organic moiety can be used to produce porous silica-organic hybrid materials. The generation of mesopores is very desirable for such materials towards application, such as immobilization of catalysts, metal-scavenging and selective chiral chromatography. Organosilica materials come in two broad categories. The first utilizes terminal organosilanes (O–Si–R), which are typically arranged within the inside of the pores, these are usually just known as "porous nanohybrids".[137] These are normally synthesized using post-modification, in order to selectively target the pore-wall silanol groups. The second are known as "periodic mesoporous organosilicas" (PMOs) which feature bridging organosilanes within the structure (O–Si–R–Si–O), either bridged across each wall of the pore, lined along the surface of the pore, or embedded with the structure of the silica material.[138] Co-condensation synthesis routes are usually used for PMOs to ensure an even distribution of organic moiety throughout the structure, and to take advantage of any morphology-directing properties the organic linker may have on the structure (see later in scheme **1.23**).

1.4.2 Synthesis methods

Grafting is often a preferred synthesis method because of its versatility and simple procedure. A mesoporous silica material is stirred in solvent alongside an organosilane.[139] The available surface silanols form silicate bonds and the organic group is subsequently attached to the material surface. Remaining surface silanols can be removed by a "passivation" procedure, in which an alcohol is used to cover the surface with alkyl groups. [139] MCM-41 was a popular porous silica material to modify during the conception of organosilica hybrids. One of the earlier examples was produced by Jacobs *et al* in which 3-mercaptopropylsilane was grafted onto MCM-41 post-calcination (figure **1.18**).[140] The yielded organosilica was used as a supported acid catalyst for the synthesis of monoglycerides from glycerol.
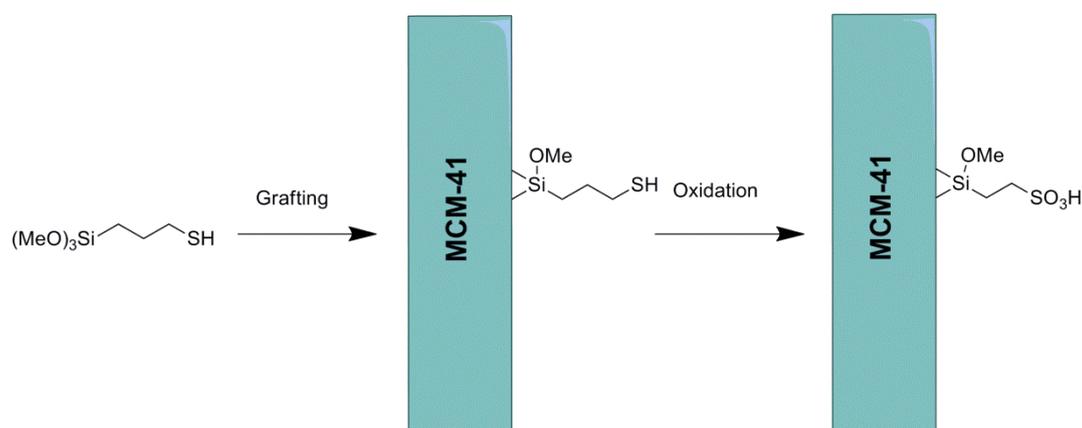
Figure 1.18 Grafting of a mercaptopropyl group onto an MCM-41 surface and subsequent oxidation. Reported by Jacobs *et al*

Disadvantages of the grafting method are related to undesired changes in pore size or structure. Inclusion of an organic group within the linker can reduce the overall surface area of the material by filling more space.[141] Moreover the integral structure of the pores can be changed if the organic moiety is large enough. The availability of the organic group within the pore also makes this method suitable for post-modification of the organic moieties. This can include modification of olefin groups and addition to amine linkages via amidation (as will be demonstrated in chapter 4). One of the more interesting examples is the coordination of metals to immobilized ligand groups, in order to create solid-state metal coordination catalysts. In the example from Jacobs *et al*, the simple mercapto-group is oxidized into a sulfonate group using post modification with H_2O_2.[140]

Co-condensation by its nature includes the organic group within the structure of the material, which is a useful if the desired effect is to alter the physical properties of the surface, for example hydrophobicity. Co-condensation proceeds via a sol-gel reaction mixture in which the

organosilane is hydrolyzed in acidic or alkaline solution in the presence of the surfactant, and the condensed Si–O–Si linkages form around the surfactant template (schemes **1.25** and **1.26**). In presence of both acid and base, the hydrolysis process occurs much more quickly than the condensation, making condensation the rate determining step. However, in the acid-catalyzed process the condensation occurs much more slowly than in the base-catalyzed process.[142] The slower condensation means that particle nucleation occurs slowly, producing more structurally integral linear siloxane networks. The disadvantage of this is that less siloxane linkages occur, resulting in a higher concentration of leftover silanol groups. As a result, silica materials produced by base-catalyzed processes tend to be denser.[143]

Hydrolysis
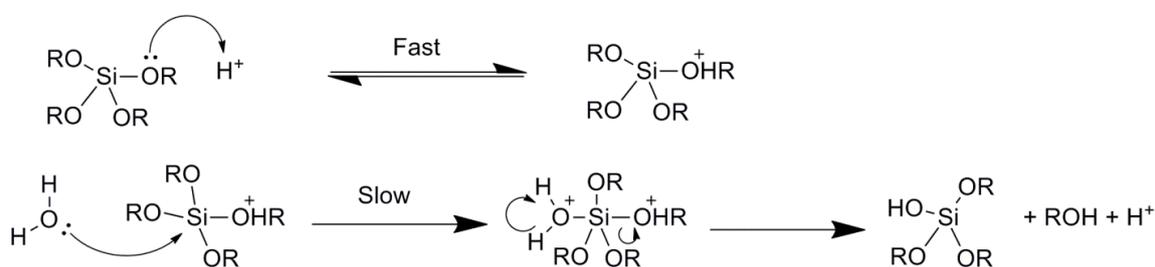
Condensation
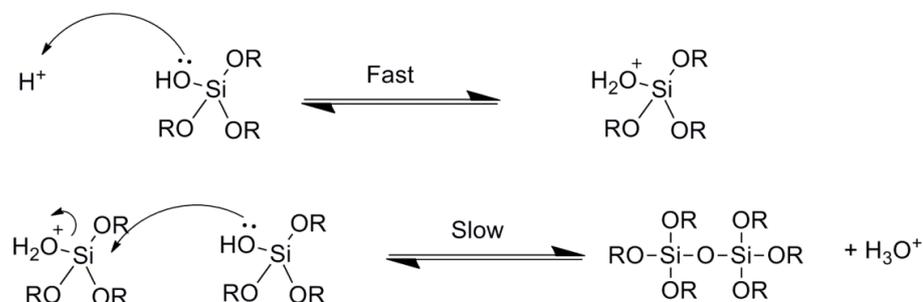
Scheme 1.25 Mechanism of the acid-catalyzed co-condensation of silanes. Adapted from reference [144]

Hydrolysis
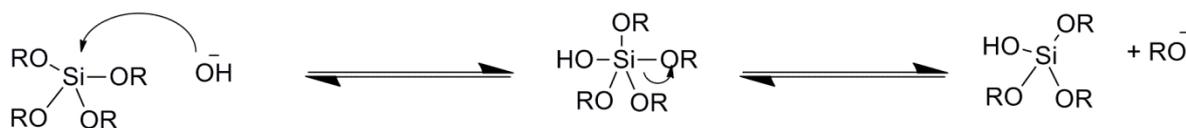
Condensation
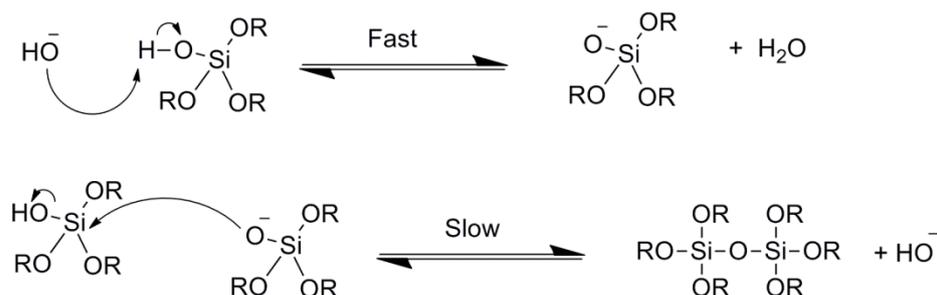
Scheme 1.26 Mechanism of the base-catalyzed co-condensation of silanes. Adapted from reference [144]

The surfactant determines the shape and arrangement of the pore network, and the arrangement of the self-assembled surfactants can also change based on the type and concentration of acid or base. [145] [142] Two broad types of surfactant are used: tetraalkylammonium salts such as CTAB, and block copolymers such as Pluronic-123 or Brij-76. [138] Naturally, the organic group also has an influence on the pore structure.Occasionally the organic units can arrange themselves around the template via their own intermolecular forces, such as π-π stacking between benzene rings.[146] However, the incorporation of more organic groups tends to disrupt the pore structure. To prevent this, the organosilane is co-condensed alongside tetraalkoxysilanes such as tetraethylorthosilicate (TEOS) to "dilute" the organic moieties within the structure by changing the Si:C ratio. When terminal organosilanes are used, the terminal alkyl groups tend to arrange together as a result of mutual repulsion through hydrophobicity; as a result the organic groups are arranged either inwards, similar to a micelle, or outwards, towards the surfactant. When bridged organosilanes are used within PMO materials, the organic moieties are often bridged across the pores, and are thus readily accessible. [147]

Terminal organosilane
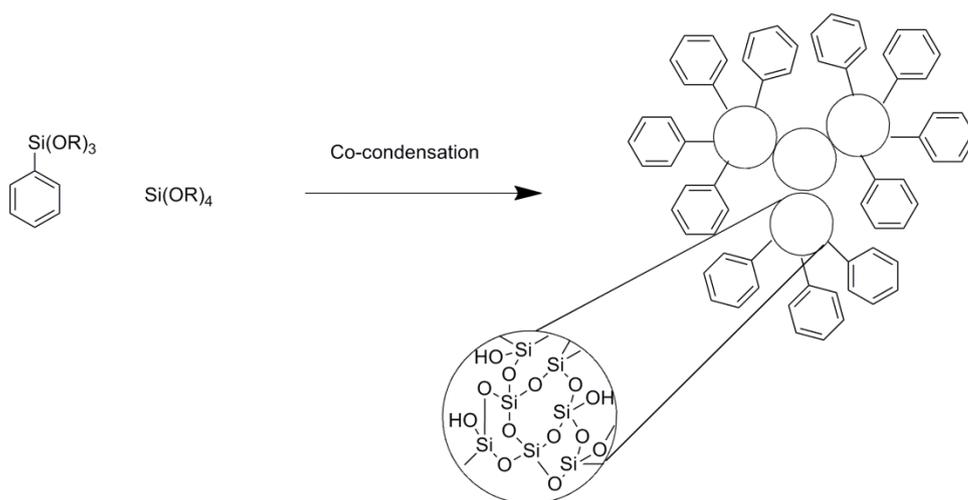
Bridged organosilane
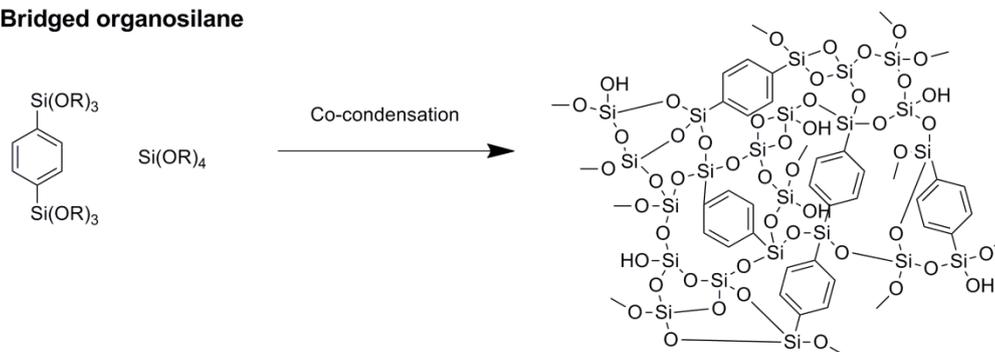
Scheme 1.27 Co-condensation of terminal (above) and bridged (below) organosilanes without surfactant. Adapted from reference [147]

PMOs were first reported independently by the groups of Ozin, Stein, and Terasaki in 1999 for a bridged ethyl organosilane, all reporting a very ordered 3-D structure (figure **1.19**).[148] [149] [150] This was later extended to include ethene, methyl, and phenyl-linkages.
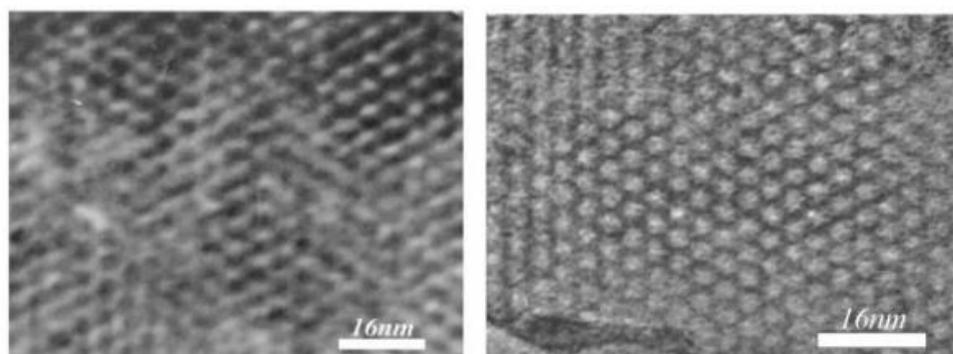
Figure 1.19 TEM images of the hexagonally-arranged ethyl-functionalized PMO reported by Ozin *et al*. Adapted from reference [148]

1.4.3 Applications

Silica is known first and foremost for its use as a stationary phase in chromatography. By introducing porosity silica, the particle size can be changed to include a size-exclusion variable and the pore size can be varied depending on the desired degree of separation. By using PMOs, the organic character can influence structure-related properties. Thus some of the drawbacks associated with normal silica phases, such as base-sensitivity or hydrophilicity, can be overcome. For normal or reversed-phase chromatographic applications, Inagaki *et al* and Fröba *et al* independently reported spherical benzene-functionalized PMO particles.[151] [152] The Fröba group followed up their report with larger particles of the same material but with tunable pore diameters synthesized using a mixture of P-123 and CTAB surfactants.[153] These materials could be used for both normal and reversed-phase chromatographic phases. The biggest opportunity stemming from organosilica chromatography is that of enantiomer separation. By including a chiral organic group within the PMO, the corresponding enantiomer of an organic compound can be selectively separated from a racemic mixture. Li *et al* published one of the first examples, a chiral *trans*-(I*R*, 2*R*)-diaminocyclohexane group attached to an ethane-bridged silane was used to produce silica spherical particles of 5-7 μm size (scheme **1.28**). [154] This was proven to be effective in HPLC for the separation of racemic amino acid mixtures.
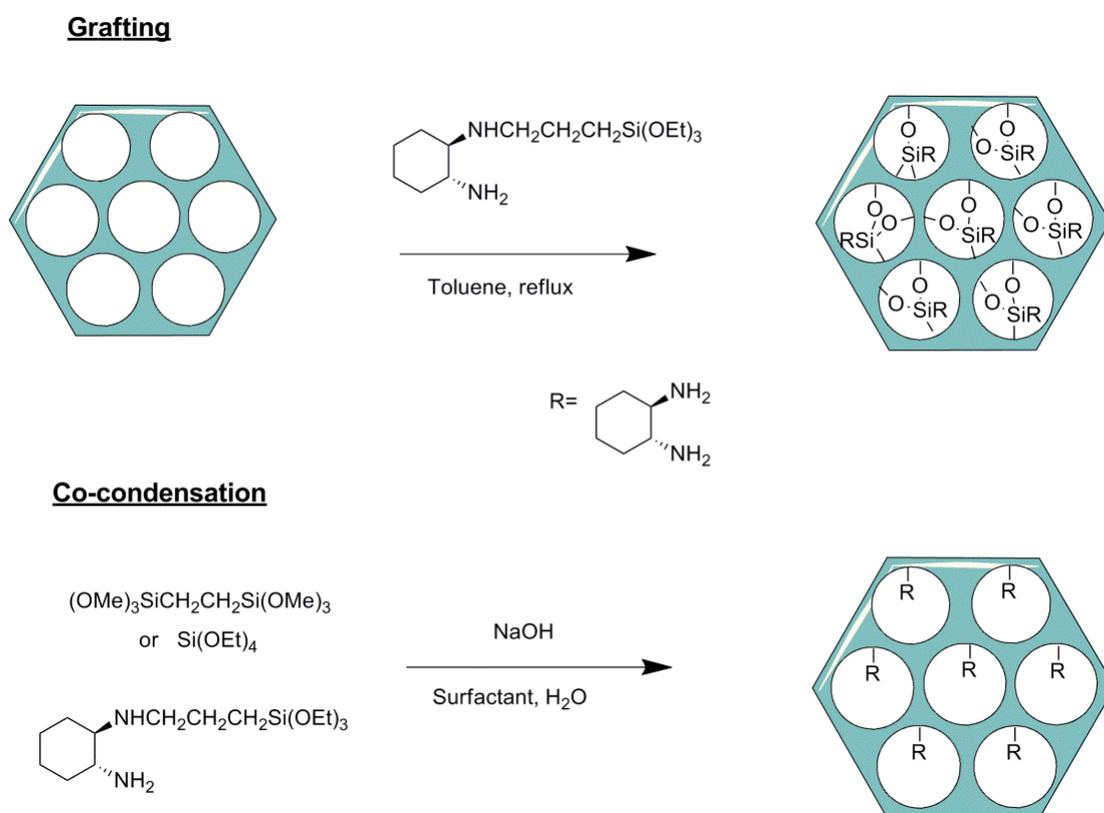
Scheme 1.28 Co-condensation and grafting syntheses of the *trans*-(I*R*,2*R*)-diaminocyclohexane-functionalized chiral PMO reported by Li *et al* [154]

Metal-scavenging is also a fruitful application field for PMOs, for removal of inorganic toxic residues for organic compounds which require particularly meticulous purification, such as pharmaceutical drug precursors. Typically this involves including an organic moiety capable of metal complexation, the most typical example being mesoporous aminopropylsilica which is commercially available; however many different heteroatomic groups have been reported. Chelating groups show particular promise, due to the entropic favorability of metal chelates. A particularly interesting example was reported by Burleigh *et al*, in which metal ions were employed in the synthesis of the PMO as a template, so that selective silica materials could be produced for particular metal ions (scheme **1.29**).[155] Copper, nickel and zinc salts were used with *N*-[3-trimethoxysilyl)propyl]ethylenediamine alongside BTEE and CTAC surfactant. The metal was removed afterwards using nitric acid, to produce a scavenger selective to the metal used during synthesis.
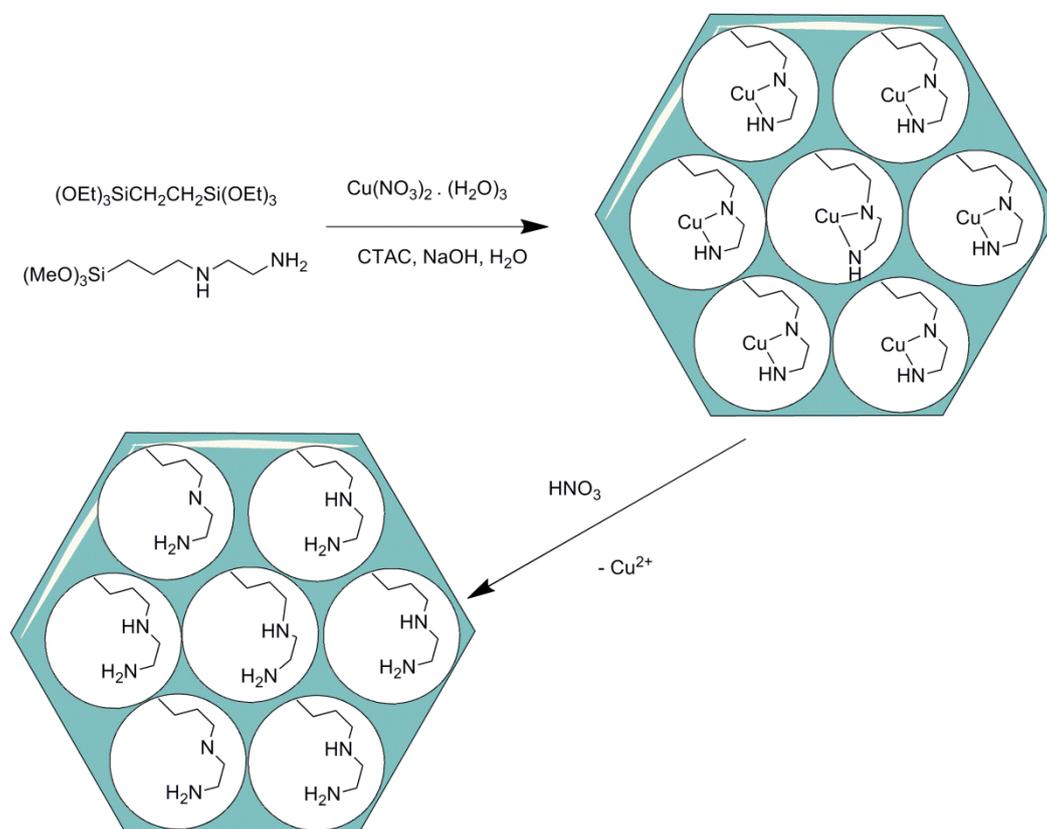
Scheme 1.29 Metal-templating approach for the synthesis of silica metal scavengers. Reported by Burleigh *et al* [155]

PMOs can also serve as heterogeneous catalysts. This presents a huge opportunity within green chemistry, as it opens up the possibility of recycling and adaptation to flow reactors. Both organocatalysts and metal catalysts can be supported onto silica by covalent or coordinate bonds. The functionalized MCM-41 material from Jacobs *et al* presented earlier in this section

was used as a supported Brønsted acid catalyst,[140] however a vast number of lewis acidic and basic examples have also been presented. Probably the biggest opportunity lies in the use of immobilized organometallic catalyst materials, since the recycling of expensive metals is desirable from a green chemistry perspective. Homogeneous catalyst immobilization elegantly combines the worlds of homogeneous and heterogeneous catalysis. Defined catalysts can be prepared which are specifically designed for the process in mind and immobilized onto a macromolecular structure, resulting in a catalyst which has a similar activity and selectivity to that of a homogeneous catalyst, and the recyclability and robustness of a heterogeneous catalyst. PMOs in particular are promising macrostructures for catalyst immobilization. The mesoporous network allows good tunable access to the active sites; and recently siloxane groups have been shown to have a stabilizing effect on metals, in work on immobilized silica catalysts presented by Thieuleux *et al* (figure **1.19**). [156]
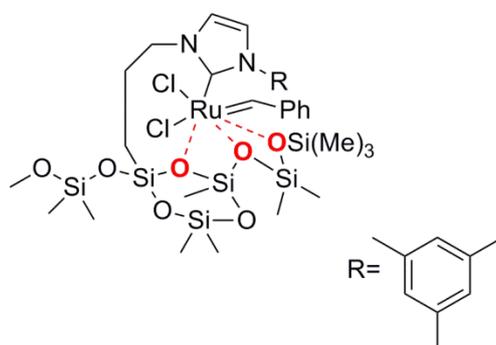
Figure 1.19 Illustration of surface-metal interactions on a silica-immobilized Ru–NHC catalyst as reported by Thieuleux *et al* [156]

The bulk of work involving supported metal catalysts focuses on Pd nanoparticles for cross-coupling reactions.[138] However, nanoparticles typically undergo composition changes upon successive reuse.[157] Strongly donating immobilized ligands are desirable for metal complex immobilisation in order to prevent significant metal leeching. Phosphines are a typical example, bis- and tris-silylated phosphines were used to synthesize Pd(II),[158] Rh(I), and Ru(II) complexes,[159] and subsequently co-condensed with TEOS and surfactant in examples presented by Li and Zhang *et al* (figure **1.20**).
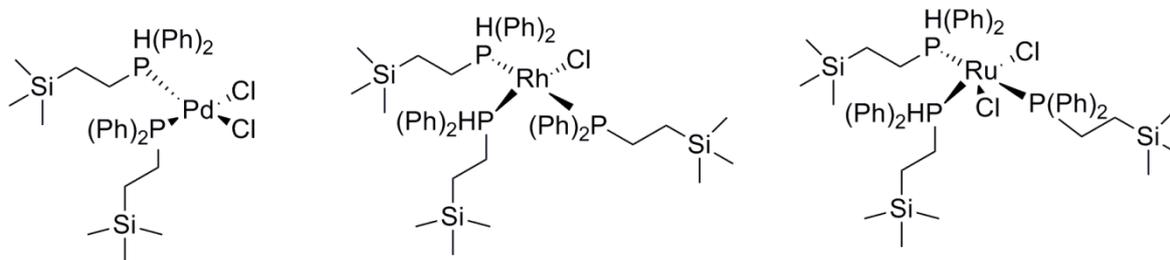
Figure 1.20 Structures of different silica-immobilized metal-phosphine complexes reported by Li (left) and Zhang (centre and right) *et al* [159] [158]

Silylated NHCs are also promising ligands for immobilization of NHC–metal complexes onto silica. PMOs featuring imidazolium salts have been presented in the literature, as will be further reviewed in the fourth chapter.

2. Synthesis and characterization of amino acid-derived NHC precursors and metal complexes

2.1 Synthesis of NHC precursors

As discussed in the previous chapter, a vast number of different *N*-heterocyclic carbene structures exist. One of the main criteria required for a stable NHC is simply the existence of at least one nitrogen atom in the α-position to the precarbenic carbon atom, to act as a π-donor/acceptor for the carbon p_π orbital. This goes to say that a number of different structures exist including sulfur, phosphorous and oxygen heterocycles.[45] However the vast majority of NHC precursor reports consist largely of imidazolium and imidazolinium salts, as a result of their simple synthesis. The first account of a heterocycle synthesis for the application of NHC precursor was reported by Arduengo in 1991.[160] This publication covered the most common synthesis of symmetrical imidazolinium salts still used to date, and also the synthesis of symmetrical imidazolium salts, which would be later developed upon by Nolan *et al.* to produce a simpler one-step procedure (scheme **2.1**).[161, 162] The three-step procedure from Arduengo involves the addition of two equivalents of a substituted primary amine to glyoxal to form a diimine, subsequent reduction to form the diamine, and finally acid-catalyzed cyclization with triethylorthoformate as the C_2 building-block. The acid counter-ion is incorporated into the final structure, thus acids such as HCl and HBF_4 are typically used in order to contribute suitable counter-ions for NHC chemistry. The imidazolium synthesis is similar to the imidazolinium synthesis, other than to skip the diimine reduction, retaining the olefin backbone and resulting in an aromatic product. The Nolan method improves on this by using paraformaldehyde and an acid catalyst, which are greener and easier to handle. These procedures share the common factor that they proceed via a Debus-Radziszewski imidazole synthesis mechanism.[163] This reaction, discovered originally as far back as 1858, proceeds in one pot almost instantly, as a result of the stability of aromatic heterocycle formation. Whilst this factor is desirable in accordance to the 12 principles of green chemistry, the Arduengo and Nolan methods still require the use of petrochemically-derived solvents and, perhaps most obviously, task-specific amines for the N-bound groups. Imidazolium salts which feature unsymmetrical N-bound groups are even less green, typically involving the nucleophilic substitution of an alkyl halide onto the imidazolium ring, or pre-synthesis of an asymmetrically-substituted diamine.[164] Fürstner *et al* described a procedure for unsymmetrical imidazolium salts in 2006 which does not require the use of alkyl halides, and instead proceeds via a N,O heterocyclic acetal intermediate; however this still requires 3 steps, and the use of a complicated precursor.[165]

Arduengo route (1991):
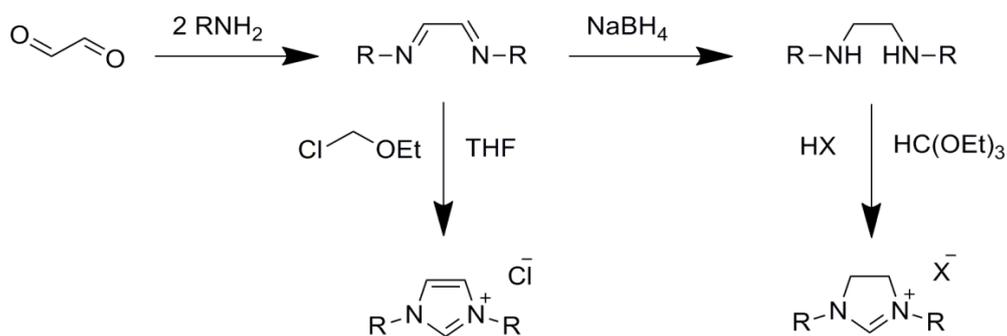
Nolan route (2000):
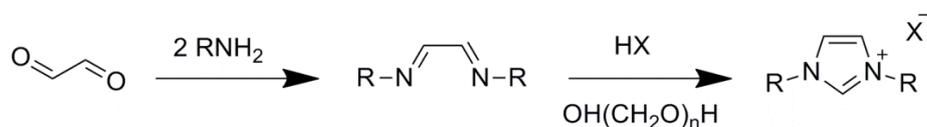
Scheme 2.1 Synthesis of imidazolium and imidazolinium NHC precursors by Arduengo[160] and Nolan[161]

A recent report from our group has seen the synthesis of substituted imidazolium salts from amino acids, pyruvaldehyde, and formaldehyde in a one-pot reaction that proceeds at room temperature in water[166]. This approach follows the principles of green chemistry on the basis that: the reactions are performed in water, at room temperature, using stoichiometric reagents that can be derived from sustainable sources. In a further account, it was proven that these zwitterionic imidazolium building blocks could be decarboxylated using hydrothermal conditions, allowing the carboxylate groups to be removed in water, in the presence of an acid (which once again serves as catalyst and counter-ion source).[167] This process results in a series of room-temperature ionic liquids, the properties of which can be tuned based on the N-bound amino acid R-group. In this particular report, both glyoxal and pyruvaldehyde were used as imidazolium backbones. Pyruvaldehyde can be easily obtained from bio-derived compounds; namely dihydroxyacetone, which can be isolated as a product of glycerol oxidation,[168-170] or more recently as an intermediate in the retro-aldol splitting of the linear glucose isomer (scheme 2.2).[171] Likewise, glyoxal can also be obtained from two-step biorefinery-upgrade procedures: pyrolysis of biomass produces bio-oil[10], which is rich in hydroxyacetaldehyde, a precursor that can yield glyoxal via selective oxidation processes and enzymatic catalysis. Whilst the current commercial standard of producing glyoxal is via the oxidation of ethylene glycol,[172] methods of producing this precursor from glucose are reported in the literature.[173, 174] A particularly recent account reports the selective production of ethylene glycol from cellulose using solid state metal

catalysts.[175] These methods present a green pathway to producing glyoxal which is already compatible with the existing industry-scale processes.
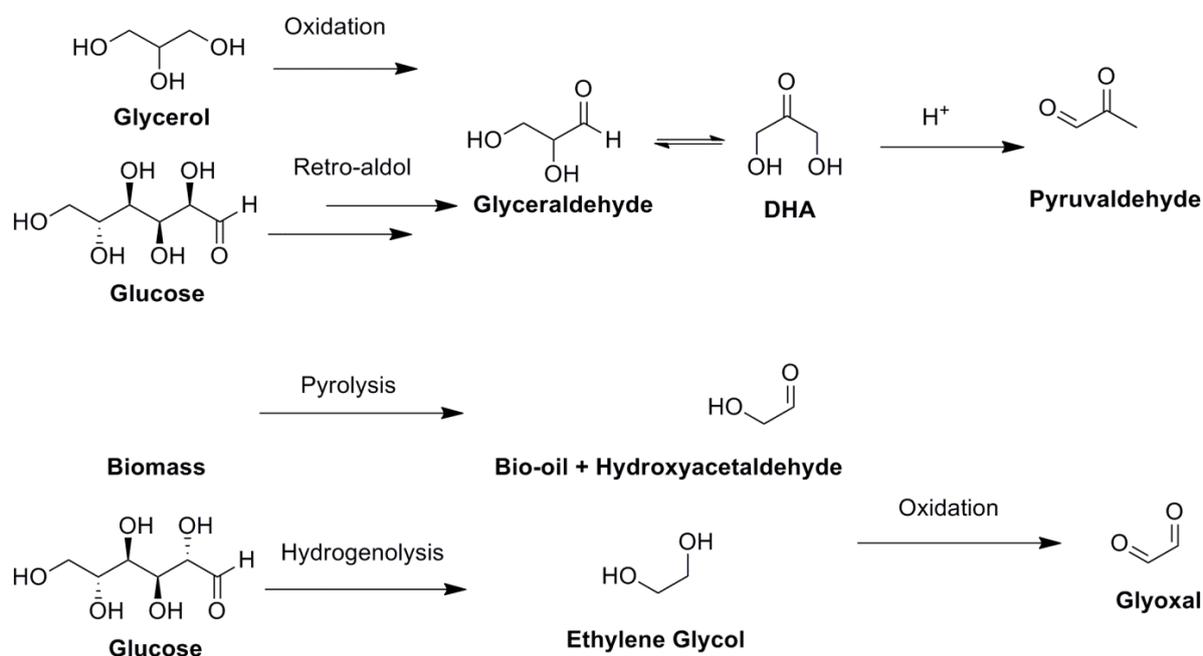
Scheme 2.2 Proposed pathways to Pyruvaldehyde and Glyoxal via biorefinery and catalytic upgrade processes

Employing primarily glyoxal as the imidazolium backbone, the amino-acid derived zwitterions were investigated for their potential as NHC precursors. Glyoxal was used in most cases to retain symmetry within the salt, since they were intended to be used for the synthesis of NHC-metal complexes. Symmetry is desirable within crystalline structures for the chance of growing single-crystals,[176] allowing the resulting complexes to be characterized using X-Ray crystallography. As opposed to within ionic liquids, where asymmetry is desirable for preventing crystallization and therefore lowering the melting point.

2.1.1 Imidazolium carboxylate zwitterions

Imidazolium carboxylate zwitterions were synthesized according to the procedure outlined in reference [166]. All zwitterionic salts were isolated as solids ranging in colour from white to brown in good to excellent yields (table **2.1**). The amino acids glycine, alanine, β-alanine and phenylalanine were used in combination with glyoxal and pyruvaldehyde backbones as a method of introducing various functionalities into the NHC precursor.

50
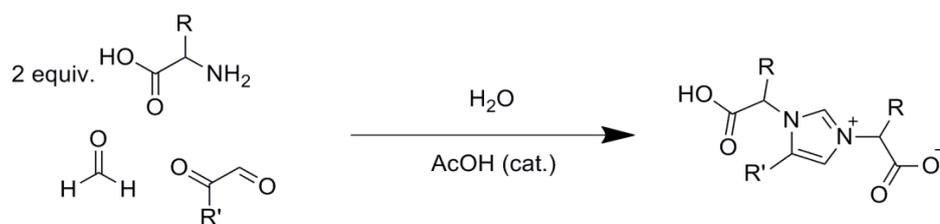
Entry	Structure	Yield [%]
1a		95
1b		99
1c		62
1d		99
1e		98
1f		95
1g		75
1h		89

Table 2.1 Synthesized zwitterions and respective yields. Reaction conditions: 1 mmol glyoxal/pyruvaldehyde, 2 mmol amino acid, 1 mmol formaldehyde, 30 mmol acetic acid, RT, 10 ml water, 1 hour. In the case of **1c**, the temperature was raised to 50 °C.

2.1.2 Imidazolium ester chlorides

Alongside the zwitterionic salts, imidazolium salts featuring halide counter-ions were also synthesized via esterification of the carboxylate in ethanol, using acetyl chloride as a source of acid catalyst HCl, thereby providing the chloride counter-ion. The resulting products are mostly viscous brown oils, aside from the ester **2a** which is a white solid (table **2.2**). NHC precursor salts with halide counter-ions represent the majority of the literature on NHC ligands, since halides are suitable 1-electron donor ligands for metal complexes adhering to the HSAB (hard/soft acid/base) rule.[177] Esterification was performed under reflux conditions in a Sohxlet apparatus with 3.5 Å molecular sieves to remove the water by-product and push the equilibrium in the direction of the desired product. In most cases full conversion was observed after 4 hours, but in particular cases such as the phenylalanine-Imi-ester (**1c**) up to 12 hours was required to fully convert both carboxylate groups. The resulting esters were susceptible to hydrolysis in air from atmospheric moisture, and thus were stored under nitrogen or argon atmosphere.
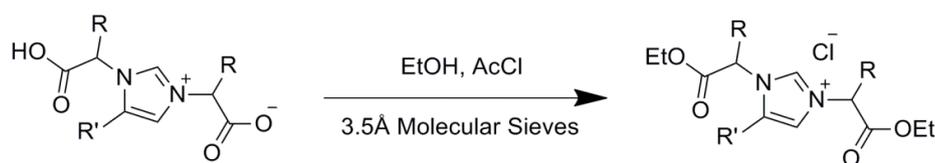
Entry	Structure	Yield [%]
2a		89
2b		84
2c		71
2d		88
2e		94

Table 2.2 Synthesized esters and respective yields. Reaction conditions: 1 mol imi carboxylate, 1.2 mol acetyl chloride, 150 ml ethanol, Soxhlet apparatus with molecular sieves under argon atmosphere, 150 °C, 4 hours.

The weakness in this synthesis route in terms of green chemistry lies in the use of acetyl chloride as HCl precursor, and therefore counter-ion source. Another method of introducing halide counter-ions without the use of HCl involves salt metathesis from a different counter-ion. This was attempted by first synthesizing the imidazolium ester using toluenesulphonic acid, and changing the resulting tosylate counter-ion using NaCl (scheme **2.5**). Synthesis of the tosylate imidazolium ester was successful in good yield, however the salt metathesis step failed in both ethanol and chloroform solvents. The most likely reason for this is that the formation of the corresponding tosylate sodium salt is not thermodynamically favourable.
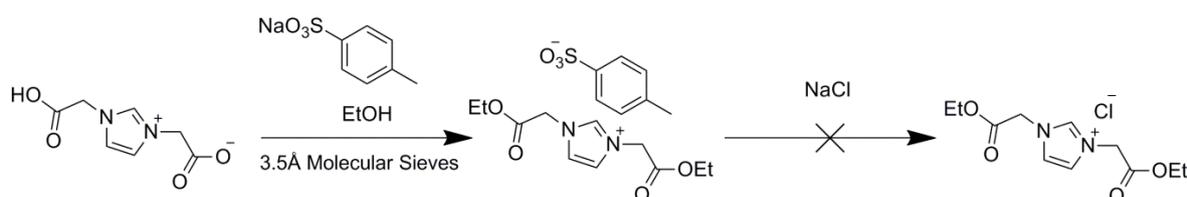
Scheme 2.3 Attempted salt metathesis via tosylate counter-ion. 1.2 equivalents of sodium chloride was used for the metathesis in ethanolic medium.

2.2   Synthesis of NHC-metal complexes

As discussed in the introduction, NHC precursors and complexes featuring carboxy-group functionalities were reported as early as 1997,[178] however reports since then have been scarce compared to NHCs without carboxy-groups. One reason for this is the relative difficulty of NHC preparation; since an NHC is prepared by deprotonating the proton present in the precarbenic C_2 position, the presence of similarly acidic protons, either as carboxylic acid protons or α-carbonyl protons, may cause non-selective deprotonation of various positions other than the C_2 position. The carboxylic acid functionality of the amino acid alanine obviously has a pK_a much lower than that of its α-position,[179, 180] but both are significantly lower than that of the C_2 position of the dimethyl substituted imidazolium cation (table **2.3**).[181] For this reason, no *free* carbene has been isolated to date featuring carboxy-group functionalities within the imidazolium structure. For this same reason, very little research has been published featuring NHC organocatalysis using carboxy-functionalized NHCs or NHC precursors featuring polar N-bound groups.[45] The bulk of NHC organocatalysis research involves the attack of the nucleophilic NHC into a carbonyl substrate, forming an intermediate capable of taking part in reverse-polarity or Umpolung chemistry. This is largely referred to as the Breslow intermediate after Breslow first postulated its existance.[49] NHC precursors featuring carbonyl groups are theoretically

susceptible to intermolecular attack on other NHC molecules, and thus unsuitable for the majority of NHC organocatalytic reactions.

Proton	pK$_a$ value in H$_2$O
	2.35
	16.50
	23.0
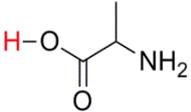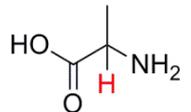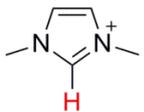
Table 2.3 Comparison of pK$_a$ values of different functional groups in H$_2$O

It was therefore more appropriate to use the carboxyl-functionalized NHC precursors reported in **2.2** for the synthesis of NHC–metal complexes. A number of similar examples exist already within the literature stemming from Herrmann's first example in 1997, which has the same structure as imidazolium ester **2a** aside from a bromide counter-ion. These were complexed simply by stirring with the metal precursor, and allowing the basic metal counter-ion to deprotonate the NHC precursor *in situ*. Most reports since have used either this *in situ* metal counter-ion deprotonation strategy, or the silver-transmetallation strategy first reported by Young *et al* in pure water.[182] This strategy has been utilized by Shaughnessy (scheme **2.4**),[81] and Santini[183] (scheme **2.5**) for charged carboxylates. In each case, the reaction was performed using pure water as the solvent, Ag$_2$O as the silver source, and NaCl as both a source of counter-ions and a measure of preventing the formation of coordination polymers. The silver adducts produced by Santini *et al* were successfully transmetallated onto gold by Hemmert *et al*.[184] Carboxylic acid-functionalized NHCs have also been coordinated to palladium via the direct metallation route with Pd(OAc)$_2$ by the Liu and Domìnguez groups.[129, 185] In both cases the ligands are chelating NHCs, the former being a pincer-type tridentate ligand with a carboxylic acid group attached to the central pyridinic coordination unit. These complexes could be utilized as recyclable precatalysts in aqueous-phase Suzuki C-C couplings, producing very high yields.
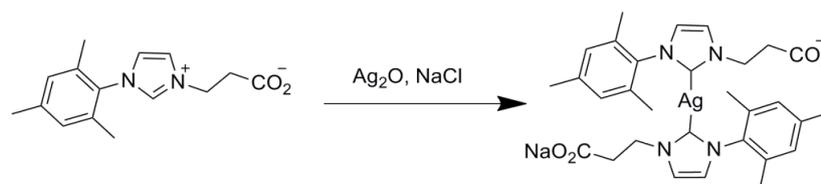
Scheme 2.4 Shaughnessy's synthesis of a bis-Ag–NHC compound from imi-zwitterions[81]
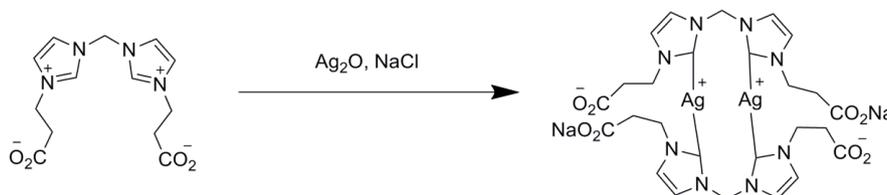
Scheme 2.5 Santini's synthesis of bis-chelating Ag–NHC compounds from imi-zwitterions[183]

Aside from carboxylate zwitterions, ester-functionalized imidazolium salts have also been reported and successfully metallated. The first example is the aforementioned report by Herrmann *et al* in which symmetric ester-functionalized precursors were directly metallated onto rhodium and palladium.[178] Further modification of the rhodium complex revealed that the ester groups retained full functionality, and could be succesfully, transesterified, hydrolyzed, and admidated; opening up possibilities for induction of water solubility. It was not until 2009 that another ester-functionalized NHC complex was reported by Domìnguez,[130] who used ester-functionalized Pd pincer complexes similar to their last report. They were reported to be very active for aqeuous-phase Suzuki couplings, but after a detailed poisoning study it was determined that the active catalyst was infact Pd(0) nanoparticles. Reports since then have been more frequent. Li *et al* were able to synthesize chelating Pd-NHC complexes which were reported as pH responsive,[131] this phenomenon was utilized in catalyst recycling during aqueous-phase Suzuki couplings. Santini and Perez both successfully transmetallated ester-functionalized NHCs using the silver adduct route onto gold (scheme **2.6**), and copper in the case of Santini.[186, 187] These could be used as both anti-cancer compounds and catalysts for C-H activation. More recent reports have seen the synthesis of ester-NHC complexes of rhodium, platinum, palladium and iridium for anti-cancer and catalysis applications.[188-190]
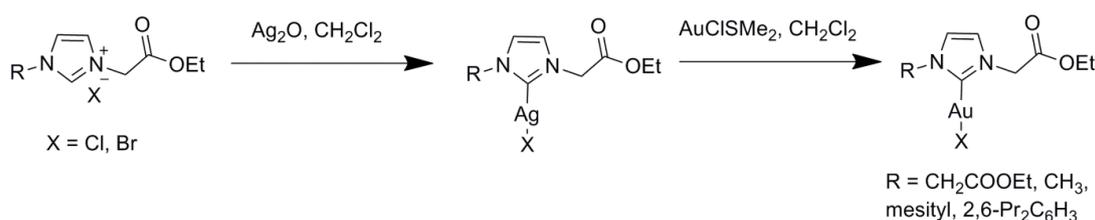
Scheme 2.6 Perez's synthesis of Ag–NHC compounds from imi-esters and subsequent transmetallation to Au

2.2.1 Imidazolium zwitterion NHC complexation

Using similar procedures to that of Santini *et al*,[191] precursor **1a** was stirred in water with Ag_2O in the presence of NaCl, at both elevated and room temperatures (scheme **2.7**). A modified attempt using NaOH as a base was also performed. Initial tests revealed a change to an orange coloured solution and the formation of a grey precipitate, however attempts to work up the reaction produced a black precipitate typical of silver residue. Upon performing this reaction using the NaOH route (scheme **2.7** Route 2) in D_2O, and NMR analysis of the reaction solution after two hours showed that the peak representing the imidazolium C_2 hydrogen had been significantly reduced as evident from peak integration, suggesting formation of a carbene adduct (figure **2.1**). The peak representing remaining C_2 protons was seen to shift downfield, this is likely a result of the formation of the carboxylate sodium salt for the rest of the unreacted zwitterion. Additionally the glycine CH_2 group and imidazolium backbone were also seen to have shifted downfield. Attempts to identify the adduct via Electrospray Mass Spectrometry (ESI-MS) in solution were unsuccessful, as no clear silver isotope pattern could be observed.
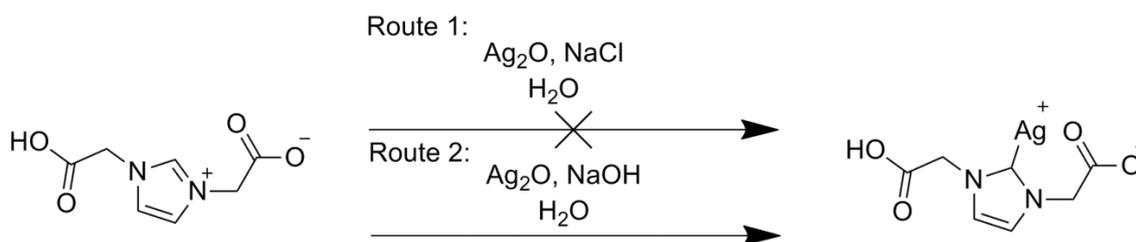
Scheme 2.7 Attempts at synthesizing Ag–NHC adducts from imi-zwitterions. Reaction conditions: 1 mmol **1a**, 1 mmol Ag_2O, 1.1 mmol NaOH/NaCl, 5 ml H_2O, 2 hours, room temperature (RT).
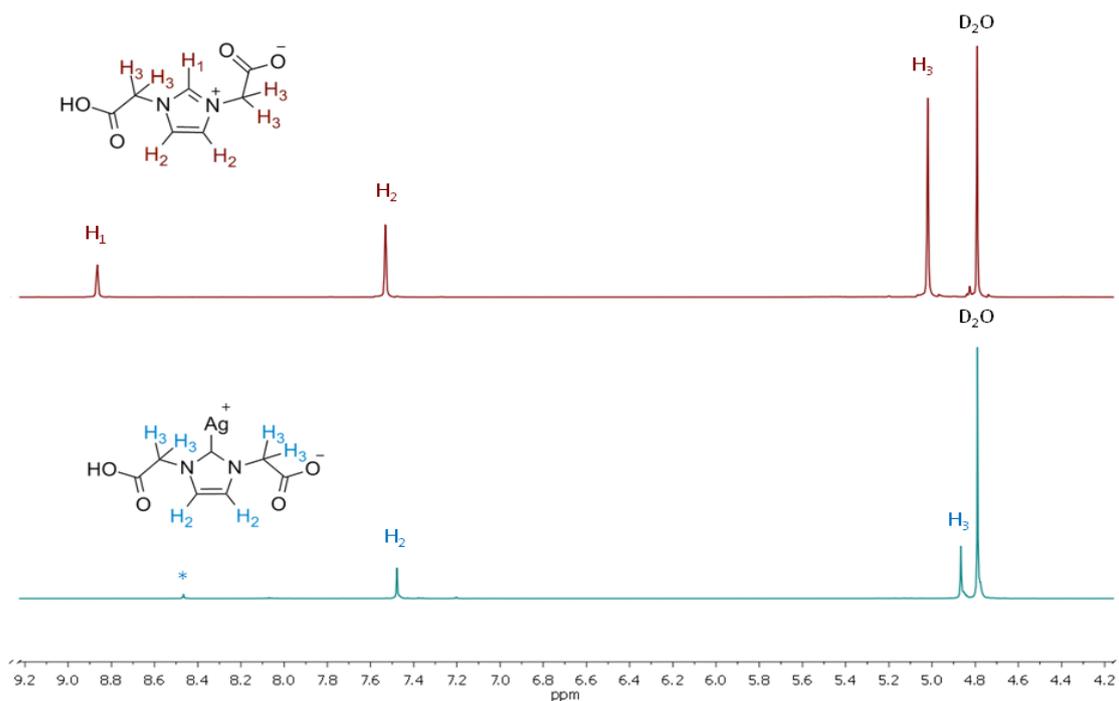
Figure 2.1 NMR evidence of Ag–NHC formation

All attempts to isolate the silver adduct resulted in the formation of a black precipitate, this is likely a result of the light sensitivity typically observed in Ag-NHC adducts. Likewise attempts to transmetallate the formed Ag adduct to palladium via Pd(OAc)$_2$ and iridium via [Ir(COD)Cl]$_2$ were unsuccessful (scheme **2.8**), also most likely a result of the sensitivity of the transmetallation agent. As this work was being carried out, Reynoso-Esparza *et al* reported the transmetallation of similar zwitterionic precursors to Au, using the same procedure to produce the Ag transmetallation intermediate.[192] The Au complexes were found to be unstable in solution, and the Ag adduct intermediates remain uncharacterized.
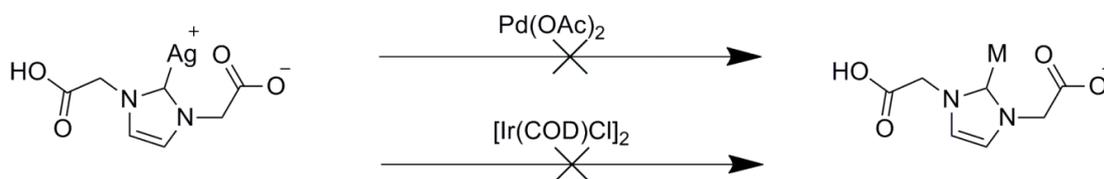
Scheme 2.8 Attempts at Ag–NHC transmetallation

2.2.2 Imidazolium ester chloride NHC complexation

2.2.2.1 Silver

Using the procedure adopted by Santini *et al*,[186] silver adducts of ester precursors **2a–2e** were attempted in acetonitrile solvent using Ag$_2$O silver source. Evidence of silver complexation was detected via ESI-MS for all precursors, however only the adduct of **2a** (**3a)** was able to be isolated in good yield (83 %) for full characterization (scheme **2.9**). The palladium complexes **4b** and **5b** (presented later) were therefore synthesised directly from the *in situ* synthesized silver adduct of **2b**. The ester precursor **2a** is solid, unlike the other precursors; this allowed for simple seperation of the adduct from its precursor, whereas in the other cases the adduct was dissolved in its viscous ionic liquid precursor, which made seperation through recrystallization impossible. All adducts were found to be air and light sensitive, however not to the same extent as the carboxylate attempts presented earlier. **3a** was found to be stable in air for up to 5 days, and stable under argon for 10 days in a vessel sheltered from light. The adducts were also found to be preferentially stable in coordinating solvents such as acetonitrile and THF as opposed to chlorinated solvents, wherein silver chloride precipitation was observed after several hours.
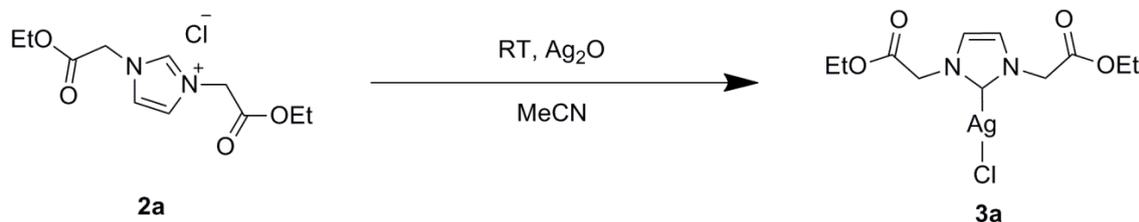
Scheme 2.9 Synthesis of Ag–NHC complex from imi-ester. Reaction conditions: 3 mmol **2a,** 3 mmol mol Ag$_2$O, 8 ml MeCN, RT, 8 hours

Complex **3a** was successfully purified for full characterization using ESI-MS, NMR and Elemental Analysis techniques. The mass spectrum for **3a** displays a peak pattern at m/z 587 and 589, typical of the isotopic pattern expected for ^{107}Ag and ^{109}Ag at the typical abundance ratios. This is also the expected peak for the [(NHC)$_2$Ag]+ bis-carbene structure rather than the mono-carbene, a common observation for linear and dimeric mono-NHC-Ag complexes. The ^{13}C NMR spectrum reveals a sharp singlet at 183.54 ppm for the carbenic carbon atom, typically observed for Ag complexes of this geometry. Despite the fact that both ^{107}Ag and ^{109}Ag have a nuclear spin of 1/2 and are therefore NMR active, the expected double-doublet motif is commonly not observed for the carbenic carbon resonance in Ag-NHC-X complexes. A proposed reason for this is the fluxional behaviour of the complex in solution, in which the NHC–Ag species can radpidly and

reversibly form a bis- NHC–Ag–NHC species. The dynamics of this fluxionality are too fast to observe on an NMR time scale.[71]

3a was additionally isolated as a single crystal for X-Ray crystallography by slow vapour diffusion of diethyl ether into a solution of **3a** in dichloromethane (figure **2.2**).
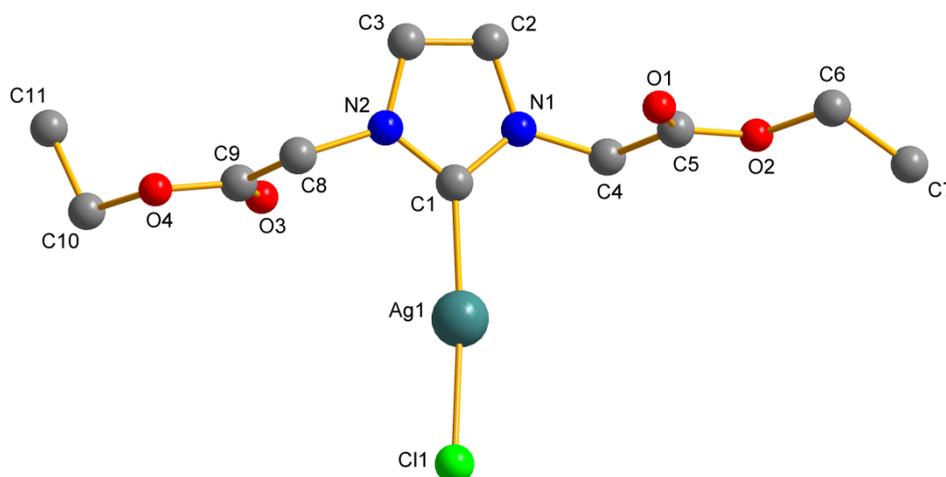
Figure 2.2 Molecular structure of **3a** monomer, H atoms omitted for clarity

Bond length [Å]	3a
Ag—C	2.097(2)
Ag—Cl	2.3882(6)
Bond angle [°]	
N—C—N	103.81(17)
Cl—Ag—C	167.53(5)

Table 2.4 Selected bond lengths and angles of **3a**

The structure was determined to be a chloride-bridged dimer, which was ascertained upon expanding the structure outside the asymmetric unit (figure **2.3**). The first indicator of this structure is the slightly distorted linear geometry, since an Ag-NHC-Cl bond angle of 167.53 ° is observed in the asymmetric unit (table **2.4**). This is supported by an intermolecular Ag-Cl distance of 2.997 Å, falling within the limit of the van der Waals radii. As this work was being conducted, the X-Ray structure of this complex was published by Santini *et al*.[191]
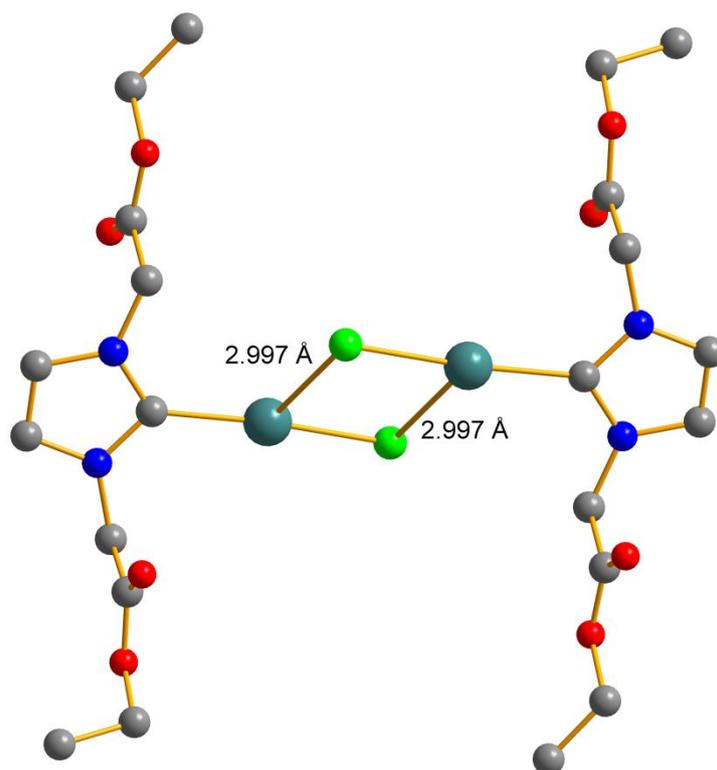
Figure 2.3 Molecular structure of **3a** dimer. Ellipsoids drawn at the 50% probability level, H atoms omitted for clarity

2.2.2.2 Bis–NHC–Palladium

The isolated silver adduct **3a** was used in a transmetallation reaction using $Pd(OAc)_2$ and $PdCl_2$ as palladium(II) sources. Two equivalents of the silver adduct were stirred in acetonitrile solvent at room temperature with the palladium source to yield a white solid and pale yellow solid in the case of $Pd(OAc)_2$ and $PdCl_2$ respectively (table **2.3**). Attempts were also made to transmetallate directly from solution for the unisolated Ag adducts, however only **2b** successfully yielded palladium complexes via this route. Imidazolium esters **2c**, **2d**, and **2e** were unsuccessful in transmetallation, possibly as a result of the comparably poor yield of the Ag adduct.
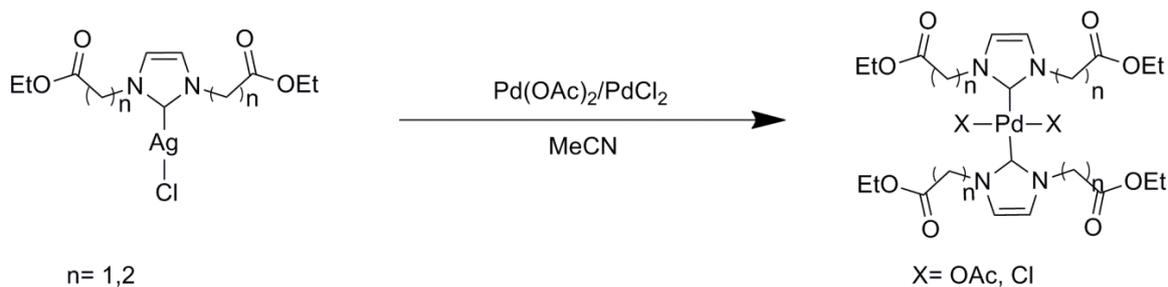
Entry	Structure	Yield [%]
4a		44
4b		22
5a		36
5b		40

Table 2.3 Synthesized bis–NHC–Pd complexes and respective yields. Reaction conditions: 3 mmol siver adduct, 1.5 mmol Pd(OAc)$_2$/PdCl$_2$, 8 ml dry acetonitrile, RT, 12 hours

^{1}H NMR analysis of each complex revealed the peak associated with the acetate CH$_3$ group (1.57 ppm for **4a** and 1.96 ppm for **4b**) in complexes **4a** and **4b** at a 1:1 ratio with the ligands, revealing that acetate remains as the coordinating anion in each complex, rather than being displaced by Cl^{-} from the silver precursor. The ESI-MS spectra reveals the expected isotopic peak pattern for [104]Pd, [105]Pd, [106]Pd, [108]Pd and [110]Pd, and the extra peaks observed for the complexes containing chlorine as a result of [35]Cl and [37]Cl. The observed fragment in each case is that of the [(NHC)$_2$PdCl][+] ion, typical of bis-NHC Pd complexes.[107]

Complexes **4a**, **5a**, and **5b** were grown as single crystals for X-Ray crystallographic analysis, complex **4b** could only crystallize in very small clusters under various conditions and was thus

unable to be analyzed. Each complex was determined to be square-planar, with the NHC ligands coordinated *trans* to each other. This geometry is typically common for bis-NHC complexes, since the steric bulk of the ligand cannot accommodate *cis* coordination around the metal centre. NHC complexes with *cis* coordination geometry have been reported previously in the literature, however only for ligands with non-bulky N-bound R groups. [51]

Complex **4a** was isolated as a single crystal by diffusing THF into a solution of the complex in CHCl$_3$ (figure **2.4**). The structure adopts a very slight distortion to the square planar geometry, with an angle of 178 ° between the NHC ligands (table **2.4**). Bond lengths are typical of those of analogous complexes, however a noteworthy comment is the slight difference in length of the Pd–C bond between the different NHC ligands. The longer Pd–C bond (see table) is assumed to be a result of the steric influence of the opposite NHC ligand, since the N-bound groups are pointed in more closely to the sphere of coordination. Despite this, the carbonyl oxygen atoms are still too far away from the metal centre to have any influence on coordination.
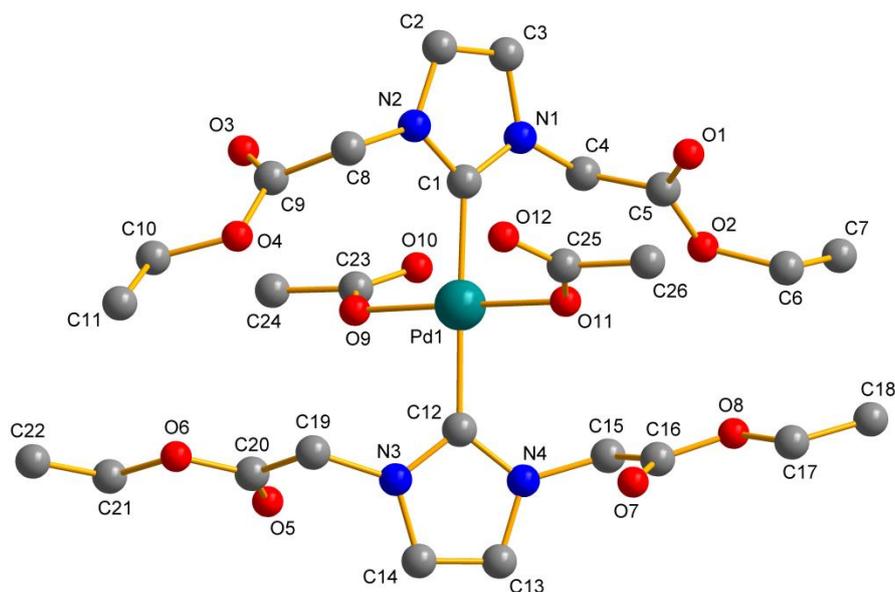
Figure 2.4 Molecular structure of **4a**. Ellipsoids drawn at the 50% probability level, H atoms omitted for clarity

| Bond length [Å]	4a
Pd—C1	2.023(2)
Pd—C12	2.039(2)
Pd—O9	2.023(2)
Pd—O11	2.020(2)
Bond angle [°]	
N—C1—N	104.8(2)
N—C12—N	104.4(2)
O—Pd—O	179.22(8)
C—Pd—C	178.28(10)
O9—Pd1—C1	91.47(9)
O9—Pd1—C12	89.21(9)
Dihedral angle [°]	
Pd/O2/C2 // N1/N2/C1-C3	68.32(6)
Pd/O2/C2 // N7/N8/C34-C36	45.82(6)

Table 2.4 Selected bond lengths and angles of **4a**

Complex **5a** and **5b** were both isolated as a single crystal by diffusing THF into a solution of the complex in CH_2Cl_2. Two molecules of **5a** were discovered within the asymmetric unit (figure **2.5**). Both structures feature very similar interatomic distances, however the dihedral angles between the NHC ligands (N-$C_{carbene}$-$C_{carbene}$-N) vary significantly; 9.2 ° was calculated for molecule 1, and 37.1 ° for molecule 2 respectively (table **2.5**). Dihedral angles between the Cl–Pd–Cl and N–C–N planes are similar, varying between 61–69°. Intermolecular interactions typically consist of interactions between Cl–H and O–H as noted from molecule packing within the unit cell, however these are not classical hydrogen bonds. For molecule **5b** (figure **2.6**), a half-molecule was found within the asymmetric unit, the full molecule is generated upon applying a C_2 symmetry element; therefore the molecule displays rotational symmetry. Similar intermolecular interactions are observed to those of **5a**. For both structures of **5a**, the carbonyl oxygen atoms face away from the plane of coordination, whereas in **5b** the oxygen atoms lie in parallel with the coordination plane. However, as with **4a**, oxygen atoms are too distant from the metal centre to have any coordination influence.
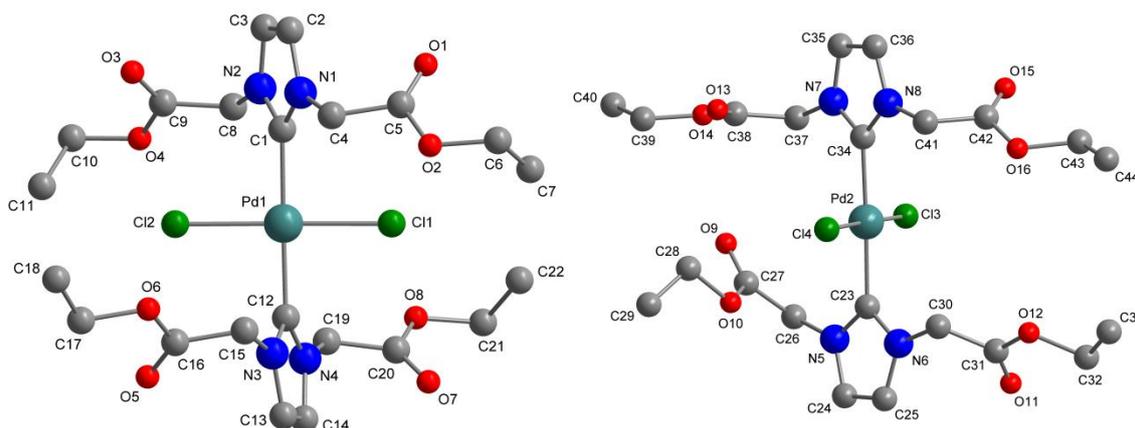
Figure 2.5 Molecular structures of **5a** molecules 1 (left) and 2 (right), orientations are not representative of the unit cell. H atoms omitted for clarity
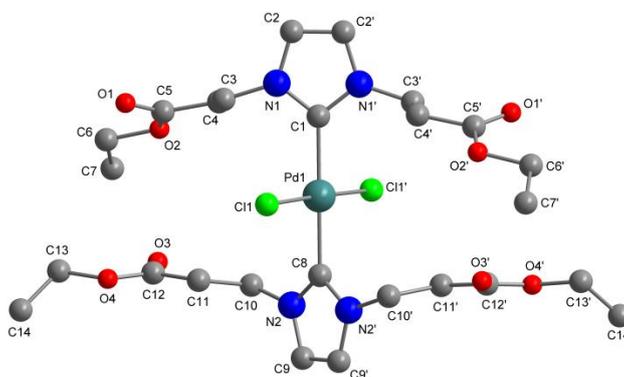
Figure 2.6 Molecular structure of **5b**, repeated atoms reproduced by symmetry. H atoms omitted for clarity

Bond length [Å]	5a	5b
Pd—C1 [C34]	2.033(3) [2.024(3)]	2.029(3)
Pd—C12 [C23] / C8	2.030(3) [2.018(3)]	2.021(3)
Pd—Cl1 [Cl3]	2.3100(8) [2.2998(9)]	2.3124(5)
Pd—Cl2 [Cl4]	2.3139(8) [2.2983(9)]	2.3124(5)
Bond angle [°]		
N—C1—N [N—C34—N]	104.1(3) [104.2(3)]	104.5(2)
N—C12/C8—N [N—C23—N]	104.2(3) [104.6(3)]	104.7(2)
Cl—Pd—Cl	178.73(3) [178.94(3)]	178.31(3)
C—Pd—C	177.0(1) [178.4(1)]	180.0
Cl1—Pd1—C1 [Cl3—Pd2—C34]	90.84(9) [91.43(9)]	90.85(1)
Cl1—Pd1—C12/C8	88.51(9)	89.15(1)
[Cl3—Pd2—C23]	[89.4(1)]	-
Dihedral angle [°]		
Pd/Cl2/C2 // N1/N2/C1-C3	68.5(1)	-
Pd/Cl2/C2 // N7/N8/C34-C36	[61.3(1)]	-
Pd/Cl2/C2 // N3/N4/C12-C14	69.0(1)	-
Pd/Cl2/C2 // N5/N6/C23-25	[69.0(1)]	-
Pd/Cl2/C2 // N1/N1_i/C1/C2/C2_i	-	68.44(7)
Pd/Cl2/C2 // N3/N4/C12-C14	-	69.0(1)

Table 2.5 Selected bond lengths and angles of **5a** and **5b**

2.2.2.3 Mono-NHC–Palladium (PEPPSI-type)

Mono-NHC Pd complexes were approached using a modified procedure to that of Organ *et al* to synthesize PEPPSI-type complexes. One equivalent of precursors **2a**–**2d** was stirred with $PdCl_2$, using pyridine as the solvent (table **2.6**). The weak base K_2CO_3 was used in order to prevent side-products from undesired α-carbonyl deprotonation. All products were produced as expected, with one coordinated NHC ligand and one labile pyridine ligand as confirmed by ^{1}H NMR. The synthesis was found to be relatively sensitive to heat, with higher temperatures generally preferred, particularly for complexes **6c** and **6d**. Temperatures of around 45 °C would tend to preferentially produce the side product $Pd(py)_4Cl_2$ (tetra-pyridine $PdCl_2$), whereas 55–60 °C produced the desired NHC complex in better yield. Complexes **6a** and **6b** were formed in much higher yield than the phenylalanine and alanine-derived complexes **6c** and **6d**, the latter case being the poorest. This is associated with a higher pK_a for the position α- to the ester group in precursors **2c** and **2d**, as a result of tertiary alkyl substitution; this is likely to cause unwanted enol-based side products. ESI-MS analysis of the crude product displayed primarily the [(NHC)Pd(py)Cl][+] fragment, however the [(NHC)PdCl][+] fragment was also present in each case; in the cases of **6c** and **6d** this was the dominant fragment.

R = CH$_2$COOEt, (CH$_2$)$_2$COOEt,
CH(CH$_2$Ph)COOEt, CH(CH$_3$)COOEt
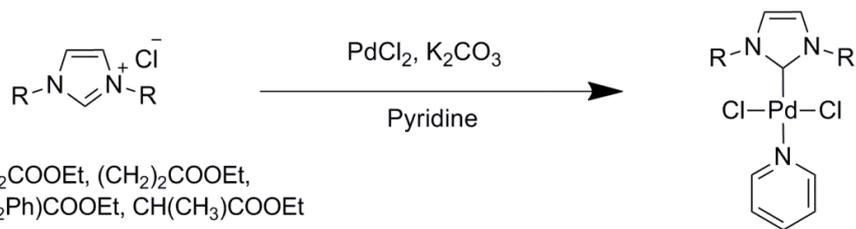
Entry	Structure	Yield [%]
6a		36
6b		30
6c		26
6d		11

Table 2.6 Synthesized Pd–PEPPSI complexes and respective yields

Complexes **6a, 6b** and **6d** were also isolated as single crystals for X-Ray analysis. **6a** and **6b** were crystallized by diffusing petroleum ether 60–80° into a solution of the respective complex in CHCl$_3$ (figures **2.7** and **2.8**), **6d** was crystallized from a solution of acetone at -20°C (figure **2.9**). The structures in each case confirm the expected coordination of the NHC *trans* to the pyridine in a square planar geometry. In each case Pd–C bond lengths are within the typical range (table **2.7**). [193] Dihedral angles between the Cl–Pd–Cl plane and the N–C–N plane of the NHC are wider in both cases than that of the angle between the Cl–Pd–Cl plane and the plane of the pyridine ring, most likely due to sterics. The packing of **6a** is completed by a chloroform molecule, interactions are observed between coordinated Cl atoms and chloroform H atoms. For **6b** only one packing interaction is observed in the unit cell between coordinated Cl and imidazolium H atoms. Outside of the unit cell, a distance between offset pyridine rings of 3.981 Å could be an

indication of intermolecular π-π stacking. The asymmetric unit of **6d** is completed by an acetone molecule. Intermolecular interactions are observed between pyridine H atoms and acetone O atoms, however this is too long a distance to be considered a classic H-bond. As with the bis complexes, oxygen atoms have no influence on the coordination sphere.
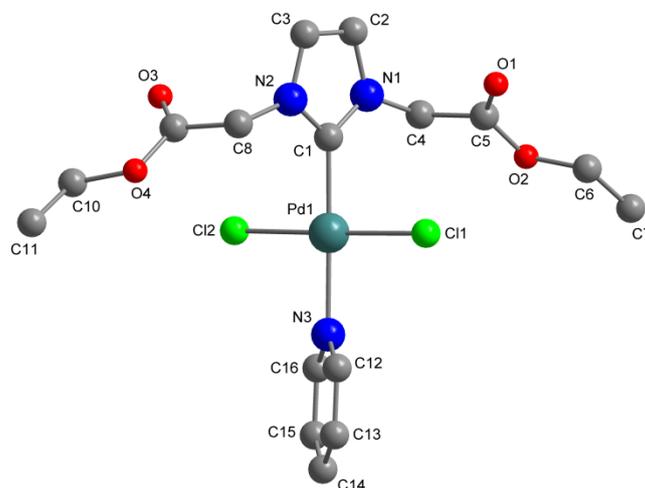
Figure 2.7 Molecular structure of **6a.** H atoms and CHCl$_3$ molecule omitted for clarity
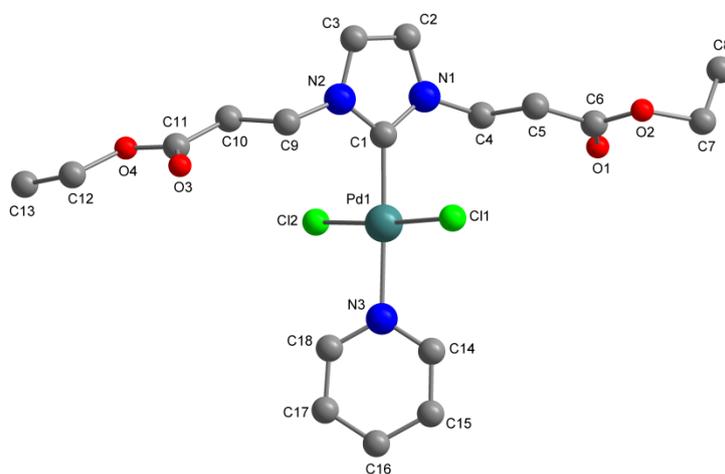
Figure 2.8 Molecular structure of **6b.** H atoms omitted for clarity
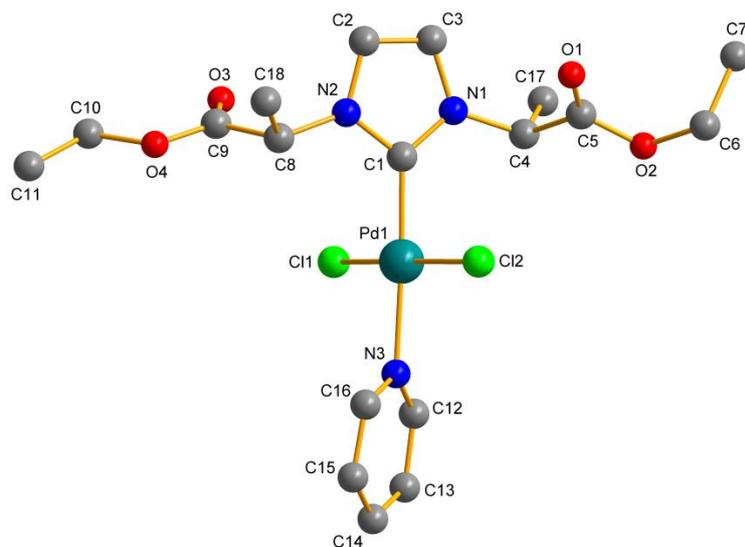
Figure 2.9 Molecular structure of **6d.** H atoms and acetone molecule omitted for clarity

Bond length [Å]	6a	6b	6d
Pd1—C1	1.969(2)	1.958(2)	1.951(14)
Pd1—N3	2.091(2)	2.110(2)	2.098(10)
Pd—Cl1	2.3046(6)	2.2988(5)	2.272(4)
Pd—Cl2	2.3014(6)	2.3167(5)	2.297(4)
Bond Angle [°]			
N1—C1—N2	105.0(2)	105.7(2)	103.6(10)
Cl1—Pd1—Cl2	177.58(3)	176.21(2)	175.15(15)
C1—Pd1—N3	178.00(9)	177.50(6)	177.3(4)
Cl1—Pd1—C1	89.12(6)	87.60(5)	89.8(4)
Cl1—Pd1—N3	90.49(6)	91.87(5)	89.2(3)
Dihedral Angle [°]			
Pd/Cl2/C2 // N1/N2/C1-C3	75.40(5)	-	75.79(32)
Pd/Cl2/C2 // N3/C12-C16	47.82(8)	-	60.48(27)
Pd/Cl2/C2 // C1/N1/C2/C3/N2	-	79.50(5)	-
Pd/Cl2/C2 // N3/C14-C18	-	39.35(7)	-

Table 2.7 Selected bond lengths and angles of **6a** and **6b**

2.2.2.4   Iridium

The iridium(I) complex **7a** was also successfully synthesized via transmetallation from silver adduct **3a** (scheme **2.10**)**.** A yellow solid was formed after stirring the adduct at room temperature with [Ir(COD)Cl]$_2$ in CH$_2$Cl$_2$. In the ^{1}H NMR spectrum, a strong AB type splitting is observed for the peak representing the NCH$_2$ protons of the N-bound group along with a strong roofing effect. This indicates a hindered rotation of the C–Ir bond, causing the otherwise equivalent protons to become diastereotopic. This same effect is observed in the analogus rhodium complex synthesized by Herrmann *et al*,[178] as well as a number of similar Ir(I)-NHC complexes synthesized by Crabtree *et al*.[194]
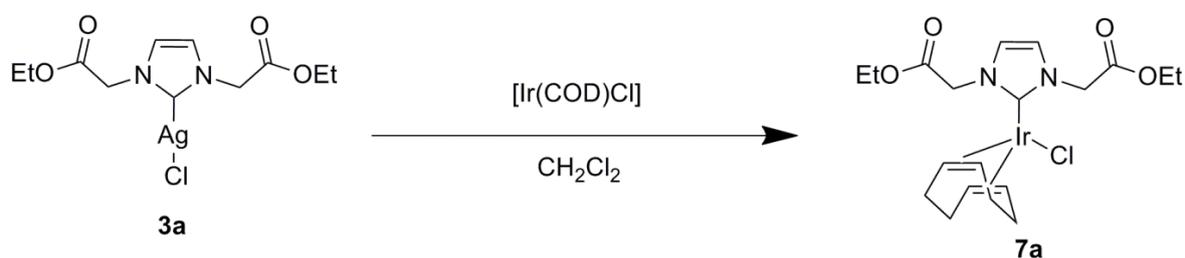
Scheme 2.10 Synthesis of **7a** via transmetallation from **3a.** Reaction conditions: 0.65 mmol **3a**, 1.3 mmol [Ir(COD)Cl]$_2$, 5ml dry CH$_2$Cl$_2$, RT, 24 hours.

Single crystals suitable for X-Ray analysis were isolated by diffusing diethyl ether into a solution of the complex in CH$_2$Cl$_2$. The structure reveals a square planar geometry of Ir(I), with the cyclooctadiene coordinations *cis* to each other and atoms C12 and C13 *trans* to the NHC, in the typical "boat" confirmation observed when coordinated to metals (figure **2.10**). The bond lengths of Ir–C12 and C13 (*trans* to NHC) are significantly longer than those of Ir–C16 and C17 (*trans* to Cl), highlighting the stronger *trans* influence in the σ-donation of the NHC ligand (table **2.8**). The torsion angle of the NHC to the Ir–Cl plane (N-C-Ir-Cl) is 88.0 °, almost a right-angle; meaning that the NHC is coordinated pretty much orthogonally to the chlorine. Intermolecular interactions in the packing are dominated by Cl–H and O–H interactions, however none of these are classical hydrogen bonds.
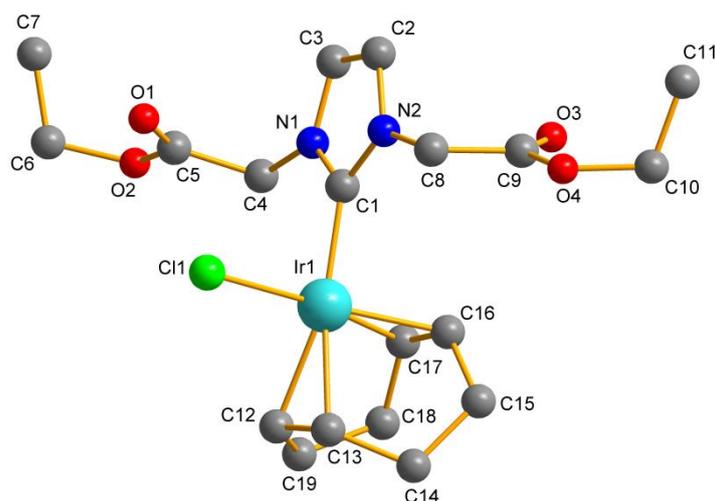
Figure 2.10 Molecular structure of **7a**. Ellipsoids drawn at the 50% probability level, H atoms omitted for clarity

Bond length [Å]	7a
Ir—C1	2.026(5)
Ir—Cl	2.352(1)
Ir—C12	2.167(5)
Ir—C13	2.196(5)
Ir—C16	2.093(4)
Ir—C17	2.118(4)
Bond angle [°]	
N—C1—N	103.9(4)
Cl—Ir—C1	89.47(11)
Cl—Ir—C12 [C13]	89.59(11) [92.80(13)]
Cl—Ir—C16 [C17]	157.80(11) [162.37(10)]
C1—Ir—C12 [C13]	156.88(16) [165.93(16)]
C1—Ir—C16 [C17]	91.86(16) [92.79(17)]
Dihedral Angle [°]	
Ir/Cl/C16-C17 // C1/N2/C2/C3/N2	86.98(18)
Ir/C12-C13 // C1/N2/C2/C3/N2	5.70(22)

Table 2.8 Selected bond lengths and angles of **7a**

2.3 Sterics and electronics

2.3.1 Bond lengths and electronics

The influence that an NHC has on a metal centre when coordinated depend on its steric and electronic properties. The factor that makes NHCs so attractive as ligands is the ability to tune these properties depending on their structure. With regards to electronics, σ-donation is the most important factor, although the ability of an NHC to π-backbond has also been shown to

influence the activity of the metal towards application.[66] A number of methods have been developed to probe the σ-donating ability of an NHC which utilize the *trans* influence phenomenon.[177] The most commonly applied method of quantifying the electronic properties of the NHC–M bond is the Tolman Electronic Parameter (TEP), which involves measuring the IR stretching frequency of the CO triple bond in metal NHC complexes with carbonyl ligands located *trans* to the NHC.[195] The greater the electron density on the metal, the greater the degree of π-backbonding into the π^*_{CO} anti-bonding orbital, thereby weakening the CO bond, which is observed via IR spectroscopy. Another method of quantitatively measuring the degree of σ-donation exerted by a ligand can be performed by observing the length of the bond coordinated *trans* to the ligand of interest for complexes of octahedral and square planar geometry, since the two ligands use the same metal d-orbitals to bond. The greater the electron density donated to the metal, the less polarized the bond of the *trans* ligand.

Since the scope of this work did not include the synthesis of $[M(NHC)(CO)_n]$ type complexes, a qualitative comparison can be made based on the length of the M–pyridine bond in the Pd-PEPPSI complexes. This is also a common method for judging σ-donor ability, utilizing the *trans* influence phenomenon.[196, 197] As expected, the Pd–C lengths of complexes **6a**, and **6b** are inversely related to the lengths of the Pd–N bond, highlighting the *trans* influence (table **2.9**). Complex **6a** features very similar bond lengths to those of typical Pd-PEPPSI complexes, in particular the commercial ligand IMes. However the Pd–C bond is significantly shorter for **6b**, likewise the Pd–N bond is longer, this could indicate an increased σ-donation ability to the Pd metal centre. The exception to this rule is the IPr-PEPPSI complex which features a longer Pd–N bond than **6b** despite also having a longer Pd–C bond, this is likely a result of the much greater steric effect exhibited by the IPr ligand. **6d** has a shorter Pd–C length than **6b**, but also a shorter Pd–N length, which does not fit the pattern. However the standard deviations for this particular structure are greater than those of the other two compounds, making this comparison statistically insignificant.

In general, the bond length comparisons for complexes **6a**, **6b**, and **6d** do not differ substantially to those of common and commercial NHC ligands within PEPPSI complexes. This suggests that the imidazolium-ester NHC ligands feature similar electronic properties to those of common NHC structures, in particular σ-donation.

Complex	Pd–C$_{carbene}$ bond length [Å]	Pd–N$_{pyridine}$ bond length [Å]
6a	1.969(2)	2.091(2)
6b	1.958(2)	2.110(2)
6d	1.951(14)	2.098(10)
IMes-PEPPSI [198]	1.969(2)	2.093(2)
IPr-PEPPSI [199]	1.964(3)	2.116(3)
IBenz-PEPPSI [196]	1.968(2)	2.093(2)
IMe-PEPPSI [200]	1.972(8)	2.084(8)

Table 2.9 *Trans* effect comparison of Pd–C and Pd–N bond lengths of Pd–PEPPSI complexes

2.3.2 Steric influence and %V_{bur}

The steric environment of a metal is closely related to the electronic properties, and plays a huge influencing factor when considering the activity of a metal complex. Most of the models used to quantify the steric influence of a ligand takes account of the physical space occupied by a ligand. The most widely used is still the Tolman Cone Angle,[195] originally used for tertiary phosphine ligands, which uses the apex angle of a cone shape centered at the metal to judge how far the van der Waals radii of the outermost ligand substituents span around the coordination centre. This model however fails for NHCs, since it assumes symmetrical substituents and full rotation of the C–M bond. Nolan and Cavallo have since proposed the percent buried volume (%V_{bur}) model, which calculates the space occupied in a spherical radius around the metal centre (figure **2.11**).[67] This model suits the steric nature of NHC ligands much better, and can easily be used to compare analogus complexes. Cavallo *et al* have since developed a piece of software (Samb*V*ca) which allows simple calculation of %V_{bur} simply using crystallographic information, available free online.[201]
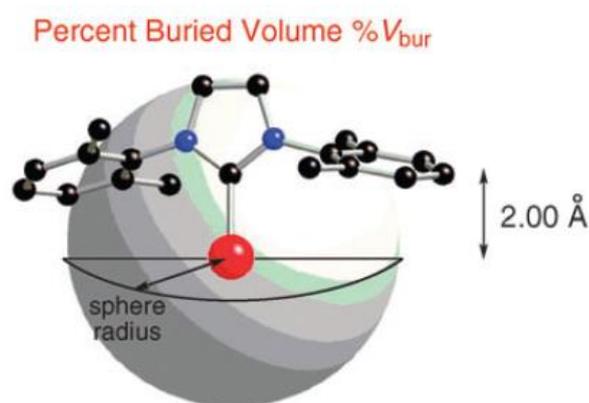
Figure 2.11 Illustration of Percent Buried Volume (%V_{bur}). Adapted from ref [69]

Values of %V_{bur} were calculated using the Samb$V$ca application for all complexes in order to compare steric environments with commercial and previously investigated NHC ligands in analogus complexes (table **2.10**). Initial observations show that the Glycine, β-alanine, and Alanine-derived ligands (**a, b** and **d** respectively) typically display a smaller percentage of coordination sphere occupation in comparison to commercial ligands for all complex types, particularly exaggerated for the smaller Ag atom. This suggests that the steric bulk of the N-bound groups does not actually manifest any effect on the metal centre, despite being longer and bulkier. This is most likely because the rotation around each bond creates several more degrees of freedom, allowing the alkyl moieities to be orientated away from the metal centre. The ligands **a b** and **d** show more steric resemblance to the IBenz ligand, which also has an extra carbon linkage; affirming the relationship between an α-CH$_2$ linkage and lower %V_{bur} values.

More interestingly, the ligand **b** shows a marginally greater buried volume in the bis–Pd complexes, whereas **a** has a significantly greater buried volume in the mono–Pd complexes. This is mostly likely a result of the different orientations of the R-group in the different solid-state packing structures of each complex, since the alkyl moieties are subject to free rotation. The poorer steric influence of **a** and **b** compared to commercial NHCs could mean that these NHCs are less well-suited for catalytic applications within which sterics play a crucial role, particularly if the catalytic cycle involves a reductive elimination step. This stands to reason that the chirality featured within ligand **d** would not be close enough to the sphere of coordination to have any steric effect on bound groups, and thus may not have a great influence in enantioselective catalysis.

Complex	%V_{bur}	Complex	%V_{bur}
(NHC)AgCl		**(NHC)PdCl$_2$(py)**	
3a	29.8	**6a**	29.8
(IMes)AgCl [69]	36.1	**6b**	27.6
(IPr)AgCl [69]	46.5	**6d**	27.3
(IBenz)AgCl [69]	32.1	**IMes-PEPPSI** [200]	34.3
		IPr-PEPPSI [199]	34.5
		IBenz-PEPPSI [196]	31.5
(NHC)$_2$PdCl$_2$		**(NHC)Ir(COD)Cl**	
5a	28.0	**7a**	27.8
5b	28.8	**(IMes)Ir(COD)Cl** [69]	33.0
(IPr)$_2$PdCl$_2$ [69]	33.9	**(IPr)Ir(COD)Cl** [69]	34.9
(IMes)$_2$PdCl$_2$ [69]	35.5		

Table 2.10 Comparison of %V_{bur} in NHC–M complexes. Samb*V*ca settings: Sphere radius 3.5 Å, bond length 2.0 Å, mesh spacing 0.05Å. Hydrogen atoms omitted from %V_{bur} calculation. All literature complex values taken from reference [69], except for the IMes, IPr and IBenz PEPPSI-type complexes which were calculated using crystallographic data provided within the referenced articles.

3.   Catalytic screenings of Pd–NHC complexes

Metal–NHC complexes have played an increasingly significant role in catalysis, a central theme within green chemistry. Since the work within this thesis has green chemistry and biorefinery at its core, catalytic reactions directed towards upgrade of bio-derived molecules were initially targeted. Initial attempts to evaluate the catalytic activity within oxidation of alcohols (**3.2**) using the bis-NHC–Pd complexes presented in chapter **1** were unsuccessful. This led us to conclude that the amino acid-derived ligands would not be catalytically competitive with a number of existing systems; however the advantage of these ligands lies instead in the easily-functionalisable α-carbonyl groups. Therefore, through hydrolysis of the ester groups, the mono-NHC–Pd complexes were successfully utilized for aqueous-phase Suzuki cross-coupling reactions with very good yields (**3.1**). This reaction, whilst still within the scope of green chemistry, allows the advantageous properties of the amino acid-derived ligands to be exploited.

3.1   Aqueous-phase Suzuki-Miyaura aryl couplings

Amino acids have not been extensively explored as bio-derived molecules for NHC functionalization. It was predicted that the amino acids' inherent water solubility could be utilized for aqueous-phase reactions. Based on the examples in part **1.3.3**, exploring amino-acid derived NHCs for their water solubility was a suitable application, and Suzuki-Miyaura couplings were chosen as an appropriate reaction to illustrate their suitability towards aqueous-phase catalysis. The ester-functionalized NHC complexes synthesized in **2.2.1** could either be inherently water soluble, or water-solubility could be induced via ester hydrolysis, in the style of Herrmann *et al* (scheme **3.1**).[178]
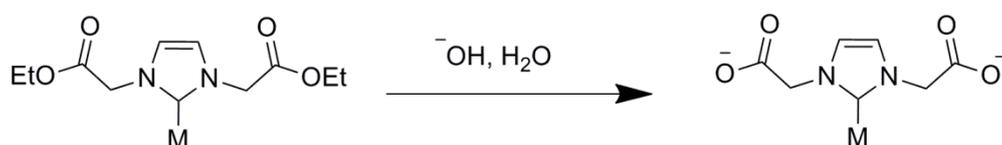
Scheme 3.1 Proposed induction of water solubility via hydrolysis of ester arms. Similar to that reported by Herrmann *et al*[178]

3.1.1   *In-situ* attempts with Pd(OAc)$_2$ and free ligand precursor

Initial attempts to evaluate the effect of the amino-acid derived ligands were performed as *in-situ* ligand and palladium(II) salt screenings in methanol solvent. The coupling of 4-

bromoanisole with phenylboronic acid was tested as a model reaction using a 1:1 ratio of Pd(OAc)$_2$ to ligand precursor. Imidazolium esters **2a**, **2b**, and **2c** were added into the reaction alongside the Pd(II) salt and reacted for 1 hour at room temperature. GC-MS analysis revealed that the esters had no favourable effect on the reaction (table **3.1**). On the contrary, conversions of the bromoanisole to the desired product 4-methoxybiphenyl were actually significantly hindered compared to a system with no free ligand, instead promoting the formation of the biphenyl by-product.
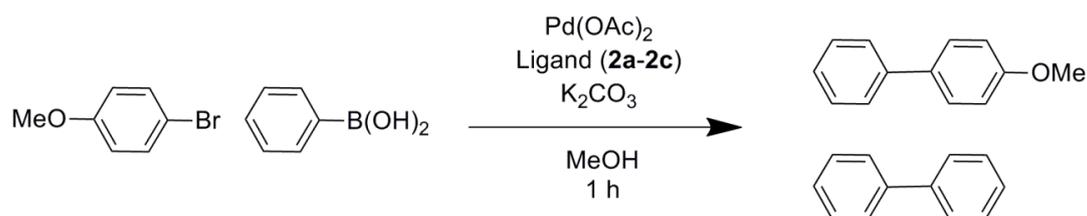
Entry	Added Ligand	Conversion (4-methoxyphenyl) (%)	Conversion (biphenyl) (%)
1	None	73	13
2	2a	56	25
3	2b	45	15
3	2c	57	24

Table 3.1 Attempted catalytic screenings and resulting conversions. Reaction conditions: 1mmol 4-bromoanisole, 1.5 mmol phenylboronic acid, 5 mol% Pd(OAc)$_2$, 5 mol% ligand precursor, 2 mmol K$_2$CO$_3$, 5 ml MeOH, room temperature.

There could be a number of possible reasons for the drop in overall yield upon introducing the imidazolium salt. Since the ester arms of the imidazolium salts are susceptible to hydrolysis, the base could be used in the hydrolysis side-reaction, rendering it unavailable for the coupling.

Another reason could be the preferred formation of a bis-complex *in-situ*, which are not as active as Pd(OAc)$_2$ under low-temperature conditions, as will be demonstrated in part **3.3.2.1**.

3.1.2 Complex screening

3.1.2.1 Water solubility

Based on the *in-situ* studies, the aqueous-phase studies were conducted using the synthesized complexes. Initially, bis-NHC complexes **4a–5b** were tested for the bromoanisole coupling in pure water at 80 °C over 24 hours. ^{1}H NMR was used to calculate yields with the addition of a trimethoxybenzene internal standard, to avoid contaminating the GC column with residual water. Analysis showed that although no biphenyl byproduct was observed, no significant difference was observed between using Pd(OAc)$_2$ and the complexes in catalysis, each producing poor yields for 4-methoxybiphenyl (table **3.2**). Attempts at optimizing the conditions, including choice of base and temperature did not bring any substantial improvement. Interestingly, raising the temperature to 100 °C significantly reduced yields.
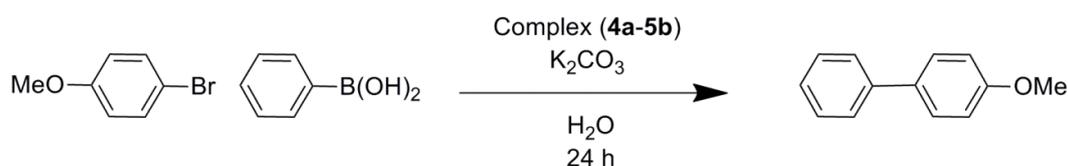
Entry	[Pd]	Temperature (°C)	Base	Yield (4-methoxybiphenyl) (%)
1	Pd(OAc)$_2$	80	K$_2$CO$_3$	28
2	**4a**	80	K$_2$CO$_3$	31
3	**4b**	80	K$_2$CO$_3$	30
4	**4b**	50	KOH	36
5	**4b**	100	K$_2$CO$_3$	5
6	**4b**	100	KOH	8
7	**4b**	100	NaOAc	2
8	**5a**	80	K$_2$CO$_3$	30
9	**5b**	80	K$_2$CO$_3$	25

Table 3.2 Attempted catalytic screenings and resulting conversions. Reaction conditions: 0.5 mmol 4-bromoanisole, 0.75 mmol phenylboronic acid, 2 mol% [Pd], 1 mmol base, 2 ml H$_2$O.

The reason for this poor activity became clear when a solubility test revealed that none of the bis-NHC complexes were soluble in water, and were resistant to hydrolysis when heated in water in the presence of base (scheme **3.2**). This was ascertained by observing the lack of colouration of the solution. Additionally, a preliminary test was performed by stirring the complex in D_2O with an excess of K_2CO_3 base, and running the subsequent NMR experiment; no evidence of dissolution or ester hydrolysis was observed.
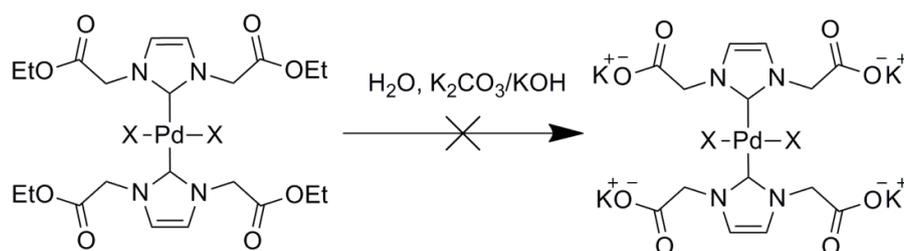
Scheme 3.2 Hydrolysis resilience of the bis–NHC complex esters in water and presence of base. Temperatures from 60–100 °C were tested.

Hydrolysis experiments on the mono–NHC complexes **6a**–**6c** were much more successful. Although not soluble as a standalone complex, stirring each complex with K_2CO_3 base and gentle heating in water produced a transparent yellow solution within one hour with no visible particles (scheme **3.3**). Upon performing the Suzuki coupling with complex **6b** in D_2O, an NMR experiment was performed after separation of the products (with ethyl acetate) to characterize the hydrolysed species. Ethanol peaks were observed in the spectrum, clearly indicating the hydrolysis of the ethyl ester N-bound groups. However the other ligand peaks appeared at a much lower intensity and were often broadened. This suggests that the water-soluble complex species manifests itself as nanoparticles; weak intensity and broadened peaks within solution NMR is typical of NHC ligand peaks bound to nanoparticles in a colloidal dispersion, as previously observed by Chaudret *et al.*[92] Concurrently, any attempt to isolate the hydrolysed complex from solution by vacuum removal of the solvent resulted in a black precipitate, suggesting agglomeration of a nanoparticle species. Dynamic light scattering (DLS) analysis was performed on the resulting dispersion to determine the size of the nanoparticles, however data acquisition was unsuccessful. This may suggest a very small nanoparticle size below the detection limit of 10 nm. Nanoparticle formation will be discussed in more detail in a later section.
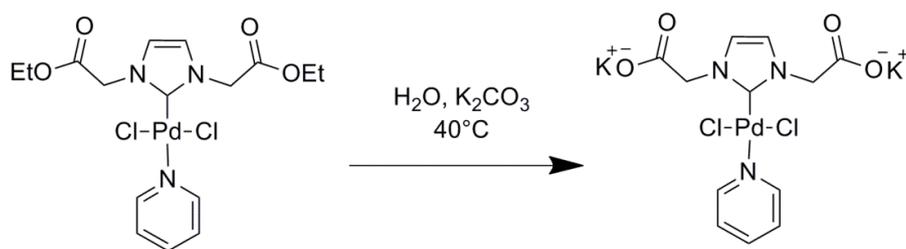
Scheme 3.3 Successful hydrolysis of mono–NHC complex esters in the presence of water and base
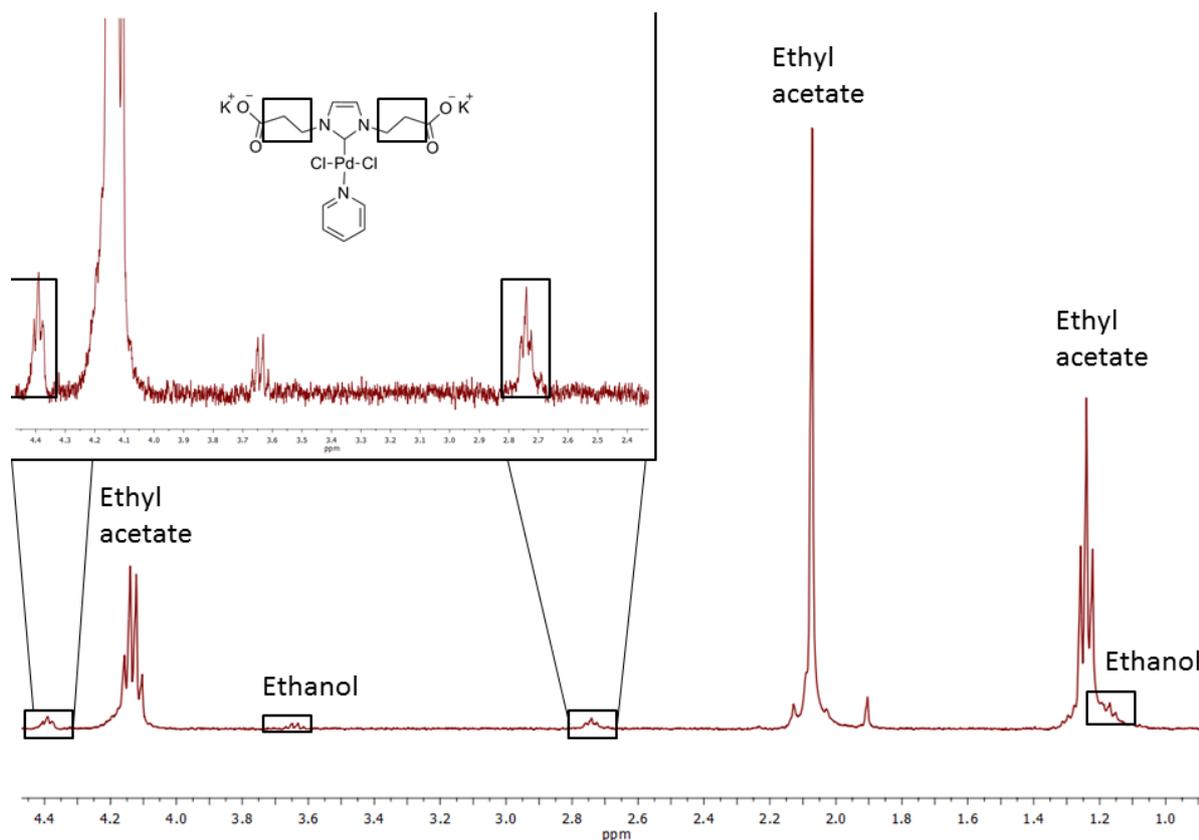
Figure 3.1 Section of the ^{1}H NMR spectrum of hydrolyzed **6b** dissolved in D_2O

Since water solubility is induced via the hydrolysis of the ester arms, the base employed within the Suzuki reaction in this case plays a second role of inducing water solubility. Therefore the active catalyst can be produced by two different strategies: pre-dissolution by hydrolysing the complex with the base prior to the start of the reaction, or *in-situ* dissolution by adding all reagents at the same time. The effect of each of these dissolution strategies upon the resulting yield was investigated using the bromoanisole coupling with complex **6b** (table **3.3**). The pre-dissolution method was determined to produce a higher yield, but not significant enough to suggest any difference between the two dissolution methods.

Pre-dissolution yield (%)	*In-situ* dissolution yield (%)
80	76

Table 3.3 Comparison of the yields from the coupling of bromoanisole and phenylboronic acid using pre-dissolved and *in-situ* dissolved precatalyst **6b.** Reaction conditions: 0.5 mmol 4-bromoanisole, 0.75 mmol phenylboronic acid, 2 mol% **6b**, 1 mmol base, 2 ml H_2O, 60 °C. Pre-dissolved catalyst was stirred at temperature in water and base for 2 hours prior to addition of reactants.

3.1.2.2 Optimization of conditions

Initial screenings of each precatalyst were performed under non-optimized conditions at 60 °C using K_2CO_3 base over 24 hours. Complexes **6a**–**6c** were tested for the bromoanisole screening alongside $Pd(OAc)_2$ (table **3.4**), complex **6d** was not screened due to poor complexation yield and difficult separation from its $PdCl_2(Py)_4$ by-product. All complexes produced significantly higher yields than those of $Pd(OAc)_2$, highlighting the enhanced stabilization of the reactive species due to the amino-acid derived NHC ligands, and the advantage of using water-soluble catalytic species. However no great difference is observed between the activities of each complex, despite the vastly different ligand structure. **6c** in particular should have a much greater steric bulk which may assist in reductive elimination of the desired biaryl.[202] This suggests that the amino acid R-groups have no great influence on the steric bulk surrounding the metal centre, supporting the $\%V_{bur}$ (percent buried volume) steric observations reported in section **2.3.2**.
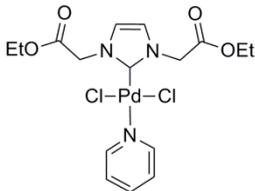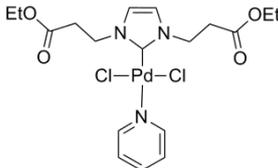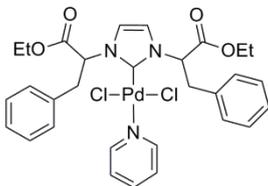
Entry	[Pd]	Yield (%)
1	**6a**	78%
2	**6b**	80%
3	**6c**	78%
4	Pd(OAc)$_2$	32%

Table 3.4 Comparison of the yields from the coupling of bromoanisole and phenylboronic acid using precatalysts **6a–6c.** Reaction conditions: 0.5 mmol 4-bromoanisole, 0.75 mmol phenylboronic acid, 2 mol% [Pd], 1 mmol K$_2$CO$_3$, 2 ml H$_2$O, 60 °C.

Optimization studies were subsequently carried out using complex **6b,** since it was seen to be slightly more active, although this is within the experimental margin of error. Base screening revealed that K$_2$CO$_3$ was still the best base of choice (table **3.5**). The inorganic hydroxide base KOH produced much poorer yields despite typically producing good activity in water-soluble Suzuki couplings; likewise the alkoxide base K^{t}BuO produced poor yields, suggesting the nucleophilicity of the alkoxy-boron intermediate does not play a crucial role in aqueous-phase. Temperature variations revealed an inverse relationship between temperature and yield beyond 60 °C. Raising the temperature above 60 °C produced lower yields, suggesting a destabilization of the active catalyst; however lower temperatures also produced poorer yields. This complicated relationship between temperature and activity suggest a compromise between activity and stability. Lower temperatures do not produce sufficient potential energy to activate the substrates, however higher temperatures encourage catalyst destabilization – further evidence pointing towards nanoparticle agglomeration. 60 °C was therefore chosen as the optimized temperature.

Entry	Base	Temperature (°C)	Yield (%)
1	K_2CO_3	60	80
2	KOH	60	43
3	t-BuOK	60	40
4	K_2CO_3	80	60
5	K_2CO_3	40	49
6	K_2CO_3	RT	32
7	KOH	80	50

Table 3.5 Comparison of the yields for the coupling of bromoanisole and phenylboronic acid using precatalyst **6b** under various conditions**.** Reaction conditions: 0.5 mmol 4-bromoanisole, 0.75 mmol phenylboronic acid, 2 mol% **6b**, 1 mmol base, 2 ml H_2O.

Finally, the effect of a phase-transfer catalyst (PTC) was evaluated by adding tetrabutylammonium bromide (TBAB) before the start of the reaction (table **3.6**). Adding tetraalkylammonium salts, otherwise known as "Jeffery conditions" (covered in section **1.3.3**), has historically improved yields within biphasic base-promoted synthesis by shuttling base between the two phases. The TBAB also plays a role in nanoparticle stabilization, as will be discussed in **3.1.2.5**. Yields were drastically improved using TBAB (1 mmol), even under non-optimized conditions. The improvement of yield at 40 °C with TBAB suggests that higher temperatures in the reactions are required to aid the transfer of substrate or base between the phases.

Entry	Base	Temperature (°C)	Yield (%)
1	K_2CO_3	40	66 [a]
2	K_2CO_3	60	92 [a]
3	t-BuOK	60	88 [a]
4	K_2CO_3	40	44 [b]
5	K_2CO_3	60	80 [b]
6	t-BuOK	60	40 [b]

Table 3.6 Comparison of the yields for the coupling of bromoanisole and phenylboronic acid using precatalyst **6b** with the addition of TBAB**.** Reaction conditions: 0.5 mmol 4-bromoanisole, 0.75 mmol phenylboronic acid, 2 mol% **6b**, 1 mmol base, 1 mmol TBAB, 2 ml H_2O. [a] with TBAB, [b] without TBAB

3.1.2.3 Substrate screening and structure-activity relationship

Using optimized conditions, **6b** was used to screen the coupling of various different aryl halides with phenylboronic acid and phenylboronic acid pincol ester to ascertain the substrate scope of the reaction with different ring positions and electron-donating or withdrawing groups (table **3.7**). A polarized C–X bond aids the oxidative addition process of the aryl halide. Electron-withdrawing groups (EWGs) therefore activate the C–X bond by drawing electron density away from the halogen, thus polarizing the bond. Electron-donating groups on the other hand deactivate the C–X bond by donating electron density towards the centre of the bond.

Substrates featuring electron withdrawing groups (EWGs), such as 4-bromoacetophenone and 1-fluoro-4-bromobenzene display better activities (entries **4** and **8**), whereas moieties featuring electron-donating groups (EDGs), such as 4-bromoanisole and 4-bromo-*N*-dimethylaniline hinder activity (entries **1** and **9**), as is typical for these reactions. Different regioisomers of bromoanisole were screened, revealing an unusual relationship between activities and the position of the EDG. The *para* (4-position) and *ortho* (2-position) anisoles display better yields than the *meta* (3-position) anisole (entries **1, 3** and **2** respectively)**.** This is despite the fact that only the 2 and 4 positions are capable of conjugating electron density to the *ipso* position of a benzene ring, thereby deactivating the C–X bond. The relatively high yield observed for the 1-bromoethylbenzene suggests that the catalyst is also effective at activating benzyl halide substrates as well as aryl halides (entry **7**). The couplings with pinacol esters were also similarly as successful as the phenylboronic acids (entries **14** and **15**), with the exception of the anisole coupling, which revealed a significantly decreased yield (entry **13**). Aryl chlorides were also tested however results were poor, generating only 11 % yield in the most active example (entries **10**, **11** and **12**). Although aryl chlorides are notoriously difficult substrates to activate in water, good yields for aryl chloride couplings have been reported for complexes with a greater steric bulk. This is believed to prevent agglomeration of the active complex into nanoparticles.

$$R \overset{}{\underset{}{\text{Ar}}}-X + \text{Ar}'-R' \xrightarrow[\substack{H_2O\ (2\ ml) \\ 60°C \\ TBAB \\ 24\ h}]{\substack{6b \\ K_2CO_3}} \text{Ph-Ar-R}$$
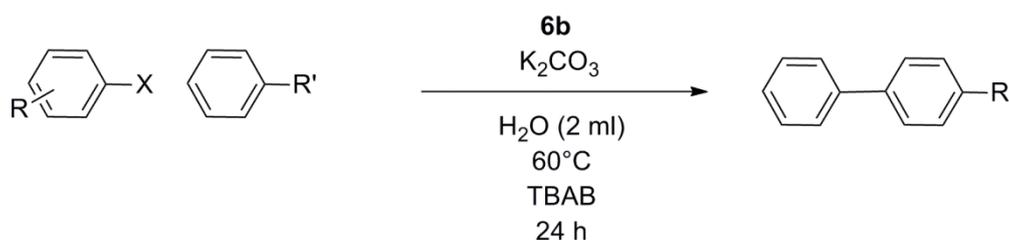
Entry	R	R'	X	Yield (%)[a]
1	4-OMe	B(OH)$_2$	Br	92, 90[b], 85[c]
2	3-OMe	B(OH)$_2$	Br	84
3	2-OMe	B(OH)$_2$	Br	93
4	4-Ac	B(OH)$_2$	Br	95, 94[b], 99[c], 90[d]
5	4-H	B(OH)$_2$	Br	81, 99[b], 56[c]
6	Napthyl	B(OH)$_2$	Br	76
7	4-CH(Br)CH$_3$	B(OH)$_2$	Br	78
8	4-F	B(OH)$_2$	Br	99, 69[c], 53[d]
9	4-N(Me)$_2$	B(OH)$_2$	Br	83
10	4-OMe	B(OH)$_2$	Cl	8
11	4-Ac	B(OH)$_2$	Cl	9
12	4-H	B(OH)$_2$	Cl	11
13	4-OMe	B(CH$_3$)$_4$C$_2$O$_2$	Br	39, 87[b]
14	4-Ac	B(CH$_3$)$_4$C$_2$O$_2$	Br	91
15	4-H	B(CH$_3$)$_4$C$_2$O$_2$	Br	99

Table 3.7 Substrate scope screenings with precatalyst **6b.** Reaction conditions: 0.5 mmol aryl halide, 0.75 mmol phenylboronic acid/ester, 1 mmol base, 1 mmol TBAB, 2 ml H$_2$O, 60 °C, 24 hours. [a] 2 mol% **6b**, [b] 1 mol% **6b**, [c] 0.1 mol% **6b**, [d] 0.01 mol% **6b.**

A number of substrates were additionally screened with a reduced catalyst loading. In most accounts where 1 mol% was used rather than 2 mol%, the yields were actually improved, the only two accounts where the yield was diminished (bromoanisole and bromoacetophenone, entries **1** and **4**) did not show a significant difference. The two most active substrates were tested with a loading of 0.01 mol%; although the 4-fluoroaryl yield was reduced (entry **8**), the acetophenone coupling was still highly active (entry **4**). The reduced activity with 2 mol% could

point once again to a catalyst deactivation through nanoparticle agglomeration, in that higher complex concentration accelerates metal agglomeration.

3.1.2.4   Kinetics and catalyst deactivation

The coupling of 4-bromoacetophenone and phenylboronic acid with 1 mol% of **6b** was taken as a model reaction to investigate the kinetic behaviour of the active catalyst (figure **3.2**). In the interest of studying the effect of catalyst dissolution on the reaction kinetics, both the pre-dissolution and *in-situ* catalyst dissolution were examined. Different reactions were set up and quenched in 5 minute-intervals. In order to prevent the reaction from continuing whilst extracting the organics using ethyl acetate, the reaction was quenched by adding 2 ml 1M HCl to neutralize any remaining base.
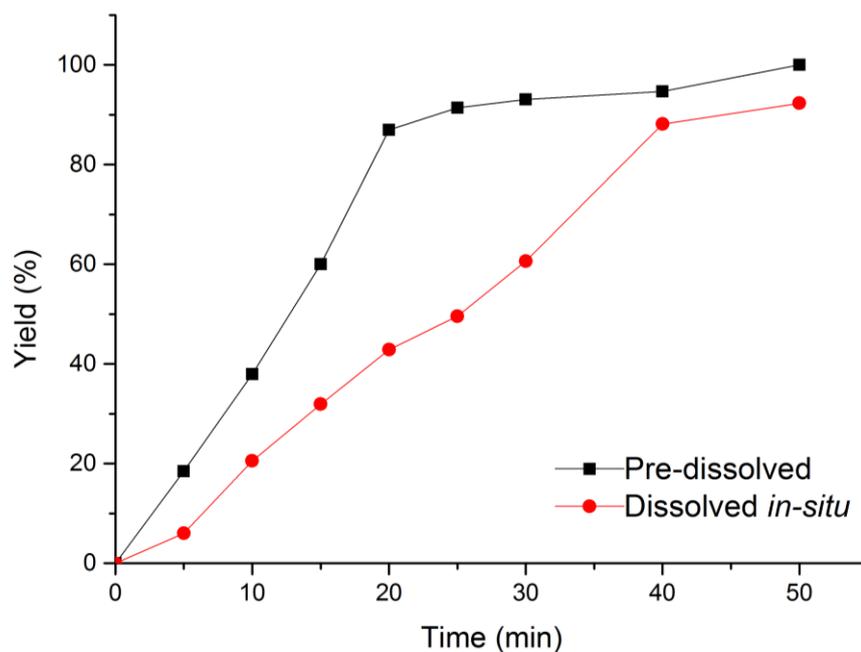
Figure 3.2 Kinetic plot of pre-dissolved and *in-situ* dissolved **6b** during the coupling of bromoacetophenone and phenylboronic acid. Reaction conditions: 0.5 mmol 4-bromoacetophenone, 0.75 mmol phenylboronic acid, 2 mol% **6b**, 1 mmol base, 1 mmol TBAB, 2 ml H_2O

The reaction proceeds rapidly with the pre-dissolution method, reaching 90% yield within 20 minutes. The 100% yield mark is not reached until 50 minutes into the reaction, followed by a sudden tail-off in reactivity. A similar story is observed for the *in-situ* system; however 90% is not reached until 40 minutes. The 100% yield mark is not reached until after 1 hour, as a result of the similar tail-off in activity observed for the pre-dissolved system. This is expected since N-

bound ester hydrolysis occurs over time, meaning that the dissolved active catalyst is slowly released into the aqueous layer, whilst a smaller amount of active catalytic species is available in the early stages of the reaction. A black precipitate was observed around the 90% yield mark in both the pre-dissolved and *in-situ* systems, suggesting that catalyst deactivation into the inactive palladium black species occurs when reagent concentrations are low. The observation of palladium black as an inactive species points further evidence to the fact that agglomeration of metal nanoparticles is the cause of catalyst deactivation.

3.1.2.5 Dependency on nanoparticles

Much evidence throughout these investigations pointed to the formation of Pd(0) nanoparticles with NHCs bound to the surface. The observation of palladium black suggested that nanoparticles were formed towards the end of the reaction. The black precipitate formed during the coupling of bromoanisole using **6b** was isolated via centrifugation of the aqueous reaction medium after separation of the products. This precipitate was analysed via transmission electron microscopy (TEM) after repeated washing with water and ethanol. Well-dispersed small nanoparticles are indeed observed (figure **3.3**).
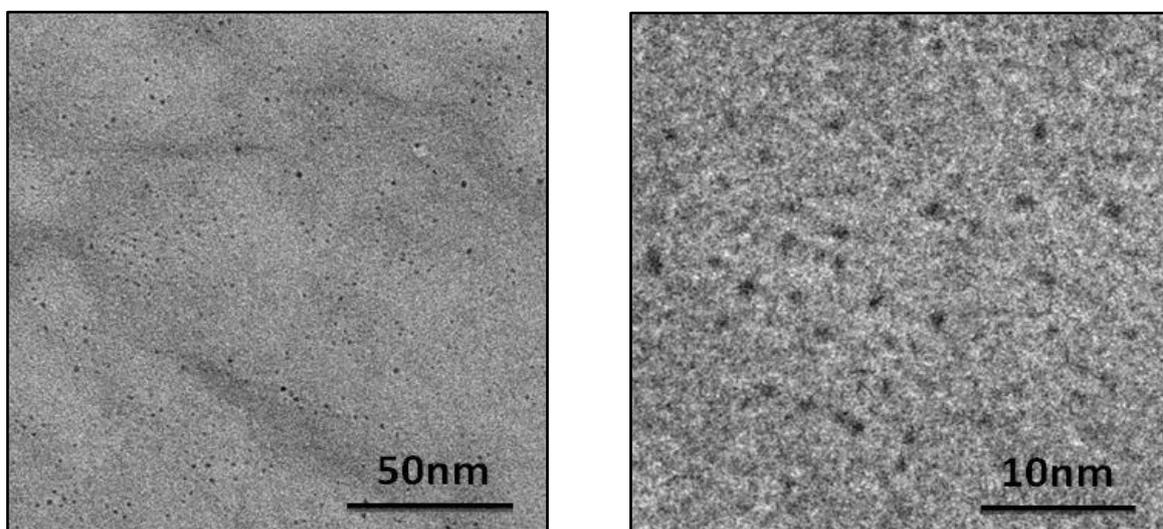
Figure 3.3 TEM images of the black precipitate isolated after the coupling of bromoanisole and phenylboronic acid with **6b**

The ^{1}H-NMR spectra of the complex dissolved in D_2O suggested that nanoparticles formed readily upon dissolution of the hydrolysed complex in water (figure **3.1**). To confirm this, TEM images were taken of the complex dissolved in water with K_2CO_3 base and TBAB prior to addition of reagents (figure **3.4**). The resulting image clearly displays dark nanoparticles gathered inside larger agglomerates, meaning that nanoparticles are formed upon dissolution of

the complex; therefore the water-soluble complex forms a colloidal dispersion of the complex with the addition of TBAB. It is worth considering the role of TBAB as a known nanoparticle stabilizer, which may contribute to the agglomerates shown in the TEM image. TBAB therefore plays two roles in the reaction, as a PTC and as a nanoparticle stabilizer.
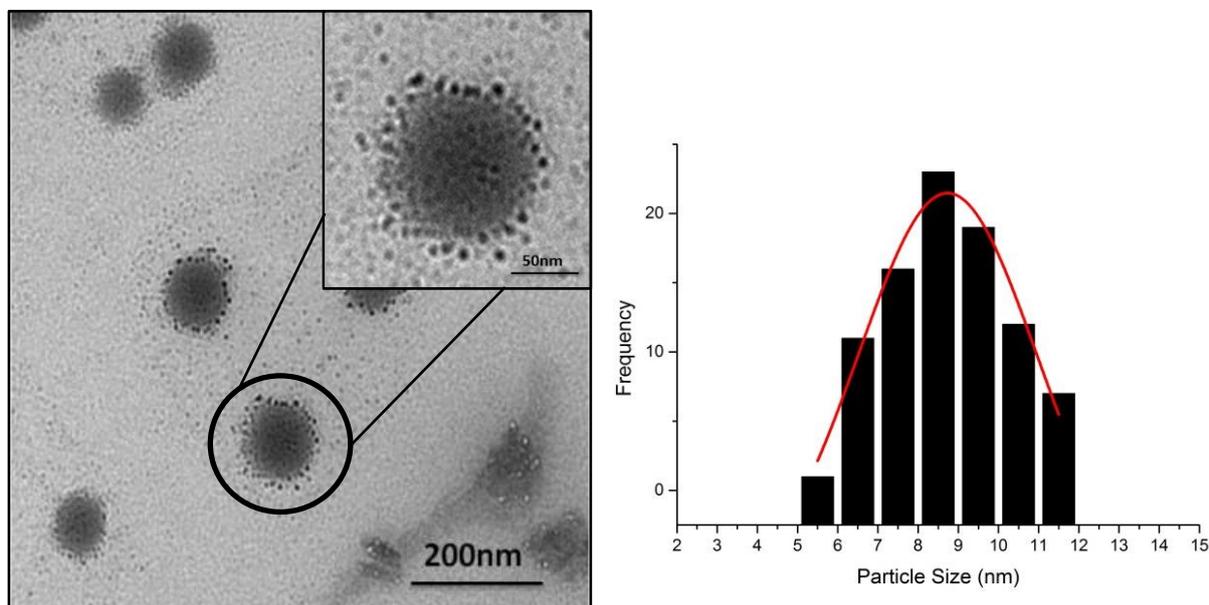
Figure 3.4 (Left) TEM image of the aqueous solution of **6b** after hydrolysis with K_2CO_3 base in the presence of TBAB. (Right) Histogram of the nanoparticle size distribution displayed within the TEM image

In order to discover whether the formed nanoparticles are active in the catalysis, mercury poisoning experiments were conducted by adding mercury to the vessel before addition of bromoanisole in its coupling with phenylboronic acid (table **3.8**). Mercury is a well-known poison for heterogeneous catalysts, and has been proven to be effective in poisoning nanoparticles; however it has no effect on dissolved homogeneous catalytic species. A Hg:Pd ratio of 300:1 was used to ensure sufficient nanoparticle poisoning. In the case of each complex, the activities were significantly diminished. Complexes **6a** and **6c** suffered significant catalyst poisoning, and **6b** was poisoned altogether. This confirms that, whilst **6a** and **6c** do no completely rely on the formation of nanoparticles for their activity, nanoparticles are mostly responsible for activity. Complex **6b** on the other hand relies completely on nanoparticles for its activity. The partial catalyst poisoning points to a "catalyst cocktail" system, in which several active species are likely to be present within the solution and within a colloidal dispersion.[203]

To further confirm the role of TBAB as nanoparticle stabilizer; an additional test was performed with an insufficient amount of Hg to completely poison **6b** (100:1), both in the presence and absence of TBAB. The results show that **6b** in the absence of TBAB is not poisoned to the same degree as with TBAB, suggesting that TBAB does indeed play the role of nanoparticle stabilizer.

Complex	Yield (without Hg) (%)	Yield (with Hg) (%)
6a	88	16
6b	92	0
6c	88	14
6b	80	32[a,b]
6b	92	8[a]

Table 3.8 Mercury poisoning test of bromoanisole and phenylboronic acid using precatalyst **6b.** Reaction conditions: 0.5 mmol 4-bromoanisole, 0.75 mmol phenylboronic acid, 2 mol% **6b**, 1 mmol base, 1 mmol TBAB, 600 mol% Hg, 2 ml H_2O, 60 °C, 24 hours. [a] 200 mol% of Hg used. [b] Performed in the absence of TBAB.

3.1.2.6   Catalyst recycling

The major advantage of water-soluble catalysts for aqueous phase synthesis is the simple facilitation of catalyst recycling, by re-using the catalytic aqueous layer. This requires a particularly stable catalyst, capable of remaining active in the presence of a large concentration of substrate. The recycling of the bromoacetophenone and phenylboronic acid coupling with **6b** was attempted by extracting products, and adding new reagents to the aqueous layer for re-use. The complexes were pre-hydrolyzed before starting the reaction to ensure water solubility of the complex is induced.

After extraction, the aqueous layer was evaporated *in vacuo* after each run in order to remove any traces of organic solvent. The residue was then re-dissolved in another 2 ml of water before adding substrates for the following run. Initial attempts to recycle the aqueous layer resulted in the catalyst leaching into the ethyl acetate solvent during extraction, as observed through the lack of activity in the second run, and ^{1}H-NMR of the extracted layer. Toluene was selected as the extraction solvent after improved screenings suggested drastically reduced catalyst leaching. This method was more successful, producing 100% yield on the first and second runs within 1

and 2 hours respectively (Figure **3.5**). However, the 3rd run only produced 10% yield over 8 hours, meaning that the active catalyst was fully deactivated. Since leaching is minimal with toluene extraction, it is assumed that most catalyst deactivation occurs as a result of nanoparticle agglomeration; however leaching of colloidal nanoparticle dispersions into the toluene cannot be ruled out. As reported in **3.1.2.3**, the bromoacetophenone coupling also proceeds to full conversion with 0.1 mol% of catalyst. Since the recycling was performed with 2 mol% loading and is deactivated early in the 3rd run, this could point to accelerated catalyst deactivation with higher catalyst loading.
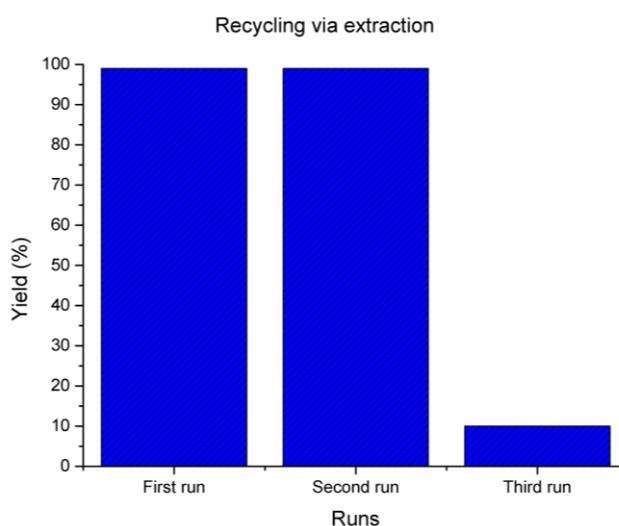
Figure 3.5 Bar chart of yields during recycling of **6b** via the extraction method

Since the carboxylate group can be altered depending on the hydrolysis agent (potassium carboxylate in the case of the potassium base and carboxylic acid in the presence of protons), the effect of pH on recycling was investigated. Change in pH-assisted recycling has been previously observed for water-soluble catalysts bearing carboxylic acid groups,[131] so the effect of quenching each reaction with 2 ml 1M HCl before toluene extraction was tested. Unfortunately no improvement to the yields of subsequent runs was observed.

3.2 Alcohol oxidation – the role of a labile ligand

The success of the Suzuki-Miyaura couplings lies with the mono-NHC Pd complexes rather than the bis-NHC complexes. Within this work, the reason for this is the induction of water-solubility by successfully hydrolysing the ester arms; however PEPPSI-type complexes in general have a history of being superior to their bis-NHC analogues. This is attributed to the coordination of a labile co-ligand, which detatches to reveal a coordination site suitable for the substrate. Aside from the poor yields of the bis-complexes in the Suzuki reaction, the decision to switch to the

PEPPSI-type complexes was influenced by earlier attempts to oxidise alcohols using the bis-NHC complexes.

The field of Pd-catalyzed alcohol oxidation is regarded as a prime example of green principles applied to homogeneous catalysis. This reaction, discovered initially by Berzelius,[204] and recently developed by Sigman,[205] Stahl,[206] Waymouth,[207] and Sheldon,[208] heavily involves the use of ligands to stabilize the catalytic intermediates. To evaluate the activity of the amino acid-derived ligands presented in **1.1,** bis-NHC complexes were chosen for initial catalytic screenings. Since oxygen is not such a sterically demanding substrate, the amino acid-derived ligands were predicted not to hinder coordination.

Initial attempts were directed towards oxidising glycerol towards its several potential oxidation products. According to a procedure similar to that of Waymouth *et al*,[209] complexes **4a** and **4b** were compared to a Pd(OAc)$_2$ and triethylamine (TEA) *in situ* system in deuterated acetonitrile, to be monitored by ^{1}H NMR (scheme **3.4**). Three equivalents of benzoquinone were used as an oxidising agent. Although the benzoquinone was seen to be completely reduced to hydroquinone, no glycerol oxidation products were observed in any of the runs.
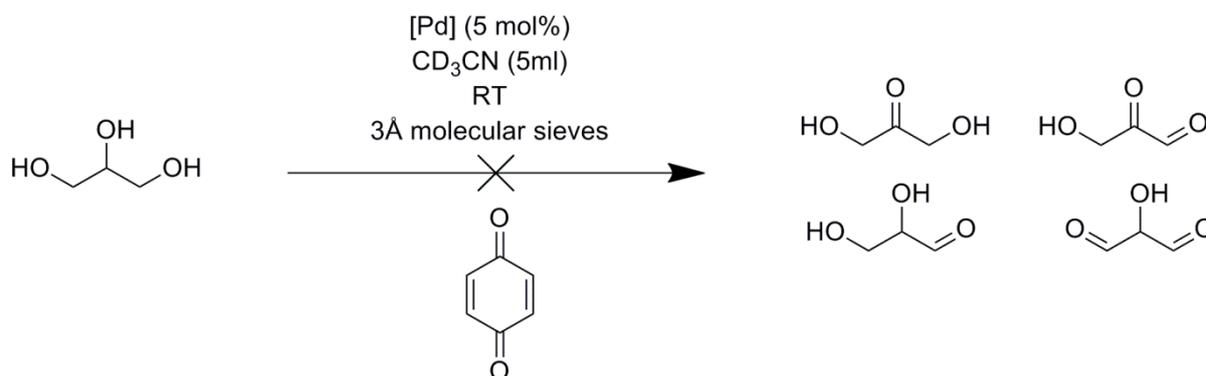
Scheme 3.4 Attempted oxidation of glycerol using complexes **4a**, **4b** and Pd(OAc)$_2$. Calculated using ^{1}H NMR analysis. Reaction conditions: 1 mmol glycerol, 3 mmol benzoquinone, 5 ml CD$_3$CN, powdered molecular sieves (100 mg), RT.

Benzyl alcohol was next attempted as a simpler substrate in a procedure similar to that of Sigman *et al*.[210] The same precatalysts were compared in a THF/toluene mixed solvent system, using a balloon of gaseous O$_2$ as the oxidising agent. Analysis of the completed reaction via GC-MS revealed that whilst full conversion of benzyl alcohol into benzaldehyde was observed in the Pd(OAc)$_2$/TEA system, complexes **4a** and **4b** produced no conversion (table **3.9**).
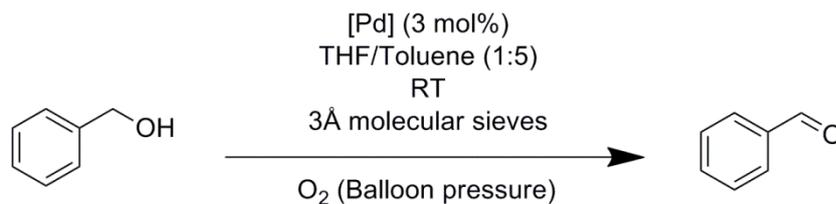
Entry	Catalyst	Conversion (%)
1	Pd(OAc)₂/TEA (1:2)	93
2	**4a**	2
3	**4b**	0
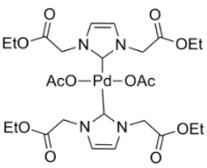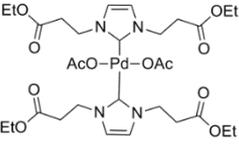
Table 3.9 Attempted catalytic screenings and resultant conversions. Calculated using GC-MS analysis. Reaction conditions: 1 mmol benzyl alcohol, 0.5 ml THF, 2.8 ml toluene, powdered molecular sieves (100 mg), RT.

The low yields through lack of activity are likely to be attributed to the bis–NHC system. The steric bulk could contribute to a lack of available coordination sites for the oxygen molecule, contrary to what was predicted. Mechanistic investigations carried out by the Waymouth group on their Pd(II)–phenanthroline system highlight the importance of an available coordination site.[209] In their case, the most successful catalyst was a mono-NHC complex with no fourth ligand, therefore leaving an empty coordination site for oxygen.

In conclusion, the bis-Pd–NHC complexes synthesised in chapter **1** were not shown to be advantageous for alcohol oxidation. However, owing to their hydrolysable ester linkages, which can induce water solubility, the PEPPSI-type Pd–NHC complexes were discovered to be very competitive for aqueous-phase Suzuki-Miyaura couplings. Excellent yields were observed with relatively fast kinetics in the presence of TBAB phase-transfer catalyst. The active catalyst was determined to be mostly in the form of Pd(0) nanoparticles, however incomplete poisoning in the presence of mercury points to a "catalyst cocktail" system. Using an extraction-and-reuse method, the catalyst was recyclable for an extra run. Most of the work presented in this chapter was published in an article within the New Journal of Chemistry.[211]

4. Imidazolium-functionalized silica materials

Imidazolium moieties as organic groups within silica hybrid materials pose many opportunities for application. The most explored utilization of these materials is as a precursor for organometallic solid-support catalysts via NHC complex formation. As a result of the strong electron-donating properties of the NHC–metal bond, immobilized carbene complexes typically show minimal leaching of metal residue; as well as opportunities for simple tuning and functionalization. Another emerging field is that of silica-immobilized ionic liquids, which show potential as catalysts, metal scavengers and ion-exchange media. A large number of reports within this research involve imidazolium-silicas. One of the first reports was published by Dai *et al*, [212] within which a symmetrical imidazolinium salt with two propyltriethoxysilane N-bound groups was used to synthesize PMOs (periodic mesoporous organosilicas) via acid and base-catalyzed co-condensation with CTAB surfactant (figure **4.1**). This particular silane precursor has been revisited in two studies: the first by Yin *et al*,[145] in which neutral surfactants were used to create an imidazolium-dilute PMO. A further study in 2011 by Hesemann *et al* highlighted the superiority of anionic surfactants for propyltriethoxysilane-functionalized imidazolium and imidazolinium compounds within PMO synthesis.[213] Whilst condensation of the pure silane resulted in a non-porous hybrid silica, dilution with TEOS resulted in a highly-structured porous material; albeit only with low imidazolium loading. An earlier report by the Hesemann group also describes the synthesis of PMO materials from unsymmetrical imidazolium silanes, featuring only one silane group.[214] Using imidazolium, and functionalized imidazole moieties (followed by post-quaternization), highly-ordered porous ionosilicas could be produced. These reports highlight the influence of the imidazolium cation charge on ordering and structure of the resulting ionosilicas.
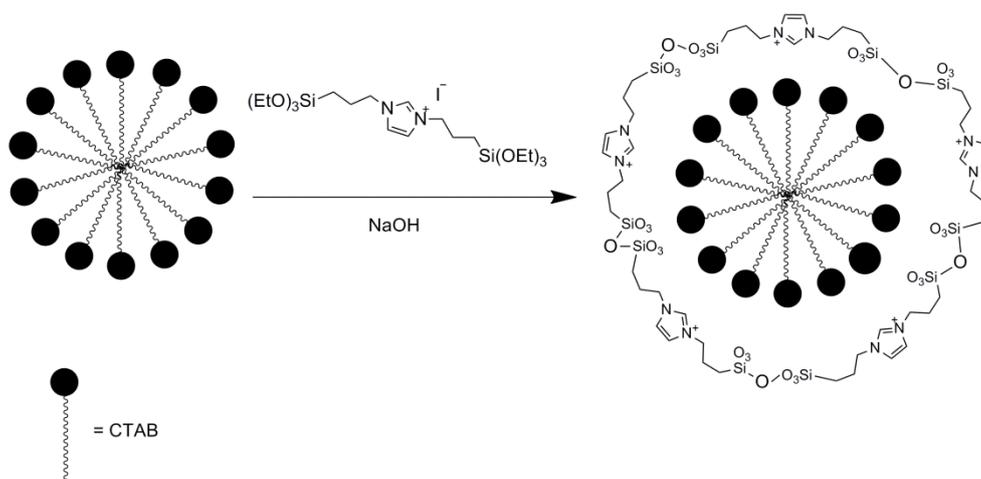
Figure 4.1 Illustration of the imidazolium silane co-condensing around a CTAB micelle, within the report from Dai *et al*. Reproduced from reference [212]

A number of similar imidazolium-functionalized PMO materials have been post-functionalized to produce supported NHC catalysts. The imidazolium propyltriethoxysilane described above was used to synthesize a PMO with non-ionic surfactant, which was post-functionalized with Pd(OAc)$_2$.[215] Although the nature of the Pd incorporation into the material was not well characterized, a well-ordered silica was produced, capable of recyclable Suzuki catalysis with low catalyst loadings. Hesemann *et al* also described a PMO synthesis using a silane analogue of IMes.[216] Once again anionic surfactants produced materials with a higher BET (Brunauer-Emmett-Teller) surface area than the PMOs produced using cationic or non-ionic surfactants, even when high dopings of the imidazolium moiety were used. This is particularly advantageous for the purposes of post-metallation, since the C2 atom is readily accessible. Within the same year, Zhang *et al* produced a PMO using an IPr silane analogue (figure **4.2**) and the bridging ethyl silane, co-condensed together using a non-ionic surfactant.[217] This was post-metallated using a variety of different Pd sources to produce silica-immobilized analogues of popular Pd–NHC catalysts, which were proven to be effective within Suzuki couplings.
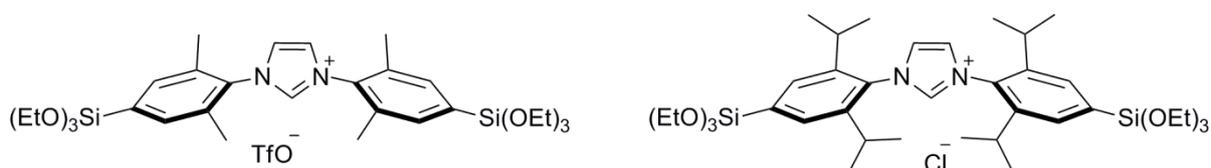
Figure 4.2 (Left) structure of the IMes silane analogue reported by Hesemann *et al*. (Right) structure of the IPr silane analogue reported by Zhang *et al*

The imidazolium salts presented within chapter **1** have the advantage of carboxy-functionalized *N*-bound groups, which offer different opportunities for functionalization. Within this regard, these imidazoliums may serve as suitable precursors for silica-functionalization, leading to possible application. Two methods of functionalization were attempted. The first, which will be described in **4.1**, involves amidation of the carboxyl groups using aminopropyl silica, a commercial mesoporous organosilica, via the acyl chloride intermediate route. The second route, described in **4.2**, involves the synthesis of a novel bridging organosilane via amidation of an ester-functionalized imidazolium salt, then synthesis of a PMO material via co-condensation.

4.1 Post-grafting via the acyl chloride

The first strategy was carried out in two steps: formation of the acyl chloride using thionyl chloride under inert atmosphere, followed by amidation with mesoporous aminopropyl silica (1mmol/g of aminopropyl groups) in the presence of Hünigs base (*N*,*N*-diisopropylethylamine) (scheme **4.1**). An excess of SOCl$_2$ was used in the first step to convert all carboxylate groups into acyl chlorides, the intermediate was used immediately in the second step after removing the

remaining SOCl₂ *in vacuo*. In the same manner, a large excess of imidazolium zwitterion starting material was used with respect to the aminopropyl groups as an attempt to ensure all supported amine groups were converted to the amide. Initially, a number of attempts with different zwitterions were performed producing relatively poor amounts of imidazolium-functionalization. During initial attempts, Imi-salts **1d**, **1e** and **1h** were used in functionalization; however elemental analysis (EA) of the final material revealed a difference in combined C, H and N content of between 3.85 and 4.49 % greater than the aminopropyl silica starting material (table **4.1**). This only equates to approximately 16% imidazolium loading through comparison of nitrogen content. Thermogravimetric analysis (TGA) of **Si-1d** displayed a mass loss difference of 7.45 % with respect to the aminopropyl silica, which is in ballpark agreement with the EA mass difference of 3.85 % after taking account for oxygen and chlorine content.
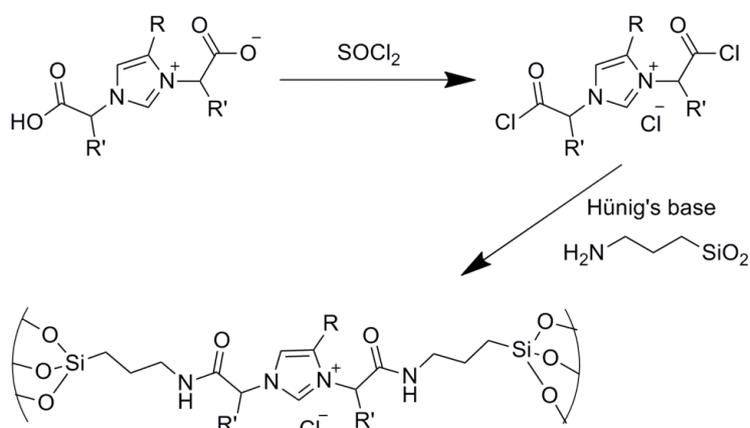
Scheme 4.1 Post-grafting strategy of hybrid material synthesis. Reaction conditions: 2.5 mmol imi-zwitterion, 6ml SOCl₂, 1g aminopropylsilica, 15ml Hünig's base.

Material	%N	%C	%H	%Total	%Difference (with respect to starting material)
Aminopropyl silica	1.63	5.57	1.82	9.02	–
Si-1e (R=Me, R'=H)	2.16	8.74	1.97	12.87	3.85
Si-1d (R=H, R'=Me)	2.49	8.94	2.08	13.51	4.49
Si-1h (R=Me, R'=Me)	1.88	9.03	2.13	13.04	4.02
Si-1e-MeCN	5.83	24.98	3.20	34.01	24.99

Table 4.1 EA values of post-grafted silica materials **Si-1e–Si-1h**, and content difference with respect to the starting material

This limited functionalization was attributed to the insolubility of the acyl chlorides in Hünig's base. A higher functionalization could be achieved by adding dry acetonitrile (10ml) during the addition of Hünig's base, thereby increasing the accessibility of the acyl chloride to the aminopropyl groups. After filtration of the silica material, the solid was dried under vacuum for 40 hours to remove all remaining traces of acetonitrile. EA reports a much higher organic content in comparison to the previous functionalization attempt, a C, H and N percentage difference of 24.99 % (table **4.1, Si-1e-MeCN**). Likewise TGA reports a mass loss difference of 43.11 % (figure **4.3**); the extra mass could be explained by oxygen and chlorine content. Comparison of the nitrogen content from the EA suggests that each aminopropyl group is occupied by an imidazolium, rather than two aminopropyl groups per imidazolium as suggested in scheme **4.1**. Therefore 1 mmol of imidazolium per gram of silica is present. Imidazolium functionalization was confirmed by infrared spectroscopy FT-IR and ^{13}C MAS-NMR analysis. Crucial to notice is that the FT-IR displays evidence of the C=O amide stretch (1599 cm^{-1}) and aromatic C=C stretching (1550-1650 cm^{-1}), however no peak is observed for nitrile CN stretching (2215-2240 cm^{-1}), confirming that no residual acetonitrile remains in the material (figure **4.3**).
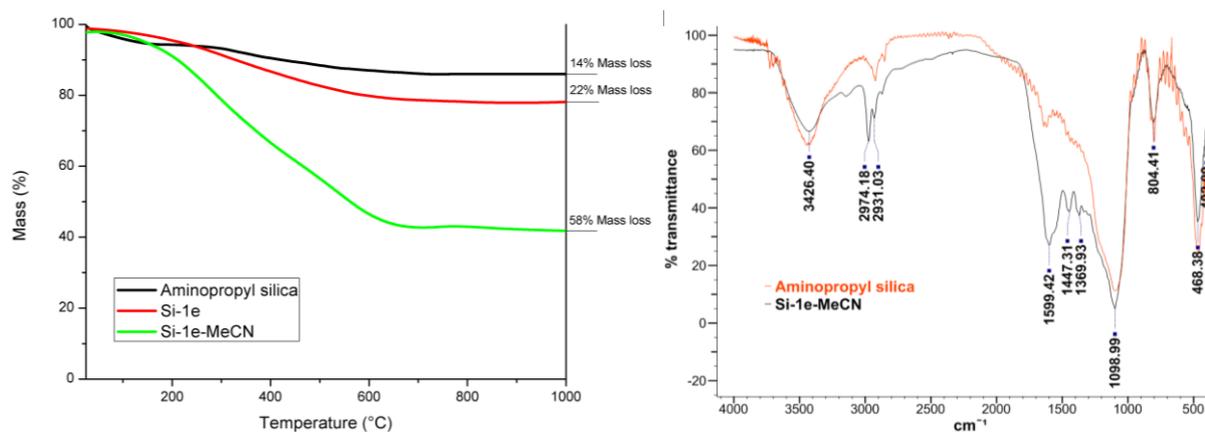
Figure 4.3 (Left) TGA curves for **Si-1e**, **Si-1e-MeCN**, and aminopropyl silica starting material. (Right) FT-IR spectra of **Si-1e-MeCN** and aminopropyl silica starting material

Analysis of the surface area via the BET method reveals that surface area decreases upon increased functionalization of imidazolium (table **4.3,** figure **4.4**). This is likely a result of silica pore sites being occupied by organic moieties. The BET curves in each case display a typical type IV adsorption isotherm, with a hysteresis loop.[218] The similarity of these curves suggests that the mesoporosity of the aminopropyl silica is retained, even after functionalization.

Material	BET surface area (m^2g^{-1})
Aminopropyl silica	330
Si-1e	252
Si-1e-MeCN	207

Table 4.3 BET surface areas of **Si-1e**, **Si-1e-MeCN**, and aminopropyl silica starting material
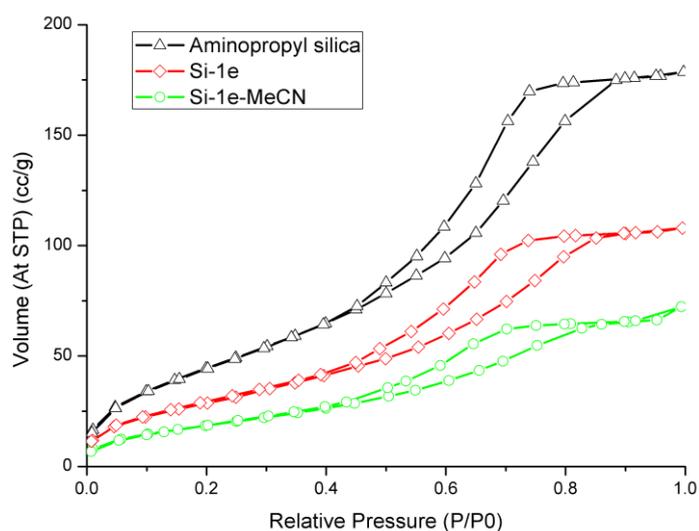
Figure 4.4 BET adsorption and desorption hysteresis curves of **Si-1e**, **Si-1e-MeCN**, and aminopropyl silica starting material

4.2   Co-condensation via silyl-amide

The second strategy was also carried out in two steps. In the first step, The imidazolium ester **2a** was amidated under inert conditions with aminopropyl(triethoxy)silane to produce bridged silane **8a.** The amidation was performed under argon atmosphere, and the product was stored in a glovebox since the silyl groups gradually hydrolyze in air. The silyl amide was characterized using ^{13}C and ^{1}H NMR analysis. This amidation was also attempted with ester precursors **2b** and **2c,** however a mixture of products was obtained that could not be separated by traditional purification methods (such as selective solvent recrystallization) which are suitable for an inert atmosphere.
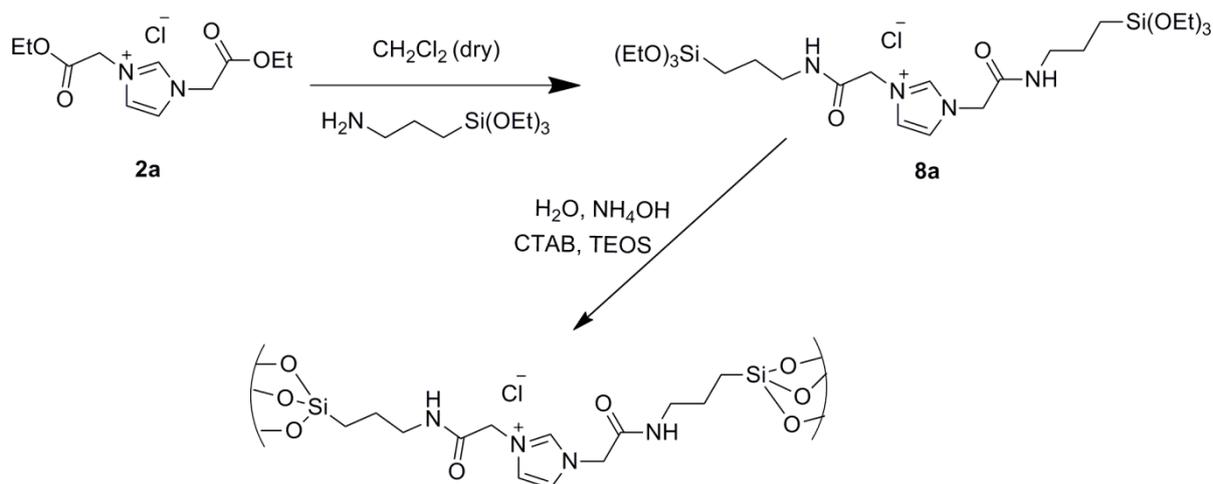
Scheme 4.3 Synthesis of bridged silane **8a** and subsequent co-condensation strategy of hybrid material synthesis

In the second step, the silane **8a** was then co-condensed using TEOS in aqueous alkaline conditions, alongside the surfactant CTAB (scheme **4.3**). Positively-charged surfactants are usually not an optimal template for positively-charged imidazolium silanes due to charge repulsion. However organosilica hybrid materials commonly use cationic and non-ionic surfactants for templating. Examples of imidazolium silanes templated with tetraalkylammonium salts have been previously reported, although this is usually in conjuction with a silane featuring long surfactant-like N-bound groups, as in a report by Hesemann *et al.*[214] Since templating was not the main priority within this study, CTAB was chosen as a non-optimized attempt at templating. A relatively large doping of imidazolium content was attempted for the co-condensation. An imi: TEOS:CTAB:NH$_3$:H$_2$O molar ratio of 1:2:0.27:18:224 was stirred together at 60 °C, the surfactant was dissolved in the aqueous ammonia solution before adding **8a** in a solution of 1 ml ethanol. The formed silica material was aged over 24 hours before being dried in a vacuum oven, similar to the procedure outlined by Hesemann *et al.*[213] EA analysis reports high values of organic content, a total of 37.12% (table **4.4**). Likewise the TGA analysis records a mass loss of 51.2%, moderately higher than the value achieved for the silica formed from the first strategy. ^{13}C MAS-NMR spectrometry confirms imidazolium inclusion into the bulk material (figure **4.5**). ^{29}Si NMR was also performed in order to ascertain the ratio between T sites (trifunctional) (SiO$_3$R) and Q sites (tetrafunctional) (SiO$_4$) within the hybrid material (figure **4.6**). Integration of the peaks reveals a 1:1 T:Q site ratio, which is in agreement with the theoretical ratio considering that there are two Si atoms in the silyl amide compared to one atom in the TEOS molecule. The integrated peaks typically representing Q3 sites (SiO$_3$OH) (-90 – -100 ppm) are greater in value than those of Q4 sites (SiO$_4$) (-105 – -120 ppm), meaning terminal silanols are still in great concentration.
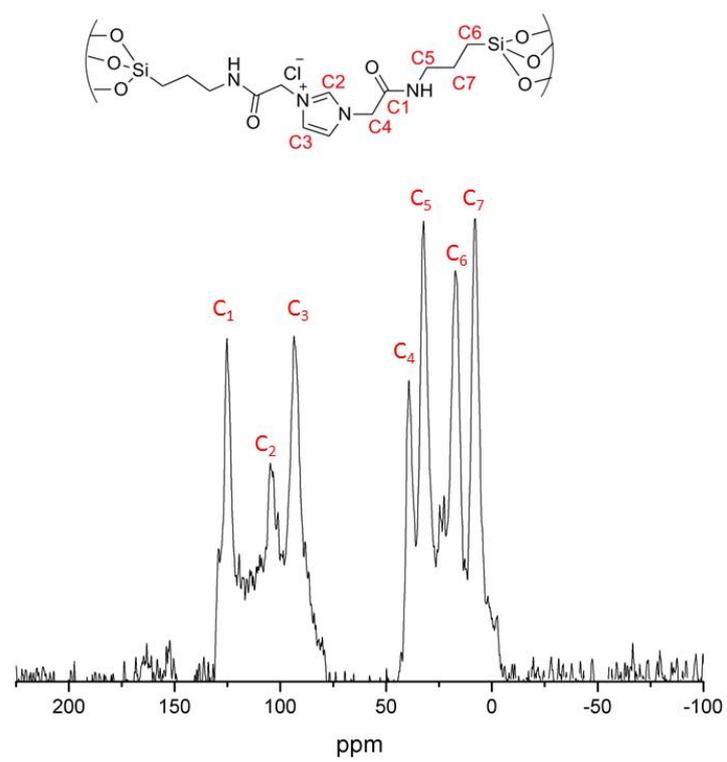
Figure 4.5 ^{13}C MAS-NMR spectrum of material **Si-8a-1:2**
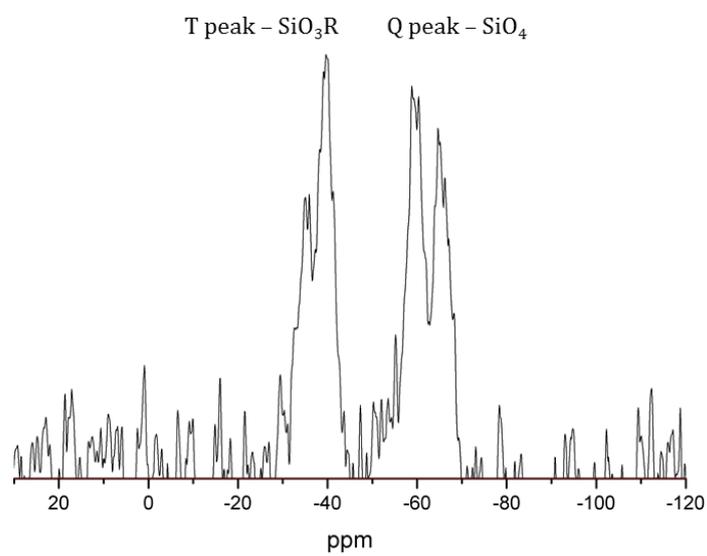
Figure 4.6 ^{29}Si MAS-NMR spectrum of material **Si-8a-1:2**

The surfactant template was washed from the material by suspending the solid in a mixture of HCl (2ml) in ethanol (100ml) without stirring overnight. This successfully removed some organic content as evidenced by EA, reporting a 5.47% difference in C, H and N content (table **4.4**). TGA also reports a mass loss of 48.8% for the washed compound, totalling in a 2.4% difference in mass, curiously smaller than the EA mass difference. Likewise, the BET surface area increases upon washing, giving the expected increase in pore density (table **4.4**), although the surface area remains particularly low, suggesting that the templating with CTAB failed, and a very dense material is produced.

Material	%N	%C	%H	%Total
Si-8a-1:2	7.76	24.71	4.65	37.12
Si-8a-1:2-W (washed)	7.37	20.25	4.03	31.65
Material	BET surface area (m^{2}g^{-1})			
Si-8a-1:2	33			
Si-8a-1:2-W	47			

Table 4.4 EA values and BET surface areas for material **Si-8a-1:2** and the surfactant-free **Si-8a-1:2-W**

In conclusion, the co-condensation method presents a safer, more versatile method of producing an organosilica material from the amino acid derived imidazoliums compared to the post-modification of aminopropylsilane. Different amounts of imidazolium can be easily incorporated into the material and easily co-condensed into silica without the use of toxic or harsh reagents. Although the opportunity for templating remains, CTAB is not an optimal surfactant for this silane. Little to no porosity is observed as evidenced by the low BET surface area. Further opportunities remain in templating through the use of non-ionic or anionic surfactants as performed in the imidazolium ionosilica templating experiments published by Hesemann *et al*,[213] which are electrostatically much more suited to the imidazolium positive charge. Furthermore, a high imidazolium content may also contribute to the lack of porosity, since the silica network is disrupted by organic moieties. This was however not a central concern as this work aimed to produce silica with a high imidazolium content regardless of density, as a step towards producing suitable precursors for supported NHC metal catalysts with a high metal content.

III   Summary and Outlook

Within this work, 1, 3-dicarboxylate imidazolium salts derived from sustainable building-blocks, produced from previous work within this group, were successfully modified to be suitable as *N*-Heterocyclic carbene ligands within metal complexes. Despite evidence of a short-lived complex produced from the carboxylate species, esterification of the carboxylate arms and inclusion of a halide counterion produced ligands suitable for complexation by traditional methods. Complexes of Ag(I), Pd(II), and Ir(I) were successfully produced using known procedures using ligands derived from glycine, alanine, β-alanine and phenylalanine. The complexes were characterized in solid state using X-Ray crystallography, which allowed for the steric and electronic comparison of these ligands to well-known NHC ligands within analogous metal complexes.

These complexes were tested for alcohol oxidation, and aqueous-phase Suzuki-Miyaura cross-couplings catalytic processes. Activities were poor for the oxidation reaction, however the advantage of easily functionalizable ester N-bound groups was utilized for the latter reaction, in which water-solubility could be induced via ester hydrolysis in the presence of base. The mono-NHC–Pd complexes were seen to be highly active in the coupling of aryl bromides with phenylboronic acid; the active catalyst of which was determined to be mostly Pd(0) nanoparticles. Kinetic studies determined that reaction proceeds quickly in the coupling of bromoacetophenone, for both pre-hydrolyzed and *in-situ* hydrolysis catalyst dissolution. The catalyst could also be recycled for an extra run by simply re-using the aqueous layer.

The imidazolium salts were also used to produce organosilica hybrid materials by post-grafting and co-condensation synthesis techniques. The former technique proved to be effective in doping imidazolium moieties onto aminopropyl silica via amidation of the carboxylate arms; however this procedure suffers in its poor consideration of green chemistry. The latter technique is a much more dynamic synthesis route which opens up possibilities of different degrees of imidazolium doping, and long range ordering via co-condensation around surfactants. Whilst the imidazolium content was successfully tunable, the resulting materials were largely nonporous; most likely as a result of the choice of a CTAB cationic surfactant and base-catalyzed condensation.

This thesis demonstrates the possibilities of using bio-derived platform chemicals for the production of homogeneous catalysts and materials, and an example of what can be achieved whilst still considering the 12 principles of green chemistry.

Further work within this field could be performed via a number of different routes. The successful induction of water-solubility using the amino-acid derived ligands could be extended to any number of different aqueous-phase homogeneous processes. The Ir(I) complex **7a** in particular could be used for any number of reactions, namely asymmetric hydrogenation, hydrogenolysis, proton/deuteron exchange, and more. Initial intentions of this project were to utilize the amino-acid derived ligands for nickel-catalyzed hydrogenolysis of aryl ethers, towards lignin refinery. However based on the inferior steric properties observed throughout this work, and their instability towards free-NHC formation, such NHCs are very unlikely to be suitable for this reaction.

Ongoing collaborative work with the Peter Hesemann group at the Université de Montpellier 2 will investigate the possibilities of producing ordered silica materials with these imidazoliums using different surfactants. This work may lead to applications relating to the ionosilica properties, such as metal scavenging, or organocatalysis.

Finally, a huge opportunity is presented by combining the homogeneous catalyst work with the silica material work. Solid-support homogeneous NHC catalysts could be produced, either by amidation of the ester arms on the pre-formed NHC metal complex, or by post-complexation of the imidazolium organosilica. This aims to produce a solid-support catalyst with similar activity to that of a homogeneous catalyst, but the advantage of simple recycling and adaptation to flow chemistry. As of yet, methods of producing similar catalysts are typically complicated and involve difficult procedures, this presents a simpler approach from readily available materials.
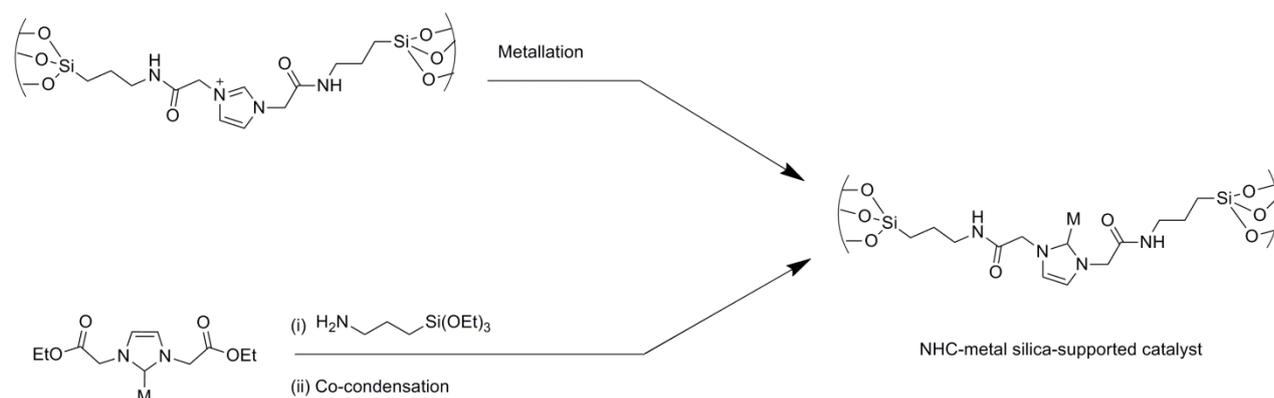
Scheme III.1 Different strategies towards a silica-supported metal–NHC catalyst

IV   Abbreviations

%V$_{bur}$ – Percent buried volume

ACS – American chemical society

AE – Atom economy

BET – Brauner-Emmett-Teller method

Boc – *tert*-butyloxycarbonyl

COD – cyclooctadiene

CTAB – cetyltrimethylammonium bromide

CTAC – cetyltrimethylammonium chloride

dba – dibenzylideneacetone

DHA – dihydroxyacetone

DLS – Dynamic light scattering

EA – Elemental analysis

EDG – electron donating group

EPA – Environmental Protection Agency

ESI-MS – Electrospray ionisation-Mass spectrometry

EtOH – ethanol

EWG – electron withdrawing group

FT-IR – Fourier transform infrared spectroscopy

GC-MS – Gas chromatography-Mass spectrometry

HMF – 5-hydroxymethylfurfural

HSAB – hard/soft acid/base

IAd – 1,3-bis(adamantyl)-imidazol-2-ylidene

IBenz – 1,3-bis(methylphenyl)-imidazol-2-ylidene

ICy – 1,3-bis(cyclohexane)-imidazol-2-ylidene

IMe – 1,3-bis(methyl)-imidazol-2-ylidene

IMes – 1,3-bis(2,4,6-trimethylphenyl)-imidazol-2-ylidene

IPr – 1,3-bis(2,6-diisopropylphenyl)-imidazol-2-ylidene

I^{t}Bu – 1,3-bis(*tert*-butyl)-imidazol-2-ylidene

LCA – Life Cycle Assessment

L-donor – 2 electron donor ligand

LUMO – lowest unoccupied molecular orbital

MAS – Magic-angle spinning

MCM-41 – Mobil Company Material-41

MeI – methyl iodide

MeOH – methanol

m-TPPMS – *meta*-triphenylphosphine monosulfonate

m-TPPTC – *meta*-triphenylphosphine tricarboxylate

m-TPPTS – *meta*-triphenylphosphine trisulfonate

NHC – *N*-Heterocyclic carbine

NMR – Nuclear magnetic resonance

OAc – acetate

OTAC – octadecyltrimethylammonium chloride

P-123 – Pluronic-123 ethylene glycol block copolymer

PEPPSI – Pyridine-enhanced precatalyst preparation, stabilization and initiation

PMO – Periodic mesoporous organosilica

PTC – Phase-transfer catalyst

PTFE – polytetrafluoroethane

p-TPPMP – *para*-triphenylphosphine monophosphonate

PXRD – Powder X-ray diffraction

py – pyridine (as coordinated ligand)

ROMP – Ring-opening metathesis polymerization

RT – room temperature

SBA-15 – Santa Barbera Amorphous-15

SICy – 1,3-bis(cyclohexane)-imidazolin-2-ylidene

SIMes – 1,3-bis(2,4,6-trimethylphenyl)-imidazolin-2-ylidene

SIPr – 1,3-bis(2,6-diisopropylphenyl)-imidazolin-2-ylidene

TEA – triethylamine

TEM – Transmission electron microscopy

TEOS – tetraethylorthosilicate

TEP – Tolman electronic parameter

TGA – Thermal gravimetric analysis

THF – Tetrahydrofuran

t-KBuO – potassium tert-butoxide

TNT – trinitrotoluene

X-donor – 1 electron donor ligand

V   Materials, Methods and Characterization

All chemicals were used as received without further treatment or purification unless otherwise specified. Metal complexation experiments were conducted using Schlenk techniques under argon atmosphere appropriate for air-sensitive reagents, intermediates, or products. An M.Braun glove box system under argon atmosphere was used for storage and preparation of particularly sensitive samples. Water used for solvent and regent purposes was purified using an SG Integra UV Plus millipore water purification system. Dry solvents were either purchased and used directly from Acros Organics, or dried by the author using appropriate solvent drying procedures; dry solvents were stored under argon or nitrogen atmosphere over 3Å molecular sieves. Deuterated solvents for NMR were purchased from Sigma Aldrich except for deuterated acetonitrile which was purchased from Acros Organics.

Sigma Aldrich

Acetic acid (≥ 99.7 %), β-alanine, ethanol (≥99.8 %), methylglyoxal (40 % aq. Solution), $Pd(OAc)_2$ (≥99.9 %), $PdCl_2$ (≥98 %), [Ir(COD)Cl]$_2$ (≥98 %), 1,3,5-trimethoxybenzene (≥99 %), 2-bromoanisole, 3-bromoanisole, triethylamine (≥97 %), benzoquinone (≥97 %), glycerol, benzyl alcohol, tetrabutylammonium hexafluorophosphate (99.9 %), phenylboronic acid (≥97 %), phenylboronic acid pinacol ester (≥98 %), potassium tert-butoxide, 4-fluoro-1-bromobenzene, 1-bromo-4-dimethylaniline, 4-bromoaceotophenone (≥99 %), 4-chloroaceotophenone (≥99 %), tetrabutylammonium bromide (≥98 %), thionyl chloride, acetyl chloride, TEOS, aminopropyl silica (1mmol/g of amino groups), aminopropyltriethoxysilane, diisopropylethylamine, d^1-chloroform, d^6-DMSO, d^8-tetrahydrofuran, D_2O.

Carl Roth

Glyoxal (40 % aq. solution), L-alanine (≥99.0%), L-phenylalanine (≥99.0%), silver(I) oxide (≥98 %), potassium hydroxide, potassium carbonate. 4-chloroanisole, 1-bromonaphthalene, HCl (37% sat. aq. solution), cetyltrimethylammonium bromide, 3Å molecular sieves.

Fischer Scientific

Chlorobenzene, bromobenzene.

AppliChem

Formaldehyde (37 % aq. Solution).

Acros Organic

Dry pyridine, dry tetrahydrofuran, dry dichloromethane, dry acetonitrile, d^3-acetonitrile.

Merck

Glycine (p.a. 99.7 %)

Imidazolium carboxylate zwitterions

These compounds were prepared according to the procedure outlined in reference []. The compounds were presented and characterized as part of another PhD thesis.

Imidazolium ester chlorides

A flask with a Soxhlet apparatus containing molecular sieves (3 Å) was charged with **1a**–**1f** (1 mol) and a stir bar under argon. Ethanol (150 ml) was then added as a reactant and solvent, followed by acetyl chloride (1.2 mol, 1.2 equiv). The mixture was refluxed at 150 °C for 4 hours. After cooling, the solution was filtered through a PTFE membrane and the solvent was removed under reduced pressure. The obtained residue was washed with diethyl ether and dried affording the desired ligand precursors, which were stored under an argon atmosphere.
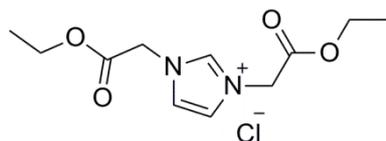
2a: White solid, yield: 89%.

^{1}H NMR (CDCl$_3$, 400MHz) δ 10.21 (s, 1H, CH$_{imi}$), 7.73 (s, 2H, CH$_{imi}$), 5.38 (s, 4H), 4.15 (q, J = 7.1 Hz, 4H), 1.21 (t, J = 7.1 Hz, 6H). ^{13}C NMR (101 MHz, CDCl$_3$) δ 166.15 (C$_{carbox}$), 139.60 (C$_{imi}$), 123.41 (C$_{imi}$), 63.05 (CH$_2$COOEt), 50.42 (CH$_2$CH$_3$), 14.14 (CH$_3$CH$_2$). ESI-MS: m/z Calcd for C$_{11}$H$_{17}$ClN$_2$O$_4$ 276.09 [M]$^+$, found 241.2 [M – Cl]$^+$. Elemental Anal: Calcd for C$_{11}$H$_{17}$ClN$_2$O$_4$: C, 47.74; H, 6.19; N, 10.12. Found: C, 47.66; H, 5.91; N, 10.05.
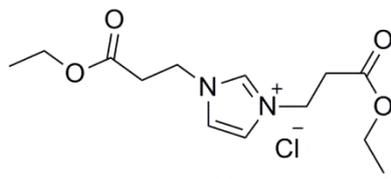
2b: Brown oil, yield: 84%.

^{1}H NMR (CDCl$_3$, 400 MHz) δ 10.67 (s, 1H, CH$_{imi}$), 7.51 (s, 2H, CH$_{imi}$), 4.65 (t, J = 5.8 Hz, 4H), 4.13 (q, J = 7.1 Hz, 4H), 3.05 (t, J = 5.8 Hz, 4H), 1.23 (t, J = 7.1 Hz, 6H). ^{13}C NMR (CDCl$_3$, 101 MHz) δ 170.40 (C$_{carbox}$), 137.80 (C$_{imi}$), 122.78 (C$_{imi}$), 61.22, 45.24, 34.60, 13.94. ESI-MS: m/z Calcd for C$_{13}$H$_{21}$ClN$_2$O$_4$ 304.12 [M]$^+$, found 269.2 [M – Cl]$^+$. Elemental Anal: Calcd for C$_{13}$H$_{21}$ClN$_2$O$_4$: C, 51.23; H, 6.95; N, 9.19. Found: C, 49.17; H, 6.59; N, 9.00.
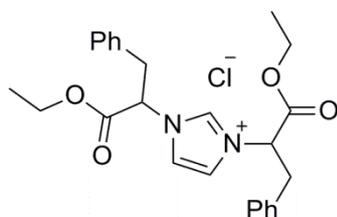
2c: Brown oil, yield: 71%.

^{1}H NMR (CDCl$_3$, 400 MHz) δ 10.77 (s, 1H, CH$_{imi}$), 7.23 – 7.21 (m, 6H), 7.16 (s, 2H, CH$_{imi}$), 7.09 – 7.06 (m, 4H), 6.01 (t, J = 7.1 Hz, 2H), 4.22 (q, J = 7.1, 1.0 Hz, 4H), 3.45 (d, J = 7.0 Hz, 4H), 1.24 (t, J = 7.1 Hz, 6H). ^{13}C NMR (CDCl$_3$, 101 MHz) δ 167.66 (C$_{carbox}$), 138.89, 133.60 (C$_{imi}$), 129.29, 129.15, 128.00, 121.15 (C$_{imi}$), 63.12, 62.72, 39.29, 14.05. ESI-MS: m/z Calcd for C$_{25}$H$_{29}$ClN$_2$O$_4$ 456.18 [M]$^+$, found 421.4 [M – Cl]$^+$. Elemental Anal: Calcd for C$_{25}$H$_{29}$ClN$_2$O$_4$: C, 65.71; H, 6.40; N, 6.13. Found: C, 65.69; H, 6.35 N, 5.99.
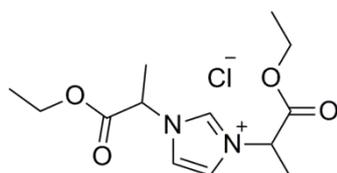
2d: Brown oil, yield 88%.

^{1}H NMR (CDCl$_3$, 400 MHz) δ 10.84 (s, 1H), 7.53 (s, 2H), 5.86 (q, J = 7.1 Hz, 2H), 4.24 (q, J = 6.9 Hz, 4H), 1.87 (d, J = 7.2 Hz, 6H), 1.29 (t, J = 7.1 Hz, 6H). ESI-MS: m/z Calcd for C$_{13}$H$_{21}$ClN$_2$O$_4$ 304.12 [M]$^+$, found 269.4 [M – Cl]$^+$.
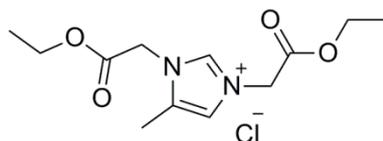
2e: Brown oil, yield 94%.

^{1}H NMR (CDCl$_3$, 400 MHz) δ 10.30 (s, 1H), 7.37 (s, 1H), 5.31 (d, J = 9.7 Hz, 4H), 4.24 – 4.19 (m, 4H), 2.26 (s, 3H), 1.27 (dd, J = 7.0, 2.7 Hz, 6H). ESI-MS: m/z Calcd for C$_{13}$H$_{21}$ClN$_2$O$_4$ 290.74 [M]$^+$, found 255.1 [M – Cl]$^+$.

NHC–Metal complexes

Ag–NHC

A Schlenk tube was charged with **2a** or **2b** (0.003 mol) and a stir bar under argon. Dry acetonitrile was added (8 ml) and the mixture was gently heated (45 °C) with stirring for 10 minutes. Silver oxide (0.64g, 0.003 mol) was then added under flow of argon and the mixture stirred at room temperature for 8 hours. The mixture was then gently heated again (45 °C) for 5 minutes to aid dissolution of the adduct, and filtered under argon by use of a cannula. The solvent was removed from the filtrate *in vacuo* to give the desired product. **3a** was isolated for characterization, whereas the unisolated residue of **3b** was simply used for further reaction.
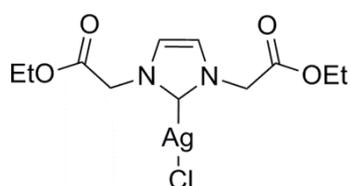
3a: White solid, yield 83%.

^{1}H NMR (CDCl$_3$, 400 MHz) δ 7.13 (s, 2H, CH$_{imi}$), 4.93 (s, 4H), 4.26 (q, *J* = 7.1 Hz, 4H), 1.32 (t, *J* = 7.2 Hz, 6H). ^{13}C NMR (CDCl$_3$, 101 MHz) δ 183.54 (C$_{carbene}$), 167.24 (C$_{carbox}$), 122.75, 62.61, 52.83, 14.21. ESI-MS: *m/z* Calcd for C$_{11}$H$_{17}$AgClN$_2$O$_4$ 384.99 [M]$^+$, found 587.3 [2L + Ag – Cl]$^+$. Elemental Anal: Calcd for C$_{11}$H$_{17}$AgClN$_2$O$_4$: C, 34.35; H, 4.46; N, 7.28. Found: C, 34.57; H, 4.28; N, 7.33.

Bis–NHC–Pd
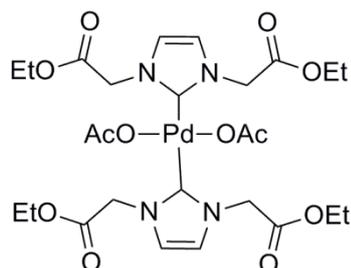
4a: A Schlenk tube was charged with **2a** (1.24g, 0.003mol) and a stir bar under argon. Dry acetonitrile was added (8ml) and stirred until dissolution. Palladium acetate (0.36g, 0.0015mol) was then added under flow of argon and mixture stirred at room temperature for 12 hours. The mixture was filtered and the precipitate dried *in vacuo.* The solid was recrystallized from CHCl$_3$ to afford the desired product. Crystals suitable for X-ray diffraction analysis were prepared from a slow diffusion chamber of CHCl$_3$/THF.

White solid, yield 44%.

^{1}H NMR (CHCl$_3$, 400 MHz) δ 6.94 (s, 2H, CH$_{imi}$), 5.57 (s, 4H), 4.23 (q, J = 7.1 Hz, 4H), 1.57 (s, 3H), 1.31 (t, J = 7.1 Hz, 6H). ^{13}C NMR (101 MHz, CDCl$_3$) δ 171.95 (C$_{carbene}$), 167.85 (CO$_{ester}$), 166.53 (CO$_{acetate}$), 122.49 (C$_{imi}$), 62.07, 52.05, 22.33, 14.25. ESI-MS: m/z 241.2 [L]$^+$, 645.1 [M – OAc]$^+$ Anal: Calcd for C$_{26}$H$_{38}$N$_4$O$_{12}$Pd: C, 44.29; H, 5.43; N, 7.95. Found: C, 43.67; H, 5.29; N, 7.95.
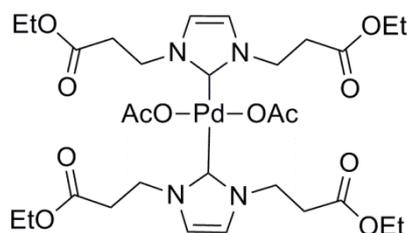
4b: A Schlenk tube was charged with 2b (1g, 0.0022mol) and a stir bar under argon. Dry acetonitrile was added (8ml) and stirred until dissolution. Palladium acetate (0.27g, 0.0011mol) was then added under flow of argon and mixture stirred at room temperature for 12 hours. The mixture was filtered and the precipitate dried *in vacuo.* The precipitate was recrystallized from a CH$_2$Cl$_2$/Et$_2$O solvent mixture to afford the desired product.

White solid, yield 22%.

^{1}H NMR (CDCl$_3$, 400 MHz) δ 7.06 (s, 2H, CH$_{imi}$), 4.36 (t, J = 6.4 Hz, 4H), 4.09 (q, J = 7.2 Hz, 5H), 2.80 (t, J = 6.4 Hz, 4H), 1.96 (s, 3H), 1.19 (t, J = 7.2 Hz, 6H). ^{13}C NMR (101 MHz, CDCl$_3$) δ 176.86 (CO$_{acetate}$), 172.20 (CO$_{ester}$), 170.51 (C$_{carbene}$), 121.39 (C$_{imi}$), 60.80, 46.22, 35.99, 22.58, 14.31. ESI-MS m/z 269.2 [L]$^+$, 701.2 [M – OAc]$^+$. Anal: Calcd for C$_{30}$H$_{46}$N$_4$O$_{12}$Pd: C, 47.34; H, 6.09; N, 7.36. Found: C, 47.22; H, 5.81; N, 7.35.
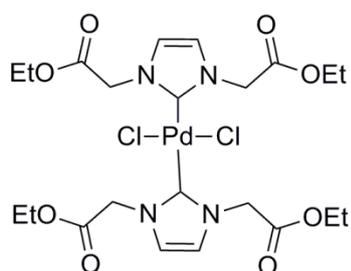
5a: A Schlenk tube was charged with 3a (0.79g, 0.002mol) and a stir bar under argon. Dry acetonitrile was added (8ml) and the mixture was stirred until dissolution. Palladium(II) chloride (0.18g, 0.001mol) was then added under flow of argon and the mixture was further

stirred at 50°C for 12 hours. The suspension was filtered and the filtrate dried *in vacuo.* The obtained crude solid was recrystallized from $CHCl_3$ to afford the desired product. Crystals suitable for X-ray analysis were prepared from a slow evaporation chamber of CH_2Cl_2/THF.

Yellow solid, yield 36%.

^{1}H NMR ($CDCl_3$, 400 MHz) δ 7.03 (s, 2H, CH_{imi}), 5.32 (s, 4H), 4.26 (q, *J* = 7.1 Hz, 4H), 1.29 (t, *J* = 7.1 Hz, 6H).^{13}C NMR (101 MHz, $CDCl_3$) δ 171.88 ($C_{carbene}$), 167.83 (C_{carbox}), 122.50, 62.03, 51.99, 14.22. ESI-MS: *m/z* Calcd for $C_{22}H_{32}Cl_2N_4O_8Pd$658.08 [M]$^+$, found 623.3 [M – Cl]$^+$. Elemental Anal. Calcd for $C_{22}H_{32}Cl_2N_4O_8Pd$: C, 40.17; H, 4.90; N, 8.52. Found: C, 40.29; H, 4.75; N, 7.84.
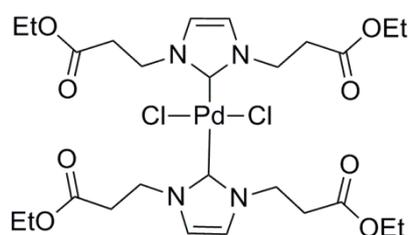
**5b**: A Schlenk tube was charged with 3b (0.94g, 0.0023mol) and a stir bar under argon. Dry acetonitrile was added (8ml) and the mixture was stirred until dissolution. Palladium(II) chloride (0.2g, 0.0011mol) was then added under flow of argon and the mixture was stirred at room temperature for 12 hours. The mixture was filtered and the filtrate was transferred to a freezer at -20°C overnight to afford the desired product. Crystals suitable for X-ray analysis were prepared from a slow evaporation chamber of CH_2Cl_2/THF.

Yellow solid, yield 33%.

^{1}H NMR ($CDCl_3$, 400 MHz) δ 6.96 (s, 2H, CH_{imi}), 4.79 (t, *J* = 6.7 Hz, 4H), 4.16 (q, *J* = 7.1 Hz, 4H), 3.23 (t, *J* = 6.7 Hz, 4H), 1.26 (t, *J* = 7.2 Hz, 6H). ^{13}C NMR (101 MHz, $CDCl_3$) δ 171.63 ($C_{carbene}$), 170.50 (C_{carbox}), 121.71, 60.98, 46.20, 35.96, 14.27. ESI-MS: *m/z* Calcd for $C_{26}H_{40}Cl_2N_4O_8Pd$ 714.13 [M]$^+$, found 679.3 [M – Cl]$^+$. Elemental Anal: Calcd for $C_{26}H_{40}Cl_2N_4O_8Pd$: C, 43.74; H, 5.65; N, 7.85. Found: C, 43.74; H, 5.44; N, 7.84.

Mono–NHC–Pd (PEPPSI)

A Schlenk tube was charged with 2a – 2c (0.0033mol), K_2CO_3 (0.004mol), Palladium(II) chloride (0.69g, 0.004mol), freshly powdered 3Å molecular sieves (80mg) and a stir bar under argon. Dry pyridine (7ml) was added and the mixture stirred at 50°C for 36 hours. The mixture was then filtered and the filtrate was evaporated to dryness. The crude solid was recrystallized from hot ethanol to afford the desired product.
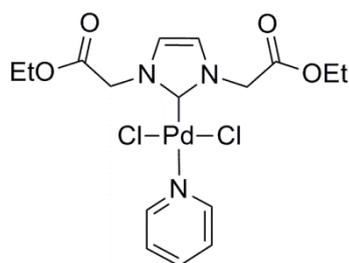
6a: Yellow solid, yield 36%. Crystals suitable for X-ray analysis were prepared from a slow evaporation chamber of $CHCl_3$/Petroleum ether 60°-80°.

^{1}H NMR (CDCl$_3$, 400 MHz) δ 8.96 – 8.94 (m, 2H), 7.79 – 7.74 (m, 1H), 7.35 (dd, J = 7.7, 6.5 Hz, 2H), 7.15 (s, 2H, CH$_{imi}$), 5.45 (s, 4H), 4.29 (q, J = 7.2 Hz, 4H), 1.32 (t, J = 7.1 Hz, 6H). ^{13}C NMR (CDCl$_3$, 101 MHz,) δ 167.33, (C$_{carbox}$) 153.19 (C$_{carbene}$), 151.44, 138.27, 124.62, 123.46, 62.27, 52.07, 14.23. ESI-MS: m/z Calcd for $C_{16}H_{21}Cl_2N_3O_4Pd$ 496.99 [M]$^+$, found 462.1 [M – Cl]$^+$. Elemental Anal: Calcd for $C_{16}H_{21}Cl_2N_3O_4Pd$: C, 38.69; H, 4.26; N, 8.46. Found: C, 38.71; H, 4.11; N, 8.40.
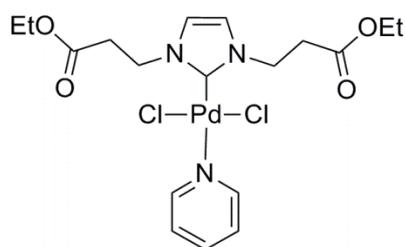
6b: Yellow solid, yield 30%. Crystals suitable for X-ray analysis were prepared from a slow evaporation chamber of $CHCl_3$/Petroleum ether 60°-80°.

^{1}H NMR (CDCl$_3$, 400 MHz) δ 8.99 – 8.97 (m, 2H), 7.79 – 7.76 (m, 1H), 7.36 (dd, J = 7.7, 6.5 Hz, 2H), 7.06 (s, 2H, CH$_{imi}$), 4.84 (t, J = 6.5 Hz, 4H), 4.15 (q, J = 7.1 Hz, 4H), 3.22 (t, J = 6.4 Hz, 4H), 1.24 (t, J = 7.1 Hz, 6H). ^{13}C NMR (CDCl$_3$, 101 MHz) δ 171.67 (C$_{carbox}$), 151.37, 149.76 (C$_{carbene}$), 138.28, 124.65, 122.97, 61.13, 46.32, 35.50, 14.28. ESI-MS: m/z Calcd for $C_{18}H_{25}Cl_2N_3O_4Pd$ 525.02 [M]$^+$,

found 489.2 [M – Cl]$^+$. Elemental Anal: Calcd for C$_{18}$H$_{25}$Cl$_2$N$_3$O$_4$Pd: C, 41.20; H, 4.80; N, 8.01. Found: C, 41.26; H, 4.72; N, 7.88.
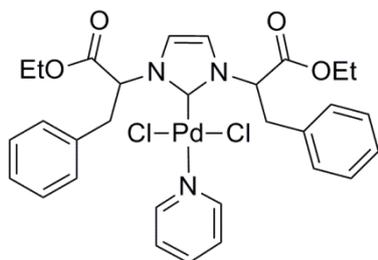
6c: Yellow solid, yield 26%.

^{1}H NMR (Acetonitrile-d_3, 400 MHz) δ 8.90 (dd, J = 6.5, 1.6 Hz, 2H), 7.94 (tt, J = 7.7, 1.7 Hz, 1H), 7.51 (dd, J = 7.7, 6.5 Hz, 2H), 7.33 – 7.26 (m, 10H), 7.22 (s, 2H, CH$_{imi}$), 6.51 (dd, J = 8.1, 6.9 Hz, 2H), 4.14 (q, J = 7.1 Hz, 4H), 3.52 (dd, J = 7.5, 2.7 Hz, 4H), 1.13 (t, J = 7.1 Hz, 6H). ^{13}C NMR (CD$_3$CN, 101 MHz) δ 170.23 (C$_{carbox}$), 151.91(C$_{carbene}$), 139.87, 136.50, 130.31, 129.52, 128.12, 125.88, 121.91, 64.83, 62.75, 39.25, 14.23. ESI-MS: m/z Calcd for C$_{30}$H$_{33}$Cl$_2$N$_3$O$_4$Pd 677.09 [M]$^+$, found 642.3 [M – Cl]$^+$. Elemental Anal: Calcd for C$_{30}$H$_{33}$Cl$_2$N$_3$O$_4$Pd: C, 53.23; H, 4.91; N, 6.21. Found: C, 53.39; H, 4.75; N, 6.27.
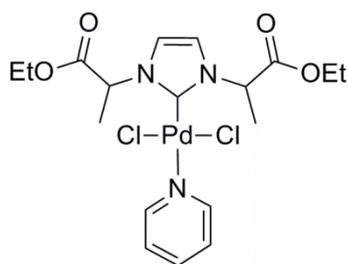
6d: Yellow solid, yield 11%. Crystals suitable for X-ray analysis were prepared from a solution of the complex in acetone at -20 °C.

^{1}H NMR (400 MHz, CDCl$_3$) δ 8.98 (dd, J = 6.5, 1.5 Hz, 2H), 7.76 (tt, J = 7.6, 1.6 Hz, 1H), 7.37 – 7.31 (m, 2H), 7.25 (s, 2H, CH$_{imi}$), 6.45 (q, J = 7.4 Hz, 2H), 4.25 (q, J = 7.1 Hz, 4H), 1.80 (d, J = 7.4 Hz, 6H), 1.30 (t, J = 7.1 Hz, 6H). ^{13}C NMR (101 MHz, CDCl$_3$) δ 170.73 (C$_{carbox}$), 151.46 (C$_{carbene}$), 151.42, 138.21, 124.56, 120.40, 62.15, 58.62, 19.18, 14.21. ESI-MS: m/z Calcd for C$_{18}$H$_{25}$Cl$_2$N$_3$O$_4$Pd 525.02 [M]$^+$, found 489.1 [M – Cl]$^+$.

Ir–NHC
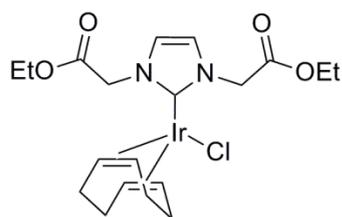
7a: In a glovebox under argon atmosphere, a Schlenk tube was charged with [Ir(COD)Cl]$_2$ (0.44g, 0.00065 mol) and **3a** (0.5g, 0.0013 mol) and a stir bar. Dry CH_2Cl_2 (5ml) was added via cannula under argon and the mixture was stirred at room temperature for 24 hours. The resulting mixture was filtered with a cannula filter under argon with gentle heating. The dark orange filtrate was dried under vacuum to produce the crude product. The yellow/red solid was recrystallized in Et$_2$O to produce the desired product as a crystalline yellow solid.

Yellow solid, yield 78%. Crystals suitable for X-ray analysis were prepared from a slow evaporation chamber of CH_2Cl_2/Petroleum ether 60°-80°.

^{1}H NMR (400 MHz, d^6-THF) δ 7.14 (s, 2H, CH$_{imi}$), 5.70 (d, J = 17.5 Hz, 2H, C$\underline{H_2}$COOEt), 4.85 (d, J = 17.5 Hz, 2H, CH$_2$COOEt), 4.53 – 4.45 (m, 2H, CH(COD)), 4.22 (tdd, J = 10.8, 7.1, 3.6 Hz, 4H, COOC$\underline{H_2}$), 2.93 – 2.77 (m, 2H, CH(COD)), 2.19 – 2.07 (m, 4H, CH$_2$(COD)), 1.69 (m, 2H, CH$_2$(COD)), 1.56 (m, 2H, CH$_2$(COD)), 1.28 (t, J = 7.1 Hz, 6H, CH$_2$C$\underline{H_3}$). ^{13}C NMR (101 MHz, d^6-THF) δ 183.89 (C$_{carbene}$), 169.27 (C$_{carbox}$), 123.02, 85.69, 62.15, 52.04, 51.88, 34.57, 30.40, 14.67. ESI-MS: m/z Calcd for $C_{21}H_{35}ClIrN_2O_4$ 607.18 [M]$^+$, found 572.4 [M – Cl]$^+$. Elemental Anal: Calcd for $C_{21}H_{35}ClIrN_2O_4$: C, 39.61; H, 4.90; N, 4.86. Found: C, 39.77; H, 4.99; N, 4.86.

Silyl amide
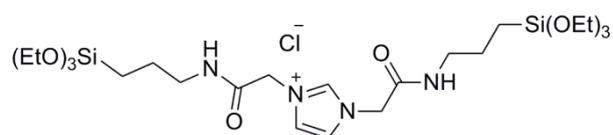
8a: **2a** (4g, 0.015 mol) was added to a two-necked round-bottom flask with a stirrer and purged with argon. Aminopropyltriethoxysilane (6.76ml 0.03 mol) was added followed by dry CH_2Cl_2 (100ml). The mixture was stirred at room temperature for 24 hours. The solvent was removed under vacuum and the resulting solid was washed with hexane followed by drying to produce the desired product. **8a** was stored in a glovebox under inert atmosphere.

White waxy solid, yield 90%.

^{1}H NMR (400 MHz, d^6-THF) δ 9.57 (s, 1H), 9.05 (t, J = 5.4 Hz, 2H), 7.71 (s, 2H), 5.26 (s, 4H), 3.79 (q, J = 7.0 Hz, 12H), 3.16 (dd, J = 13.0, 6.8 Hz, 4H), 1.60 (dt, J = 15.7, 7.8 Hz, 4H), 1.18 (t, J = 7.0 Hz, 18H), 0.70 – 0.57 (m, 4H). ^{13}C NMR (101 MHz, d^6-THF) δ 165.79, 139.61, 123.91, 58.95, 52.30, 43.17, 23.88, 18.91, 8.84. ESI-MS: m/z Calcd for $C_{25}H_{51}ClN_4O_8Si_2$ 627.32 [M]$^+$, found 591.3 [M – Cl]$^+$. Elemental Anal: Calcd for $C_{25}H_{51}ClN_4O_8Si_2$: C, 47.87; H, 8.19; N, 8.93. Found: C, 46.17; H, 7.59; N, 8.59.

Procedure for the catalytic oxidation of glycerol

Benzoquinone (0.324g, 3mmol) molecular sieves (3Å, 100mg), and [Pd] (**4a**, **4b** or Pd(OAc)$_2$, 0.05mmol) was weighed into a round-bottom flask with a stir bar. Glycerol (0.074ml, 1mmol) was then added dissolved in 0.5 ml water, (in the case of Pd(OAc)$_2$, triethylamine (0.014ml, 0.1 mol) was added at this point). Acetonitrile-d^3 (5ml) was then added and the mixture was stirred for 1 hour. The mixture was then filtered with a syringe filter and immediately analysed using ^{1}H NMR.

Procedure for the catalytic oxidation of benzyl alcohol

[Pd] (**4a**, **4b** or Pd(OAc)$_2$) (0.03mmol), was weighed into a two-necked round-bottom flask alongside molecular sieves (200mg) and a stir bar. A mixture of THF and Toluene (1:5 equivalents) (3.2ml) was then added. The flask was purged slowly under vacuum and then refilled with oxygen gas three times, a balloon of oxygen gas was then added using needle and septum. Benzyl alcohol (0.121ml, 1mmol) was then added and the mixture stirred at room temperature for 3 hours. The resulting mixture was filtered over a plug of celite and subsequently submitted for GC-MS analysis.

Procedure for the electrocatalytic reduction of CO$_2$

Tetrabutylammonium hexafluorophosphine (0.387g, 0.1 mol) and [Pd] (**4a**, **4b**, **5a** or **5b**, 0.1mmol) were added to a two-necked flask under nitrogen atmosphere. Dry acetonitrile (10ml) was added with a needle and the solids were shaken until dissolution. The solution was then pipetted into a nitrogen or CO$_2$-purged electrochemical chamber with a 7mm^2 glassy carbon working electrode, an Ag/AgNO$_3$ reference electrode, and a platinum wire counter electrode. The corresponding gas was slowly bubbled into the solution over 10 minutes, after which the experiment was begun. CVs were run at 100mV/s between a range of -2.7 V and 2V for 5 cycles, the 3rd cycle was taken in each case. The setup was calibrated using ferrocene as a standard against the Ag/AgNO$_3$ electrode. Electrodes were cleaned using alumina paste and rinsed with ethanol and water before drying over a flow of nitrogen.

Procedure for the Suzuki-Miyaura catalytic screenings in methanol

A reaction vial was charged with base (2.0mmol), phenylboronic acid/pinacol ester (1.5mmol), [Pd] (Pd(OAc)$_2$ with ligands **2a–2c** (1 equivalent)) (0.05mmol) and a stir bar under air. Methanol (5ml) was added, followed by aryl halide (1 mmol). The mixture was stirred at room temperature for 1 hour. Upon completion, the mixture was cooled to 5°C. The resulting mixture was filtered over a plug of celite and subsequently submitted for GC-MS analysis.

Procedure for the Suzuki-Miyaura catalytic screenings in water

A reaction vial was charged with base (1.0mmol), phenylboronic acid/pinacol ester (0.75mmol), TBAB (1.0mmol), [Pd] (complexes **4a–6c**) (0.01mmol) and a stir bar under air. Water (2ml) was added, followed by aryl halide (0.5mmol). The mixture was stirred at 60°C for 24 hours. Upon completion, the mixture was cooled to 5°C. The products were then extracted with ethyl acetate (2x5ml), filtered, and evaporated to dryness. The residue was directly dissolved in CDCl$_3$ for ^{1}H NMR analysis. Yields were calculated using trimethoxybenzene (0.3mmol) as an internal standard.

Procedure for the kinetic experiments for the Suzuki-Miyaura catalytic screenings in water

A reaction vial was charged with K$_2$CO$_3$ (1.0mmol), phenylboronic acid (0.75mmol), TBAB (0.1mmol), complex **6b** (0.01mmol) and a stir bar under air. Water (2ml) was added, followed by bromoacetophenone (0.5mmol). The mixture was stirred at 60°C for the allotted time. The reaction was quenched by adding 2ml HCl (1M) and cooling the mixture to 5°C. The products were then extracted with ethyl acetate (2x5ml), filtered, and evaporated to dryness. The residue was directly dissolved in CDCl$_3$ for ^{1}H NMR analysis. Yields were calculated using trimethoxybenzene (0.3mmol) as an internal standard.

Procedure for the mercury poisoning experiments

A reaction vial was charged with base (1.0mmol), complex (0.01mmol) and a stir bar under air. Water (2ml) was added, and the mixture was stirred at 60°C for 2 hours to pre-dissolve the complex. Mercury was added (3mmol), followed by phenylboronic acid (0.75mmol) and bromoanisole (0.5mmol). The reaction was stirred for 24 hours under 60°C heating. Upon completion, the mixture was cooled to 5°C. The products were then extracted with ethyl acetate (2x5ml), filtered, and evaporated to dryness. The residue was directly dissolved in CDCl$_3$ for ^{1}H NMR analysis. Yields were calculated using trimethoxybenzene (0.3mmol) as an internal standard.

Procedure for the catalyst recycling

A reaction vial was charged with K_2CO_3 (1.0mmol), phenylboronic acid (0.75mmol), complex **6b** (0.01mmol) and a stir bar under air. Water (2ml) was added, followed by bromoacetophenone (0.5mmol). The mixture was stirred at 60°C for 1 hour. The mixture was then cooled to 5°C. The products were then extracted with ethyl acetate (2x5ml), filtered, and evaporated to dryness. The residue was directly dissolved in $CDCl_3$ for 1H NMR analysis. Yields were calculated using trimethoxybenzene (0.3mmol) as an internal standard. The aqueous layer was evaporated to dryness and the residue was redissolved in 2ml water, this was recharged with base, reactants and TBAB and used for the next run.

General procedure for the grafting of imidazolium zwitterion carboxylate 1e onto aminopropyl silica

1e (0.5g, 2.5mmol) was added to a three-necked flask with a stirrer and purged with argon. $SOCl_2$ (6ml) was added and the reaction was stirred at 50 °C for 2 hours, and then at 70 °C for a subsequent 2 hours. The residue was then vacuumed to dryness using a trap with NaOH solution to neutralize the gaseous HCl. Diisopropylethylamine (Hünig's base) (15ml) was then added, followed by aminopropyl silica (1g) which had been dried for 4 hours in an oven at 60 °C. The reaction was then stirred for 24 hours at room temperature. Ethanol was added to quench the remaining acyl chloride and the mixture was filtered. The resulting solid was dried in a vacuum oven at 40 °C for 48 hours to produce the desired material.

Procedure for the co-condensation of 8a with TEOS

An aqueous ammonia solution (3.5M) (17ml) was added to a round-bottom flask followed by CTAB surfactant, the solution was stirred for 1 hour at room temperature. **8a** (2.1g, 3.3mmol) was then added in a 1ml solution of ethanol, followed by tetraethoxyorthosilicate (1.5ml, 6.6mmol). The general ratio of **8a**:TEOS:CTAB:NH_3:H_2O was 1:2:0.27:18:224. The solution was stirred at 60°C for 12 hours, followed by heating without stirring at 90 °C for another 24 hours. The solution was filtered, washed with water and dried in a vacuum oven at 40 °C for 24 hours to yield the desired material. To wash out the surfactant, the material was suspended in ethanol (100ml) with 37% HCl solution (2ml) for 24 hours and filtered; the resulting material was dried in a vacuum oven at 40 °C for 24 hours.

VI   Applied Characterization Methods

NMR spectrometry

Nucleus-localized protons (or nucleons) exhibit a spin property, this means that the dipole produced from the nucleus' overall charge has angular momentum. The ratio of the magnetic dipole (μ) of a nucleus versus its angular momentum (L) produced by the spin is expressed as the magnetogyric ratio (γ):

$$\gamma = \frac{\mu}{L}$$

When an external magnetic field is applied (B_0), these spins can be aligned in the direction of the field (z-axis). The aligned orientation depends on the spin state of the nucleon, of which there are two, corresponding to the spin quantum number ($m_z = \frac{1}{2}$ or $-\frac{1}{2}$). By applying a radio frequency (RF) pulse perpendicular to the aligned spins (x-axis), the spins can be inverted, causing the vector of the magnetic dipoles to be pushed away from the direction of the external field B_0 (towards the x-y plane). The relaxation of the spin states back to their alignment along B_0 indicated as relaxation decay lifetime (T_1), and the relaxation of the nuclei back to their original spin-states (decay lifetime T_2) produce an emitted radio frequency which can be measured using a magnetic coil. The signal produced from this decay is recorded as an FID (free induction decay), which is different depending on the nuclei present. Only nuclei with odd numbers of nucleons produce an FID (^{1}H, ^{13}C, etc.), since the relaxation of spin states with equal number cancel each other out. The FID can be processed by Fourier Transform to produce the NMR spectrum.

Nuclei with differing degrees of electron density surrounding them produce different FID signals, and therefore different spectra. Nuclei surrounded by many electrons (shielded) resonate at lower frequencies than those surrounded by fewer electrons (deshielded). The difference in resonance frequency (chemical shift δ) of each nucleus is given with respect to a standard, which is usually TMS (tetramethylsilane $\delta=0$).

Spin-spin coupling also plays a role in the final NMR spectrum. Both directly and through their bonding electrons, nuclei spins can interact with each other, each interaction possessing different energies. On the spectrum, this manifests as signal splitting, which can be predicted using the rule that each signal is split corresponding to the number of neighbouring protons plus one (n + 1 rule). All of this information can be used to determine the environment of each NMR active nucleus within the sample, and thus determine the samples' structure.

All solution NMR experiments within this thesis were performed by the author. Proton ([1]H 400MHz) and ^{13}C decoupled experiments (101MHz) were performed on Bruker Spectrospin 400MHz Ultrashield and Ascend 400MHz spectrometers using deuterated solvents, referencing chemical shifts to the residual solvent signal.

Solid state NMR spectrometry follows the same physical principles as solution NMR; however the orientation-dependency is greatly exaggerated. The anisotropic interactions which in solution NMR are averaged out by Brownian motion are fixed in place due to the solid state of the sample. This results in very broad spectra stemming from the extra signals produced within the FID. A number of techniques can be used to counter this. The two most used techniques are cross-polarization (CP) and magic-angle spinning (MAS).

CP involves transferring polarization from abundant nuclear spins (such as ^{1}H nuclei) to more dilute spins (such as ^{13}C). This relies on the strong dipolar coupling observed within abundant nuclei, the T_1 relaxation frequencies of the abundant and dilute nuclei are matched by adjusting the power of the RF pulse on each channel. This matching of relaxation frequencies (Hartmann-Hahn match) allows the transfer of spin polarization from the abundant to the dilute nuclei.

MAS attempts to average out the anisotropic interactions by spinning the sample to a greater or equal rate of the interactions themselves. The Hamiltonian function of both the dipolar and chemical shielding interactions contain the term $3\cos^2\theta - 1$, where θ is an angle with respect to B_0. By solving the term for zero, $\theta = 54.74\,°$, this is known as the "magic angle". By spinning the sample at this angle with respect to B_0, the magnitudes of any anisotropic interaction containing that term is reduced to zero. Combining the CP and MAS techniques produces high-resolution solid-state NMR spectra, known as CP MAS NMR spectra.

Silicon-29 NMR experiments are also commonly used within solid-state NMR. [29]Si features a negative magnetogyric ratio so therefore many of the Si-NMR spectra feature peaks within the negative ppm range with respect to TMS. A large degree of splitting is often observed within organosilica samples therefore decoupling experiments tend to be performed. Narrow-band RF pulses are also often used to prevent noise as a result of silicon contained within the glass sample tube.

CP MAS ^{13}C and [29]Si experiments were performed at the Université de Montpellier 2 by the Peter Hesemann group using a Bruker ASX 400 device using a 3.2 mm probe head. [13]C experiments were performed using combined CP and MAS techniques, [29]Si experiments were performed using a one-pulse technique using an acquisition frequency of 59.59 kHz.

Mass spectrometry (MS)

Neutral analyte compounds can be ionized using a suitable device such as an electron gun. By propelling the charged analyte in the gas phase through a magnetic field towards a detector, and judging the trajectory and deflection of the analyte, the mass of the ionized sample can be determined. The mass spectrum allows for the detection of the analyte according to the mass-to-charge ratio (m/z) of the molecular ion and its relative abundance. Fragmentation of the parent ion into smaller daughter ions allows the elucidation of various structural features. Various methods of ionization and detection are available. The most common ionization techniques are electron ionisation (EI) and electrospray ionisation (ESI).

Within this thesis, only ESI was used, as a popular technique for analysing organic and organometallic analytes. Although EI is often used within organometallics, since it produces predictable fragmentation patterns (typically metal plus charged ligand species); ESI was used since easily fragmentable linkages occur within the ligand structure (such as carbonyl linkages). Within ESI, the analyte dissolved within an eluent is ionised as a solution, and sprayed from a fine capillary producing an aerosol of gaseous ionized analyte with its solvent. The gaseous analyte is then desolvated in a process called "nebulisation", in which the sample is sprayed into a region of warm bath gas to evaporate the ionized solvent.

Mass spectrometry was performed by the author on a Thermo Scientific Velos Pro MS system coupled with a liquid chromatography injection system without the use of a column. Water soluble samples were performed in water as eluent with formic acid ionizing agent. Organic soluble samples were performed in methanol as eluent with formic acid ionizing agent. Metal complexes were performed in acetonitrile eluent without ionizing agent.

X-Ray diffraction

A crystalline solid has a structure which repeats identically in three dimensions. The central repeated motif (unit cell) can be split into planes according to its 3D Bravais lattice, along which atoms are arranged. The points at which the atoms intercept the lattice planes are termed Miller indices; both these and the spacing between the planes (d) uniquely describe the arrangement of a unit cell. X-Rays are scattered by the electron density within atoms into a diffraction pattern. The resulting diffraction pattern is caused by constructive and destructive interference between diffracted waves from the d-spacings, and is unique to each crystal. Therefore, diffracting X-Rays from a sample at various different angles can produce structural information about a crystal unit cell and any molecules contained there within. Assuming constructive interference between diffracted X-Rays, the relationship between the wavelength of incident light (λ), spacing between

lattice planes (d) and the angle of incident light with respect to the lattice plane (the Bragg angle θ) is described by Bragg's Law:

$$n\lambda = 2d sin\theta$$

Using the Bragg angle and d-spacing, the Miller indices can be ascertained for any given crystal geometry. Within a powder diffraction sample (PXRD), many microcrystalline particles are randomly arranged, so the commonly occurring diffraction patterns are subtracted from background diffractions.

Within this work, PXRD measurements were recorded by the author on a Bruker D8 diffractometer using Cu-Kα radiation (λ = 0.154 nm) and a scintillation counter (KeveX Detector). Match! Software was used to view and compare diffraction patterns.

Single-crystal XRD requires a single crystal of the sample and is thus much more difficult to obtain, however the resulting diffraction pattern provides much more structural information than that of PXRD. Since the intensity of each diffracted light wave is directly proportional to the electron density within the material, this can be used to produce a 3D pattern of electron density within the unit cell. This relationship is described within the structure factor equation:

$$I = \frac{LptF^2}{K}$$

Where I is the intensity of each light "reflexion" and F is the structure factor, which can be Fourier transformed to give the electron density at point (x,y,z) described by the Miller indices. The electron density pattern can be solved using "direct methods" or "Patterson methods" which use probability densities to ascertain the atom position, among others such as heavy-atom methods. The structure is then refined by least squares minimization and comparison to known atom sizes and bond lengths to produce the final molecular structure. The reliability of the final structure is represented by the R factor.

Single-crystal diffraction data was obtained and solved by Prof. Uwe Schilde and Frau Alexandra Kelling at the Potsdam Universität inorganic chemistry department, using single crystals grown by the author. The crystals were mounted on a glass fibre. Intensity data were collected at 210 K using a STOE Imaging Plate Diffraction System IPDS-2 with graphite monochromatized Mo-Kα radiation (λ = 0.71073 Å) at 50 kV and 40 mA. The data were corrected for Lorentz and polarisation effects using the program X-Area1. Numerical absorption corrections were applied using optimized shape. The structures were solved by direct methods (SHELXS-2013/1), and refined with full-matrix least-squares on F^2 using the program SHELXL-2014/72b. Non-hydrogen atoms were refined with anisotropic temperature factors. Refinement data for each

crystal structure is presented in the appendix. Images for this thesis were produced using the DIAMOND software package with the POV-RAY imaging add-on. Bond lengths, angles, and crystal parameters were collected using the DIAMOND software and PLATON freeware programs.

Fourier transform infrared (FT-IR) spectroscopy

The chemical bonds between molecules vibrate within the energy range of infrared light. Bonds can therefore absorb infrared light and vibrate at a specific frequency, causing the dipole moment between two atoms to change. The frequency depends on the energy of the bond and the nature of the vibration. The Fourier transformed pattern of absorbed infrared light produces an FT-IR spectrum which can be used to ascertain the types of bonds contained within the molecule. Samples pressed into discs diluted with KBr were used within this work in order to enhance the resolution between minor peaks and dominating peaks, typically common for organosilica materials.

Infrared spectra were recorded on a ThermoScientific Nicolet iS5 FT-IR spectrometer using a prepared KBr disc at a resolution of 4 cm^{-1} and averaged over 16 scans.

Elemental analysis

In order to obtain the percentage of hydrogen, carbon, nitrogen, and various other heteroatoms within a sample, combustion of the sample within a saturated oxygen atmosphere can be performed. The gaseous compounds CO_2, NO_2, and H_2O are formed from combustion and can be quantified by collection in traps. The content and purity of a sample can be judged using this technique.

Elemental analysis was performed by Frau Silvia Porik using a varioMICRO V 1.4.1 device from Elementar Analysensysteme GmbH.

Thermogravimetric analysis (TGA)

A sample can be thermally decomposed under inert (N_2) or oxidative (air) atmosphere. By measuring the change in mass of the sample with respect to time and temperature, a thermal decomposition model of the sample can be obtained. Within this work, TGA was used to ascertain the organic content of an organic-inorganic hybrid material.

TGA analysis was performed by Frau Ursula Lubahn on a Netzsch TG209 F1 Iris device with a heating rate of 10 K/min from 25 °C to 1000 °C.

Gas chromatography (GC)

The individual molecular substituents of a mixture can be separated by injecting the sample into an eluent (mobile phase) and forced through a porous solid (stationary phase). The individual molecules can thereby be separated in order of size and often polarity (depending on the type of mobile phase) according to the principles of chromatography. Gas chromatography allows this to be performed rapidly in the gas phase for volatile samples. The samples, dissolved in an appropriate solvent, are vaporized and forced through a column containing the stationary phase within a carrier gas mobile phase. Within this work, GC was used coupled with MS to separate and quantify the substituents of a catalytic reaction.

GC-MS analysis was performed by the author using an Agilent Technologies 5975 gas chromatograph equipped with a MS detector and a capillary column (HP-5MS, 30 m, 0.25 mm, 0.25 μm). The temperature program started with an isothermal step at 50 °C for 2 min, the temperature was then increased to 300 °C at a rate of 30 °C/min and maintained for 1 min. MS spectra were referenced according to the NIST 08 database with a retention index allowance of ± 100.

Nitrogen sorption

The surface area and respective pore size of a material can be obtained by saturating the material with N_2 under a range of pressures. The resulting data can be fit to an isotherm model in order to evaluate the surface information. Within this work, surface area was calculated according to the Brauner-Emmett-Teller (BET) isotherm.

Nitrogen sorption measurements were performed by Frau Irina Shekova using a Quantachrome Quadrasorb device at the temperature of liquid nitrogen. The samples were previously degassed at 150 °C for 20 hours and analyzed with QuadraWin analysis software (version 5.05).

Transmission electron microscopy (TEM)

A traditional light microscope uses a series of lenses to magnify an image using light within the visible spectrum. Since the De Broglie wavelength of an electron is magnitudes shorter than that of a photon, using an electron beam can produce images with extortionate magnification in high resolution. For TEM, an electron beam is fired at a sample through a collimating lens, the beam is diffracted by the sample and the diffracted electrons are focused onto an imaging plate using a focusing lens. Likewise, relaxation of outer-shell electrons to inner shells emits X-Ray radiation. The pattern of the X-Rays can also be used to obtain information about the crystal lattice using the d spacing between planes. Within this work, nanoparticles were observed using the heavy contrast between the high electron density of metal particles compared to other particles within the solution.

TEM images were recorded by Dr. Valerio Molinari and Frau Heike Runge using a Zeiss EM 912Ω microscope operated at an acceleration voltage of 120 kV.

VII   Bibliography

1. U. IUCN, WWF, 1980.
2. EPA, ed. EPA, 1990
3. W. Anastas J. C., P. T. , *Green Chemistry: Theory and Practice*, Oxford University Press, 1998.
4. B. M. Trost, *Science*, 1991, 1471–1477.
5. R. A. Sheldon, *Chem. Ind. (London, U. K.)*, 1992.
6. R. A. Sheldon, *C. R. Acad. Sci. Paris, IIc, Chimie/Chemistry*, 2000, 541-551.
7. C. Jiménez-González, A. D. Curzons, D. J. C. Constable and V. L. Cunningham, *The International Journal of Life Cycle Assessment*, **9**, 114-121.
8. M. R. Yates and C. Y. Barlow, *Resources, Conservation and Recycling*, 2013, **78**, 54-66.
9. V. Nallathambi Gunaseelan, *Biomass and Bioenergy*, 1997, **13**, 83-114.
10. D. Mohan, C. U. Pittman and P. H. Steele, *Energy & Fuels*, 2006, **20**, 848-889.
11. S. Yin, Y. Pan and Z. Tan, *International Journal of Green Energy*, 2011, **8**, 234-247.
12. P. Kumar, D. M. Barrett, M. J. Delwiche and P. Stroeve, *Industrial & Engineering Chemistry Research*, 2009, **48**, 3713-3729.
13. C. Teater, Z. Yue, J. MacLellan, Y. Liu and W. Liao, *Bioresource Technology*, 2011, **102**, 1856-1862.
14. M. Wang, M. Leitch and C. Xu, *European Polymer Journal*, 2009, **45**, 3380-3388.
15. T. Werpy and G. Petersen, *Top Value Added Chemicals from Biomass: Volume I -- Results of Screening for Potential Candidates from Sugars and Synthesis Gas*, 2004.
16. A. A. Rosatella, S. P. Simeonov, R. F. M. Frade and C. A. M. Afonso, *Green Chemistry*, 2011, **13**, 754-793.
17. H. W. Tan, A. R. Abdul Aziz and M. K. Aroua, *Renewable and Sustainable Energy Reviews*, 2013, **27**, 118-127.
18. R. Vanholme, B. Demedts, K. Morreel, J. Ralph and W. Boerjan, *Plant Physiology*, 2010, **153**, 895-905.
19. J. Zakzeski, P. C. A. Bruijnincx, A. L. Jongerius and B. M. Weckhuysen, *Chemical Reviews*, 2010, **110**, 3552-3599.
20. M. B. Hocking, *Journal of Chemical Education*, 1997, **74**, 1055.
21. M. Zaheer and R. Kempe, *ACS Catalysis*, 2015, **5**, 1675-1684.
22. M. Ikeda, in *Microbial Production of l-Amino Acids*, eds. R. Faurie, J. Thommel, B. Bathe, V. G. Debabov, S. Huebner, M. Ikeda, E. Kimura, A. Marx, B. Möckel, U. Mueller and W. Pfefferle, Springer, Berlin, 2003, pp. 1-35.
23. H. Enei, K. Yokozeki and K. Akashi, *Recent progress in microbial production of amino acids*, CRC Press, 1989.
24. N. Y. a. X. Chen, *Nature*, 2015, **524**, 155-157.
25. B. Cornils and W. A. Herrmann, in *Aqueous-Phase Organometallic Catalysis*, Wiley-VCH Verlag GmbH & Co. KGaA, 2005, pp. 1-24.
26. F.-S. Han, *Chemical Society Reviews*, 2013, **42**, 5270-5298.
27. FDA, ed. U. S. D. o. H. a. H. S.-F. a. D. Administration, 2012.
28. K. Alfonsi, J. Colberg, P. J. Dunn, T. Fevig, S. Jennings, T. A. Johnson, H. P. Kleine, C. Knight, M. A. Nagy, D. A. Perry and M. Stefaniak, *Green Chemistry*, 2008, **10**, 31-36.
29. D. C. Rideout and R. Breslow, *Journal of the American Chemical Society*, 1980, **102**, 7816-7817.
30. R. Breslow, *Accounts of Chemical Research*, 1991, **24**, 159-164.
31. A. Lubineau, *The Journal of Organic Chemistry*, 1986, **51**, 2142-2144.
32. T. R. Furlani and J. Gao, *The Journal of Organic Chemistry*, 1996, **61**, 5492-5497.
33. S. Narayan, J. Muldoon, M. Finn, V. V. Fokin, H. C. Kolb and K. B. Sharpless, *Angewandte Chemie International Edition*, 2005, **44**, 3157-3157.
34. W. A. Herrmann and F. E. Kühn, in *Aqueous-Phase Organometallic Catalysis*, Wiley-VCH Verlag GmbH & Co. KGaA, 2005, pp. 44-56.
35. K. H. Shaughnessy, *Chemical Reviews*, 2009, **109**, 643-710.

36. S. Ahrland, J. Chatt, N. R. Davies and A. A. Williams, *Journal of the Chemical Society (Resumed)*, 1958, 276-288.
37. B. Cornils and E. G. Kuntz, *Journal of Organometallic Chemistry*, 1995, **502**, 177-186.
38. A. L. Casalnuovo and J. C. Calabrese, *Journal of the American Chemical Society*, 1990, **112**, 4324-4330.
39. M. Lautens, A. Roy, K. Fukuoka, K. Fagnou and B. Martín-Matute, *Journal of the American Chemical Society*, 2001, **123**, 5358-5359.
40. W. A. Herrmann, C. W. Kohlpaintner, B. E. Hanson and X. Kang, in *Inorganic Syntheses*, John Wiley & Sons, Inc., 2007, pp. 8-25.
41. C.-J. Li, *Chemical Reviews*, 2005, **105**, 3095-3166.
42. L.-A. Schaper, S. J. Hock, W. A. Herrmann and F. E. Kühn, *Angewandte Chemie International Edition*, 2013, **52**, 270-289.
43. F. Joó, *Aqueous organometallic catalysis*, Springer Science & Business Media, 2006.
44. D. G. Blackmond, A. Armstrong, V. Coombe and A. Wells, *Angewandte Chemie International Edition*, 2007, **46**, 3798-3800.
45. L. Benhamou, E. Chardon, G. Lavigne, S. Bellemin-Laponnaz and V. César, *Chemical Reviews*, 2011, **111**, 2705-2733.
46. K. Öfele, *Journal of Organometallic Chemistry*, 1968, **12**, P42-P43.
47. H. W. Wanzlick and H. Schönherr, *J. Angew. Chem., Int. Ed.*, 1968, **7**, 141.
48. A. J. Arduengo, R. L. Harlow and M. Kline, *J. Am. Chem. Soc.*, 1991, **113**, 361.
49. R. Breslow, *Journal of the American Chemical Society*, 1958, **80**, 3719-3726.
50. D. Enders, K. Breuer, G. Raabe, J. Runsink, J. H. Teles, J.-P. Melder, K. Ebel and S. Brode, *Angewandte Chemie International Edition in English*, 1995, **34**, 1021-1023.
51. W. A. Herrmann, M. Elison, J. Fischer, C. Köcher and G. R. J. Artus, *Angewandte Chemie International Edition in English*, 1995, **34**, 2371-2374.
52. M. Scholl, S. Ding, C. W. Lee and R. H. Grubbs, *Org. Lett.*, 1999, **1**, 953.
53. D. Bourissou, O. Guerret, F. P. Gabbaï and G. Bertrand, *Chemical Reviews*, 2000, **100**, 39-92.
54. S. T. Liddle, I. S. Edworthy and P. L. Arnold, *Chemical Society Reviews*, 2007, **36**, 1732-1744.
55. D. J. Nelson and S. P. Nolan, *Chemical Society Reviews*, 2013, **42**, 6723-6753.
56. A. J. Arduengo, F. Davidson, H. V. R. Dias, J. R. Goerlich, D. Khasnis, W. J. Marshall and T. K. Prakasha, *Journal of the American Chemical Society*, 1997, **119**, 12742-12749.
57. M. K. Denk, A. Thadani, K. Hatano and A. J. Lough, *Angewandte Chemie International Edition in English*, 1997, **36**, 2607-2609.
58. A. J. Arduengo, H. V. R. Dias, R. L. Harlow and M. Kline, *Journal of the American Chemical Society*, 1992, **114**, 5530-5534.
59. J. C. Green, R. G. Scurr, P. L. Arnold and F. Geoffrey N. Cloke, *Chemical Communications*, 1997, 1963-1964.
60. J. C. Garrison, R. S. Simons, W. G. Kofron, C. A. Tessier and W. J. Youngs, *Chemical Communications*, 2001, 1780-1781.
61. A. A. D. Tulloch, A. A. Danopoulos, S. Kleinhenz, M. E. Light, M. B. Hursthouse and G. Eastham, *Organometallics*, 2001, **20**, 2027-2031.
62. X. Hu, Y. Tang, P. Gantzel and K. Meyer, *Organometallics*, 2003, **22**, 612-614.
63. N. M. Scott, R. Dorta, E. D. Stevens, A. Correa, L. Cavallo and S. P. Nolan, *Journal of the American Chemical Society*, 2005, **127**, 3516-3526.
64. H. Jacobsen, A. Correa, C. Costabile and L. Cavallo, *Journal of Organometallic Chemistry*, 2006, **691**, 4350-4358.
65. A. J. Arduengo, *Accounts of Chemical Research*, 1999, **32**, 913-921.
66. H. Baier, P. Metzner, T. Körzdörfer, A. Kelling and H.-J. Holdt, *European Journal of Inorganic Chemistry*, 2014, **2014**, 2952-2960.
67. A. C. Hillier, W. J. Sommer, B. S. Yong, J. L. Petersen, L. Cavallo and S. P. Nolan, *Organometallics*, 2003, **22**, 4322-4326.

68.	S. Leuthäußer, D. Schwarz and H. Plenio, *Chemistry – A European Journal*, 2007, **13**, 7195-7203.
69.	H. Clavier and S. P. Nolan, *Chemical Communications*, 2010, **46**, 841-861.
70.	C. Segarra, E. Mas-Marzá, M. Benítez, J. A. Mata and E. Peris, *Angewandte Chemie International Edition*, 2012, **51**, 10841-10845.
71.	H. M. J. Wang and I. J. B. Lin, *Organometallics*, 1998, **17**, 972.
72.	A. Krüger, E. Kluser, H. Müller-Bunz, A. Neels and M. Albrecht, *European Journal of Inorganic Chemistry*, 2012, **2012**, 1394-1402.
73.	B. Cetinkaya, P. Dixneuf and M. F. Lappert, *Journal of the Chemical Society, Dalton Transactions*, 1974, 1827-1833.
74.	B. Liu, Y. Zhang, D. Xu and W. Chen, *Chemical Communications*, 2011, **47**, 2883-2885.
75.	T. M. Trnka, J. P. Morgan, M. S. Sanford, T. E. Wilhelm, M. Scholl, T.-L. Choi, S. Ding, M. W. Day and R. H. Grubbs, *Journal of the American Chemical Society*, 2003, **125**, 2546-2558.
76.	A. S. K. Hashmi, C. Lothschütz, C. Böhling, T. Hengst, C. Hubbert and F. Rominger, *Advanced Synthesis & Catalysis*, 2010, **352**, 3001-3012.
77.	B. Liu, Q. Xia and W. Chen, *Angewandte Chemie International Edition*, 2009, **48**, 5513-5516.
78.	B. R. M. Lake, E. K. Bullough, T. J. Williams, A. C. Whitwood, M. A. Little and C. E. Willans, *Chemical Communications*, 2012, **48**, 4887-4889.
79.	G. W. Nyce, S. Csihony, R. M. Waymouth and J. L. Hedrick, *Chemistry – A European Journal*, 2004, **10**, 3839-3839.
80.	E. Levin, E. Ivry, C. E. Diesendruck and N. G. Lemcoff, *Chemical Reviews*, 2015, **115**, 4607-4692.
81.	L. R. Moore, S. M. Cooks, M. S. Anderson, H.-J. Schanz, S. T. Griffin, R. D. Rogers, M. C. Kirk and K. H. Shaughnessy, *Organometallics*, 2006, **25**, 5151-5158.
82.	A. Almássy, C. E. Nagy, A. C. Bényei and F. Joó, *Organometallics*, 2010, **29**, 2484-2490.
83.	C. Fleckenstein, S. Roy, Leuthau and H. Plenio, *Chemical Communications*, 2007, 2870-2872.
84.	S. Roy and H. Plenio, *Advanced Synthesis & Catalysis*, 2010, **352**, 1014-1022.
85.	İ. Özdemir, B. Yiğit, B. Çetinkaya, D. Ülkü, M. N. Tahir and C. Arıcı, *Journal of Organometallic Chemistry*, 2001, **633**, 27-32.
86.	J. P. Jordan and R. H. Grubbs, *Angewandte Chemie International Edition*, 2007, **46**, 5152-5155.
87.	A. Melaiye, R. S. Simons, A. Milsted, F. Pingitore, C. Wesdemiotis, C. A. Tessier and W. J. Youngs, *Journal of Medicinal Chemistry*, 2004, **47**, 973-977.
88.	B. Karimi and P. Fadavi Akhavan, *Chemical Communications*, 2011, **47**, 7686-7688.
89.	J. S. Bradley, G. Schmid, D. V. Talapin, E. V. Shevchenko and H. Weller, in *Nanoparticles*, Wiley-VCH Verlag GmbH & Co. KGaA, 2005, pp. 185-238.
90.	L. S. Ott, M. L. Cline, M. Deetlefs, K. R. Seddon and R. G. Finke, *Journal of the American Chemical Society*, 2005, **127**, 5758-5759.
91.	F. Bernardi, J. D. Scholten, G. H. Fecher, J. Dupont and J. Morais, *Chemical Physics Letters*, 2009, **479**, 113-116.
92.	P. Lara, O. Rivada-Wheelaghan, S. Conejero, R. Poteau, K. Philippot and B. Chaudret, *Angewandte Chemie International Edition*, 2011, **50**, 12080-12084.
93.	C. M. Crudden, J. H. Horton, I. I. Ebralidze, O. V. Zenkina, A. B. McLean, B. Drevniok, Z. She, H.-B. Kraatz, N. J. Mosey, T. Seki, E. C. Keske, J. D. Leake, A. Rousina-Webb and G. Wu, *Nat Chem*, 2014, **6**, 409-414.
94.	O. R. M. S. Kharasch, *Constable, London*, 1954, 1384.
95.	A. O. King, N. Okukado and E.-i. Negishi, *Journal of the Chemical Society, Chemical Communications*, 1977, 683-684.
96.	Y. Hatanaka and T. Hiyama, *Synlett*, 1991, **1991**, 845-853.
97.	D. Milstein and J. K. Stille, *Journal of the American Chemical Society*, 1978, **100**, 3636-3638.

98. N. Miyaura and A. Suzuki, *Journal of the Chemical Society, Chemical Communications*, 1979, 866-867.
99. R. F. Heck and J. P. Nolley, *The Journal of Organic Chemistry*, 1972, **37**, 2320-2322.
100. T. Mizoroki, K. Mori and A. Ozaki, *Bulletin of the Chemical Society of Japan*, 1971, **44**, 581-581.
101. K. Sonogashira, *Journal of Organometallic Chemistry*, 2002, **653**, 46-49.
102. A. Suzuki, *Pure Appl. Chem.*, 1985, **57**, 1749-1758.
103. G. B. Smith, G. C. Dezeny, D. L. Hughes, A. O. King and T. R. Verhoeven, *The Journal of Organic Chemistry*, 1994, **59**, 8151-8156.
104. C. Amatore, A. Jutand and G. Le Duc, *Chemistry – A European Journal*, 2011, **17**, 2492-2503.
105. C. Zhang, J. Huang, M. L. Trudell and S. P. Nolan, *The Journal of Organic Chemistry*, 1999, **64**, 3804-3805.
106. G. A. Grasa, M. S. Viciu, J. Huang, C. Zhang, M. L. Trudell and S. P. Nolan, *Organometallics*, 2002, **21**, 2866-2873.
107. H. Lebel, M. K. Janes, A. B. Charette and S. P. Nolan, *Journal of the American Chemical Society*, 2004, **126**, 5046-5047.
108. G. Altenhoff, R. Goddard, C. W. Lehmann and F. Glorius, *Angewandte Chemie International Edition*, 2003, **42**, 3690-3693.
109. W. A. Herrmann, V. P. W. Böhm, C. W. K. Gstöttmayr, M. Grosche, C.-P. Reisinger and T. Weskamp, *Journal of Organometallic Chemistry*, 2001, **617–618**, 616-628.
110. M. S. Viciu, R. F. Germaneau, O. Navarro-Fernandez, E. D. Stevens and S. P. Nolan, *Organometallics*, 2002, **21**, 5470-5472.
111. O. Navarro, H. Kaur, P. Mahjoor and S. P. Nolan, *The Journal of Organic Chemistry*, 2004, **69**, 3173-3180.
112. N. Marion, O. Navarro, J. Mei, E. D. Stevens, N. M. Scott and S. P. Nolan, *Journal of the American Chemical Society*, 2006, **128**, 4101-4111.
113. C. J. O'Brien, E. A. B. Kantchev, C. Valente, N. Hadei, G. A. Chass, A. Lough, A. C. Hopkinson and M. G. Organ, *Chemistry – A European Journal*, 2006, **12**, 4743-4748.
114. J. Nasielski, N. Hadei, G. Achonduh, E. A. B. Kantchev, C. J. O'Brien, A. Lough and M. G. Organ, *Chemistry – A European Journal*, 2010, **16**, 10844-10853.
115. E. Comer and M. G. Organ, *Chemistry – A European Journal*, 2005, **11**, 7223-7227.
116. D. J. Darensbourg and C. G. Ortiz, in *Aqueous-Phase Organometallic Catalysis*, Wiley-VCH Verlag GmbH & Co. KGaA, 2005, pp. 70-99.
117. M.-O. Simon and C.-J. Li, *Chemical Society Reviews*, 2012, **41**, 1415-1427.
118. T. Jeffery, *Tetrahedron*, 1996, **52**, 10113-10130.
119. L. Bai, J.-X. Wang and Y. Zhang, *Green Chemistry*, 2003, **5**, 615-617.
120. C. Dupuis, K. Adiey, L. Charruault, V. Michelet, M. Savignac and J.-P. Genêt, *Tetrahedron Letters*, 2001, **42**, 6523-6526.
121. N. B. V. Didier, *Journal of Chemical Research (S)*, 2000, 429-431.
122. R. Amengual, E. Genin, V. Michelet, M. Savignac and J.-P. Genêt, *Advanced Synthesis & Catalysis*, 2002, **344**, 393-398.
123. K. H. Shaughnessy, *Metal-Catalyzed Reactions in Water*, Wiley-VCH Verlag GmbH & Co. KGaA, 2013, pp. 1-46.
124. M. Beller, J. G. E. Krauter and A. Zapf, *Angewandte Chemie International Edition in English*, 1997, **36**, 772-774.
125. C. A. Fleckenstein and H. Plenio, *Chemistry – A European Journal*, 2007, **13**, 2701-2716.
126. C. Zhou, J. Wang, L. Li, R. Wang and M. Hong, *Green Chemistry*, 2011, **13**, 2100-2106.
127. L. Botella and C. Nájera, *Angewandte Chemie International Edition*, 2002, **41**, 179-181.
128. R. Zhong, A. Pothig, Y. Feng, K. Riener, W. A. Herrmann and F. E. Kühn, *Green Chemistry*, 2014, **16**, 4955-4962.
129. F. Churruca, R. SanMartin, B. Inés, I. Tellitu and E. Domínguez, *Advanced Synthesis & Catalysis*, 2006, **348**, 1836-1840.

130. B. Inés, R. SanMartin, M. J. Moure and E. Domínguez, *Advanced Synthesis & Catalysis*, 2009, **351**, 2124-2132.
131. L. Li, J. Wang, C. Zhou, R. Wang and M. Hong, *Green Chemistry*, 2011, **13**, 2071-2077.
132. C.-C. Yang, P.-S. Lin, F.-C. Liu, I. J. B. Lin, G.-H. Lee and S.-M. Peng, *Organometallics*, 2010, **29**, 5959-5971.
133. F.-T. Luo and H.-K. Lo, *Journal of Organometallic Chemistry*, 2011, **696**, 1262-1265.
134. C. T. Kresge, M. E. Leonowicz, W. J. Roth, J. C. Vartuli and J. S. Beck, *Nature*, 1992, **359**, 710-712.
135. C. V. James, J. R. Wielsaw and F. D. Thomas, in *Dekker Encyclopedia of Nanoscience and Nanotechnology, Second Edition*, Taylor & Francis, 2009, vol. null, pp. 2029-2043.
136. D. Zhao, J. Feng, Q. Huo, N. Melosh, G. H. Fredrickson, B. F. Chmelka and G. D. Stucky, *Science*, 1998, **279**, 548-552.
137. F. de Clippel, M. Dusselier, S. Van de Vyver, L. Peng, P. A. Jacobs and B. F. Sels, *Green Chemistry*, 2013, **15**, 1398-1430.
138. P. Van Der Voort, D. Esquivel, E. De Canck, F. Goethals, I. Van Driessche and F. J. Romero-Salguero, *Chemical Society Reviews*, 2013, **42**, 3913-3955.
139. K. Moller and T. Bein, *Chemistry of Materials*, 1998, **10**, 2950-2963.
140. W. D. Bossaert, D. E. De Vos, W. M. Van Rhijn, J. Bullen, P. J. Grobet and P. A. Jacobs, *Journal of Catalysis*, 1999, **182**, 156-164.
141. M. H. Lim and A. Stein, *Chemistry of Materials*, 1999, **11**, 3285-3295.
142. L. L. Hench and J. K. West, *Chemical Reviews*, 1990, **90**, 33-72.
143. G. W. S. C. Jeffrey Brinker, *Sol-Gel Science - The Physics and Chemistry of Sol-Gel Processing*, Academic Press, 1990.
144. Z. ALOthman, *Materials*, 2012, **5**, 2874.
145. I. C. Tilgner, P. Fischer, F. M. Bohnen, H. Rehage and W. F. Maier, *Microporous Materials*, 1995, **5**, 77-90.
146. J. Pang, V. T. John, D. A. Loy, Z. Yang and Y. Lu, *Advanced Materials*, 2005, **17**, 704-707.
147. G. Kickelbick, in *Hybrid Materials*, Wiley-VCH Verlag GmbH & Co. KGaA, 2007, pp. 1-48.
148. T. Asefa, M. J. MacLachlan, N. Coombs and G. A. Ozin, *Nature*, 1999, **402**, 867-871.
149. B. J. Melde, B. T. Holland, C. F. Blanford and A. Stein, *Chemistry of Materials*, 1999, **11**, 3302-3308.
150. S. Inagaki, S. Guan, Y. Fukushima, T. Ohsuna and O. Terasaki, *Journal of the American Chemical Society*, 1999, **121**, 9611-9614.
151. M. P. Kapoor and S. Inagaki, *Chemistry Letters*, 2004, **33**, 88-89.
152. V. Rebbin, M. Jakubowski, S. Pötz and M. Fröba, *Microporous and mesoporous materials*, 2004, **72**, 99-104.
153. V. Rebbin, R. Schmidt and M. Fröba, *Angewandte Chemie International Edition*, 2006, **45**, 5210-5214.
154. G. Zhu, D. Jiang, Q. Yang, J. Yang and C. Li, *Journal of Chromatography A*, 2007, **1149**, 219-227.
155. M. C. Burleigh, S. Dai, E. W. Hagaman and J. S. Lin, *Chemistry of Materials*, 2001, **13**, 2537-2546.
156. M. K. Samantaray, J. Alauzun, D. Gajan, S. Kavitake, A. Mehdi, L. Veyre, M. Lelli, A. Lesage, L. Emsley, C. Copéret and C. Thieuleux, *Journal of the American Chemical Society*, 2013, **135**, 3193-3199.
157. A. Corma, D. Das, H. García and A. Leyva, *Journal of Catalysis*, 2005, **229**, 322-331.
158. F. Zhang, C. Kang, Y. Wei and H. Li, *Advanced Functional Materials*, 2011, **21**, 3189-3197.
159. J. Huang, F. Zhu, W. He, F. Zhang, W. Wang and H. Li, *Journal of the American Chemical Society*, 2010, **132**, 1492-1493.
160. A. J. Arduengo Iii, R. Krafczyk, R. Schmutzler, H. A. Craig, J. R. Goerlich, W. J. Marshall and M. Unverzagt, *Tetrahedron*, 1999, **55**, 14523-14534.
161. L. Jafarpour, E. D. Stevens and S. P. Nolan, *Journal of Organometallic Chemistry*, 2000, **606**, 49-54.
162. *U.S Pat.*, US 7,109,348 B1, 2006.

163. H. Debus, *Justus Liebigs Annalen der Chemie*, 1858, **107**, 199-208.
164. M. B. Dinger, P. Nieczypor and J. C. Mol, *Organometallics*, 2003, **22**, 5291-5296.
165. A. Furstner, M. Alcarazo, V. Cesar and C. W. Lehmann, *Chemical Communications*, 2006, 2176-2178.
166. D. Esposito, S. Kirchhecker and M. Antonietti, *Chemistry – A European Journal*, 2013, **19**, 15097-15100.
167. S. Kirchhecker, M. Antonietti and D. Esposito, *Green Chemistry*, 2014, **16**, 3705-3709.
168. S. Carrettin, P. McMorn, P. Johnston, K. Griffin and G. J. Hutchings, *Chemical Communications*, 2002, 696-697.
169. S. Carrettin, P. McMorn, P. Johnston, K. Griffin, C. J. Kiely and G. J. Hutchings, *Physical Chemistry Chemical Physics*, 2003, **5**, 1329-1336.
170. Y. Shen, S. Zhang, H. Li, Y. Ren and H. Liu, *Chemistry – A European Journal*, 2010, **16**, 7368-7371.
171. D. Esposito and M. Antonietti, *ChemSusChem*, 2013, **6**, 989-992.
172. *The MAK-Collection for Occupational Health and Safety*, Wiley-VCH Verlag GmbH & Co. KGaA, 2002.
173. G. Zhao, M. Zheng, J. Zhang, A. Wang and T. Zhang, *Industrial & Engineering Chemistry Research*, 2013, **52**, 9566-9572.
174. R. Ooms, M. Dusselier, J. A. Geboers, B. Op de Beeck, R. Verhaeven, E. Gobechiya, J. A. Martens, A. Redl and B. F. Sels, *Green Chemistry*, 2014, **16**, 695-707.
175. R. Sun, M. Zheng, J. Pang, X. Liu, J. Wang, X. Pan, A. Wang, X. Wang and T. Zhang, *ACS Catalysis*, 2016, **6**, 191-201.
176. G. E. Ham, *Journal of Polymer Science*, 1962, **61**, 293-301.
177. C. E. H. a. A. G. Sharpe, *Inorganic Chemistry*, 3rd edn., Pearson, UK, 2008.
178. W. A. Herrmann, L. J. Gooβen and M. Spiegler, *Journal of Organometallic Chemistry*, 1997, **547**, 357-366.
179. T. J. Berg JM, Stryer L. , *Biochemistry*, 5th edn., New York: W H Freeman, 2002.
180. E. D. Stroud, D. J. Fife and G. G. Smith, *The Journal of Organic Chemistry*, 1983, **48**, 5368-5369.
181. T. L. Amyes, S. T. Diver, J. P. Richard, F. M. Rivas and K. Toth, *Journal of the American Chemical Society*, 2004, **126**, 4366-4374.
182. J. C. Garrison, R. S. Simons, C. A. Tessier and W. J. Youngs, *Journal of Organometallic Chemistry*, 2003, **673**, 1-4.
183. G. Papini, M. Pellei, G. Gioia Lobbia, A. Burini and C. Santini, *Dalton Transactions*, 2009, 6985-6990.
184. J. Cure, R. Poteau, I. C. Gerber, H. Gornitzka and C. Hemmert, *Organometallics*, 2012, **31**, 619-626.
185. T. Tu, X. Feng, Z. Wang and X. Liu, *Dalton Transactions*, 2010, **39**, 10598-10600.
186. M. Pellei, V. Gandin, M. Marinelli, C. Marzano, M. Yousufuddin, H. V. R. Dias and C. Santini, *Inorganic Chemistry*, 2012, **51**, 9873-9882.
187. M. Delgado-Rebollo, Á. Beltrán, A. Prieto, M. Mar Díaz-Requejo, A. M. Echavarren and P. J. Pérez, *European Journal of Inorganic Chemistry*, 2012, **2012**, 1380-1386.
188. J. DePasquale, N. J. White, E. J. Ennis, M. Zeller, J. P. Foley and E. T. Papish, *Polyhedron*, 2013, **58**, 162-170.
189. D. Gulcemal, A. G. Gokce, S. Gulcemal and B. Cetinkaya, *RSC Advances*, 2014, **4**, 26222-26230.
190. G. Dahm, C. Bailly, L. Karmazin and S. Bellemin-Laponnaz, *Journal of Organometallic Chemistry*, 2015, **794**, 115-124.
191. V. Gandin, M. Pellei, M. Marinelli, C. Marzano, A. Dolmella, M. Giorgetti and C. Santini, *Journal of Inorganic Biochemistry*, 2013, **129**, 135-144.
192. M. A. Reynoso-Esparza, I. I. Rangel-Salas, A. A. Peregrina-Lucano, J. G. Alvarado-Rodríguez, F. A. López-Dellamary-Toral, R. Manríquez-González, M. L. Espinosa-Macías and S. A. Cortes-Llamas, *Polyhedron*, 2014, **81**, 564-571.

193. L. Cavallo and C. S. J. Cazin, in *N-Heterocyclic Carbenes in Transition Metal Catalysis and Organocatalysis*, ed. S. J. C. Cazin, Springer Netherlands, Dordrecht, 2011, pp. 1-22.
194. A. R. Chianese, X. Li, M. C. Janzen, J. W. Faller and R. H. Crabtree, *Organometallics*, 2003, **22**, 1663-1667.
195. C. A. Tolman, *Chemical Reviews*, 1977, **77**, 313-348.
196. K.-T. Chan, Y.-H. Tsai, W.-S. Lin, J.-R. Wu, S.-J. Chen, F.-X. Liao, C.-H. Hu and H. M. Lee, *Organometallics*, 2010, **29**, 463-472.
197. H. V. Huynh, Y. Han, R. Jothibasu and J. A. Yang, *Organometallics*, 2009, **28**, 5395-5404.
198. H. Baier, A. Kelling and H.-J. Holdt, *European Journal of Inorganic Chemistry*, 2015, **2015**, 1950-1957.
199. Y. C. Shi, Zhengyuan; Peng, Yu; Shi, Zhan; Pang, Guangsheng, *Journal of Chemical Research*, 2011, **35**, 161-162.
200. A. Zanardi, J. A. Mata and E. Peris, *Organometallics*, 2009, **28**, 4335-4339.
201. A. Poater, B. Cosenza, A. Correa, S. Giudice, F. Ragone, V. Scarano and L. Cavallo, *European Journal of Inorganic Chemistry*, 2009, **2009**, 1759-1766.
202. R. H. Crabtree, in *The Organometallic Chemistry of the Transition Metals*, John Wiley & Sons, Inc., 2005, pp. 159-182.
203. A. S. Kashin and V. P. Ananikov, *The Journal of Organic Chemistry*, 2013, **78**, 11117-11125.
204. Berzelius, *Ann.*, 1828, **13**, 435.
205. M. J. Schultz, C. C. Park and M. S. Sigman, *Chemical Communications*, 2002, 3034-3035.
206. B. A. Steinhoff, S. R. Fix and S. S. Stahl, *Journal of the American Chemical Society*, 2002, **124**, 766-767.
207. R. M. Painter, D. M. Pearson and R. M. Waymouth, *Angewandte Chemie*, 2010, **122**, 9646-9649.
208. I. W. C. E. Arends, G.-J. ten Brink and R. A. Sheldon, *Journal of Molecular Catalysis A: Chemical*, 2006, **251**, 246-254.
209. K. Chung, S. M. Banik, A. G. De Crisci, D. M. Pearson, T. R. Blake, J. V. Olsson, A. J. Ingram, R. N. Zare and R. M. Waymouth, *Journal of the American Chemical Society*, 2013, **135**, 7593-7602.
210. M. J. Schultz, S. S. Hamilton, D. R. Jensen and M. S. Sigman, *The Journal of Organic Chemistry*, 2005, **70**, 3343-3352.
211. E. Steeples, A. Kelling, U. Schilde and D. Esposito, *New Journal of Chemistry*, 2016.
212. B. Lee, H.-J. Im, H. Luo, E. W. Hagaman and S. Dai, *Langmuir*, 2005, **21**, 5372-5376.
213. T. P. Nguyen, P. Hesemann and J. J. E. Moreau, *Microporous and Mesoporous Materials*, 2011, **142**, 292-300.
214. B. Gadenne, P. Hesemann and J. J. E. Moreau, *Chemical Communications*, 2004, 1768-1769.
215. B. Karimi, D. Elhamifar, J. H. Clark and A. J. Hunt, *Chemistry – A European Journal*, 2010, **16**, 8047-8053.
216. T. P. Nguyen, P. Hesemann, P. Gaveau and J. J. E. Moreau, *Journal of Materials Chemistry*, 2009, **19**, 4164-4171.
217. G. Li, H. Yang, W. Li and G. Zhang, *Green Chemistry*, 2011, **13**, 2939-2947.
218. K. S. W. Sing, D. H. Everett, R. A. W. Haul, L. Moscou, R. A. Pierotti, J. Rouquerol and T. Siemieniewska, in *Handbook of Heterogeneous Catalysis*, Wiley-VCH Verlag GmbH & Co. KGaA, 2008.

VIII Appendix

1   Crystal data and structure refinement

Compound	3a
Chemical formula	$C_{11}H_{16}AgClN_2O_4$
Molecular weight / g·mol^{-1}	383.58
Crystal system	monoclinic
Space group	$P2_1/c$ (no. 14)
a / Å	10.4357(5)
b / Å	16.0846(12)
c / Å	8.4037(6)
β / °	91.325(5)
Unit cell volume / Å^3	1410.22(16)
Temperature / K	210(2)
Z	4
Density (calculated) / g·cm^{-1}	1.807
Radiation type	Mo-Kα
μ / mm^{-1}	1.629
Reflections collected	8855
Independent reflections	2468
R_{int}	0.0431
R_1 / wR_2 [$I > 2\sigma(I)$]	0.0197 / 0.0473
R_1 / wR_2 (all data)	0.0256 / 0.0493
Goodness of fit on F^2	0.990

Compound	4a
Chemical formula	$C_{26}H_{38}N_4O_{12}Pd$
Molecular weight / g·mol^{-1}	705.02
Crystal system	orthorhombic
Space group	*Pbca* (no. 61)
a / Å	11.8365(3)
b / Å	20.4164(5)
c / Å	26.5774(8)
Unit cell volume / Å^3	6422.66(30)
Temperature / K	210(2)
Z	8
Density (calculated) / g·cm^{-1}	1.458
Radiation type	Mo-Kα
μ / mm^{-1}	0.642
Reflections collected	47369
Independent reflections	6800
R_{int}	0.0539
R_1 / wR_2 [$I > 2\sigma(I)$]	0.0319 / 0.0749
R_1 / wR_2 (all data)	0.0629 / 0.0851
Goodness of fit on F^2	0.984

Compound	5a
Chemical formula	$C_{22}H_{32}Cl_2N_4O_8Pd$
Molecular weight / g·mol^{-1}	657.81
Crystal system	monoclinic
Space group	$P2_1/n$ (no. 14)
a / Å	12.2261(3)
b / Å	27.7257(6)
c / Å	17.0282(4)
β / °	99.793(2)
Unit cell volume / Å^3	5688.1(2)
Temperature / K	210(2)
Z	8
Density (calculated) / g·cm^{-1}	1.536
Radiation type	Mo-Kα
μ / mm^{-1}	0.890
Reflections collected	69663
Independent reflections	9541
R_{int}	0.0616
R_1 / wR_2 [$I > 2\sigma(I)$]	0.0297 / 0.0823
R_1 / wR_2 (all data)	0.0362 / 0.0846
Goodness of fit on F^2	1.093

Compound	5b
Chemical formula	$C_{26}H_{40}Cl_2N_4O_8Pd$
Molecular weight / g·mol^{-1}	713.92
Crystal system	monoclinic
Space group	$C2/c$ (no. 15)
a / Å	10.3920(5)
b / Å	12.0677(7)
c / Å	25.5618(10)
β / °	98.377(3)
Unit cell volume / Å^3	3171.4(3)
Temperature / K	210(2)
Z	4
Density (calculated) / g·cm^{-1}	1.495
Radiation type	Mo-Kα
μ / mm^{-1}	0.804
Reflections collected	10088
Independent reflections	2804
R_{int}	0.0178
R_1 / wR_2 [$I > 2\sigma(I)$]	0.0234 / 0.0601
R_1 / wR_2 (all data)	0.0251 / 0.0610
Goodness of fit on F^2	1.052

Compound	6a·CHCl₃
Chemical formula	$C_{17}H_{22}Cl_5N_3O_4Pd$
Molecular weight / g·mol^{-1}	616.02
Crystal system	monoclinic
Space group	$P2_1/c$ (no. 14)
a / Å	11.7256(4)
b / Å	23.0938(8)
c / Å	9.0944(6)
β / °	99.520(4)
Unit cell volume / Å³	2428.7(2)
Temperature / K	210(2)
Z	4
Density (calculated) / g·cm^{-1}	1.685
Radiation type	Mo-Kα
μ / mm^{-1}	1.342
Reflections collected	15567
Independent reflections	4269
R_{int}	0.0364
R_1 / wR_2 [$I > 2\sigma(I)$]	0.0241 / 0.0581
R_1 / wR_2 (all data)	0.0327 / 0.0613
Goodness of fit on F^2	1.015

Compound	6b
Chemical formula	$C_{18}H_{25}Cl_2N_3O_4Pd$
Molecular weight / g·mol^{-1}	524.71
Crystal system	triclinic
Space group	$P\bar{1}$ (no. 2)
a / Å	9.4985(8)
b / Å	9.7104(7)
c / Å	12.2951(10)
α / °	93.265(6)
β / °	95.848(6)
γ / °	98.828(6)
Unit cell volume / Å^3	1111.72(15)
Temperature / K	210(2)
Z	2
Density (calculated) / g·cm^{-1}	1.567
Radiation type	Mo-Kα
μ / mm^{-1}	1.102
Reflections collected	14413
Independent reflections	3924
R_{int}	0.0243
R_1 / wR_2 [$I > 2\sigma(I)$]	0.0194 / 0.0525
R_1 / wR_2 (all data)	0.0213 / 0.0533
Goodness of fit on F^2	1.059

Compound	$\mathbf{6d}\cdot C_3H_6O$
Chemical formula	$C_{21}H_{31}Cl_2N_3O_5Pd$
Molecular weight / $g\cdot mol^{-1}$	582.79
Crystal system	triclinic
Space group	$P1$ (no. 1)
a / Å	8.5177(5)
b / Å	8.6938(5)
c / Å	10.4595(6)
α / °	107.624(4)
β / °	94.891(4)
γ / °	114.239(4)
Unit cell volume / Å^3	653.24(7)
Temperature / K	210(2)
Z	1
Density (calculated) / $g\cdot cm^{-1}$	1.481
Radiation type	Mo-Kα
μ / mm^{-1}	0.949
Reflections collected	10136
Independent reflections	5276
R_{int}	0.0547
R_1 / wR_2 [$I > 2\sigma(I)$]	0.0430 / 0.1145
R_1 / wR_2 (all data)	0.0430 / 0.1145
Goodness of fit on F^2	1.064

Compound	7a
Chemical formula	$C_{19}H_{28}ClIrN_2O_4$
Molecular weight / g·mol^{-1}	576.08
Crystal system	monoclinic
Space group	$P2_1/n$ (no. 14)
a / Å	15.7787(5)
b / Å	7.7401(2)
c / Å	16.6047(6)
β / °	91.031(3
Unit cell volume / Å^3	2027.58(11)
Temperature / K	210(2)
Z	4
Density (calculated) / g·cm^{-1}	1.887
Radiation type	Mo-Kα
μ / mm^{-1}	6.744
Reflections collected	25265
Independent reflections	3560
R_{int}	0.1242
R_1 / wR_2 [$I > 2\sigma(I)$]	0.0264/ 0.0660
R_1 / wR_2 (all data)	0.0269 / 0.0664
Goodness of fit on F^2	1.193

2   List of Publications

Journal articles

Amino acid-derived N-heterocyclic carbene palladium complexes for aqueous phase Suzuki-Miyaura couplings.

Steeples, E. Kelling, A. Schilde, U and Esposito, D.

New Journal of Chemistry – DOI: 10.1039/c5nj03337c

Conference contributions

Amino acid-derived N-Heterocyclic carbene palladium complexes for Suzuki-Miyaura couplings in water: the duality of hetero- and homogeneity – *accepted for poster presentation*

18th IUPAC International Symposium on Organometallic Chemistry directed towards Organic Synthesis – Sitges, Barcelona, 2015

3   Declaration

Die vorliegende Dissertation entstand in dem Zeitraum zwischen Oktober 2013 und Oktober 2015 am Max-Planck-Institut für Kolloid- und Grenzflächenforschung, unter der Betreuung von Prof. Dr. Markus Antonietti.

Hiermit erkläre ich, dass die vorliegende Arbeit selbstständig angefertigt und keine anderen als die angegebenen Hilfsmittel und Quellen verwendet wurden.

I declare herein, that the work reported within this thesis was produced independently, and nothing other than the referenced materials and sources was used.

Elliot Steeples